MSc by Research

Student: Kieran Mulready

Student No: ▮▮▮▮▮▮▮

Date: 28 August 2020

Sensors and Methods for Railway Signalling Equipment Monitoring

Submitted to Swansea University in fulfilment of

the requirements for the

Degree of Master of Science by Research

Swansea University 2020

ABSTRACT

Signalling upgrade projects that have been installed in equipment rooms in the recent past have limited capability to monitor performance of certain types of external circuits. To modify the equipment rooms on the commissioned railway would prove very expensive to implement and would be unacceptable in terms of delays caused to passenger services due to re-commissioning circuits after modification, to comply with rail signalling standards.

The use of magnetoresistive sensors to provide performance data on point circuit operation and point operation is investigated. The sensors are bench tested on their ability to measure current in a circuit in a non-intrusive manner. The effect of shielding on the sensor performance is tested and found to be significant.

The response of the sensors with various levels of amplification produces linear responses across a range of circuit gain. The output of the sensor circuit is demonstrated for various periods of interruption of conductor current.
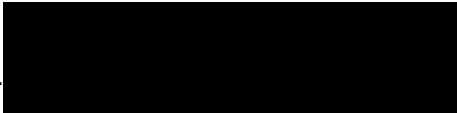
A three-axis accelerometer is mounted on a linear actuator to demonstrate the type of output expected from similar sensors mounted on a set of points. Measurements of current in point detection circuits and acceleration forces resulting from vibration of out of tolerance mechanical assemblies can provide valuable information on performance and possible threats to safe operation of equipment.

The sensors seem capable of measuring the current in a conductor with a comparatively high degree of sensitivity. There is development work required on shielding the sensor from magnetic fields other than those being measured. The accelerometer work is at a demonstration level and requires development. The future testing work with accelerometers should be at a facility where multiple point moves can be made; with the capability to introduce faults to the point mechanisms. Methods can then be developed for analysis of the vibration signatures produced by the various faults.
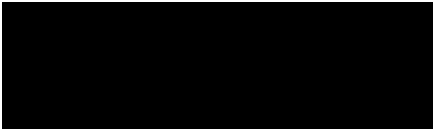
Declarations and Statements

Declaration

This work has not previously been accepted in substance for any degree and is not being concurrently submitted in candidature for any degree.

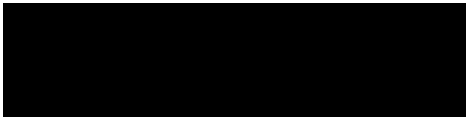Signed …⬛⬛⬛⬛⬛⬛⬛⬛⬛⬛⬛.. Date: 28th August 2020

Statement 1

This work is the result of my own independent study/investigation, except where otherwise stated. Other sources are acknowledged by footnotes giving explicit references. A bibliography is appended.

Signed ……⬛⬛⬛⬛⬛⬛⬛ Date: 28th August 2020

Statement 2

I hereby give my consent for my work, if relevant and accepted, to be available for photocopying and for inter-library loan, and for the title and summary to be made available to outside organisations.

Signed …⬛⬛⬛⬛⬛⬛ Date: 28th August 2020

Sensors and Methods for Railway Signalling Equipment Monitoring

Contents

List of Figures

List of Tables

Acronyms

ABS	Acrylonitrile Butadiene Styrene (thermoplastic polymer)
AC	Alternating Current
ADC	Analogue to Digital Converter
AMR	Anisotropic Magneto-Resistive
AN	Detection Normal Contact
BCRRE	Birmingham Centre for Railway Research and Education
BR	Detection Reverse Contact
CCTF	Control Cable Termination Frame
CGS	Centimetre-Gram-Second System
CM	Condition Monitoring
CMS	Cable Management System
C-SVM	Classification Support Vector Machine
CTFC	Cable Termination Frame Cabinet
DC	Direct Current
DMM	Digital Multimeter
DTW	Dynamic Time Warping
EMC	Electromagnetic Compatibility
EPM	Electric Point Machine
FD	Fault Detection
FDD	Fault Detection and Diagnosis
FDI	Fault Detection and Identification
FMS	Fault Management System
FPL	Facing Point Lock
HI	Health Indicator
HMI	Human Machine Interface

I/O	Input/Output
ISO	International Organisation for Standardisation
LU	London Underground
MDA	Machine Degradation-level Assessment
MOSFET	Metal Oxide Semiconductor Field Effect Transistor
MQE	Minimum Quantisation Error
MRS	Magnetic Resistive Sensor
NLR	Normal Latch Relay
NR	Network Rail
NW	Normal Point Valve solenoid
P1	Point Number Designation
P&LD	Point Lock and Detection
PCA	Principal Component Analysis
POE	Points Operating Equipment
RC	Radio Control
RCF	Rolling Contact Fatigue
RLR	Reverse Latch Relay
RMS	Root Mean Square
RPM	Railway Point Machine
RW	Reverse Point Valve Solenoid
S&C	Switches and Crossings
SI	International System of Units
SOM	Self Organising Map
SPD	Surge Protection Device
STME	Single Throw Mechanical Equipment
STP	Screened Twisted Pair
SVDD	Support Vector Data Description

SVM   Support Vector Machine

WL   Point Groundlock Valve Solenoid(based on signalling alphabet)

WMR   Point Move Relay(based on signalling alphabet)

WNR   Point Normal Relay(based on signalling alphabet)

WRR   Point Reverse Relay(based on signalling alphabet)

1 ACKNOWLEDGMENTS

I would like to take this opportunity to thank my thesis supervisor, Dr. Pavel Loskot, for his help and support throughout my research project.

I also thank my family for their patience and support throughout my period of study. Without the support of all of these people then I would not be able to submit this work.

2 INTRODUCTION

Over the last decade a number of major re-signalling projects have taken place on the London Underground system that have a minimum project lifetime of forty years. The targeted outcome is to explore means by which both centralised performance information and a local information interface for a first response maintainer can be provided.

The current level of fault reporting in the "live" system is at a comparatively high system level in order to provide a degree of latency in the safety critical data handling functionality. Fault responses are dealt with according to their effect on the ability of the system to operate safely while providing an acceptable level of service availability.

Currently preventative maintenance activities focus on:

- Time/number of operation-based change out of line replaceable components (e.g. relays)

- Time based checks of equipment set up and operation for electro-mechanical components (e.g. point machines).

- Time based testing of component properties such as insulation resistance values in the case of copper cabling and checking for core to core faults where multicore cables have been utilised in the design.

The lines that have been re-signalled have a basic requirement to route trains safely and reliably to meet scheduled timetables. Point machines are a major system component by which the desired routing for trains is selected.

The research considers the suitability of combined information gathered from sensors in the signalling equipment rooms and on the point switches to use for

condition monitoring purposes. A review of current literature has been conducted on the condition monitoring of point machines, and this indicates that there is value in investigating the use of the particular sensor combination proposed.

The hypothesis is, that non-invasive sensors measuring detection current and point switch acceleration can combine the information that they provide to allow condition monitoring of 4ft electro-pneumatic point machines used on the London Underground. This condition monitoring introduces a further means by which maintenance decisions can be made. The detection current sensors would be mounted in the equipment room cabinets and the point acceleration sensors would be mounted on the switch rails.

This project investigates introducing devices to monitor the performance of the point machines. The aim of the project is to investigate the suitability of two particular sensors to provide information on the operation of railway signalling equipment. The sensors are to be used for conductor current sensing and acceleration on mechanical components. These systems have not been installed with current monitors for the great majority of circuits installed in the new signalling equipment rooms. This project proposes using non-intrusive sensors to be retrofitted, to provide a means of current monitoring without resorting to costly major modification programmes.

The sensors in question are magnetoresistive for use in current sensing of the point detection circuit, and accelerometers for the measurement of forces on the point machines. The accelerometer used for the measurement of the moving mechanical parts measures acceleration in three axes.

The main focus of the discussion is the use of the magnetoresistive current sensor in monitoring of detection circuits and current flowing in associated equipment room conductors. The use of accelerometers is explored as a means of monitoring the condition of moving parts and linkages of point mechanical assemblies.

The object of this activity is to explore ways of using the individual sensors to feed information to a sensor hub to provide maintenance information on the wayside signalling system of an urban rapid transit rail system. The signalling system is presented as a typical system rather than a specific system in the interests of commercial sensitivity. The type of equipment described, and the implementation of the system requirements are to be found on a number of proprietary products.

The information from each sensor is gathered at a local hub and then transferred to a centralised hub. The aims are to provide the capability information to the first response maintainer and the centralised hub for system performance information to be processed.

The sensor hub implementation needs to provide for additional sensor capability where particular information may be required in future to come to decisions on extension of system lifetime or individual components. The data obtained via the sensor network is to improve performance of both planned and reactive maintenance activities. The local sensor network can have no direct interface with the system at a level that may compromise the operational safety integrity.

The difference between safety related and safety critical systems is explained by Smith [1, p.331] "Safety-critical systems are those which, on their own, achieve or maintain a safe state for equipment under their control." This is defined further in London Underground standard on Signalling-functional requirements for interlocking systems [2, p.57] as a vital system being safety critical and a non-vital system being safety related. Points form a part of the route interlocking system and as such are part of a safety critical system. The failure of a vital sub-system or system results in a direct risk of serious injury or fatality; the failure of a safety-related subsystem or system would need to occur in combination with other failures to result in serious injury or fatality.

There follows a description of the implementation of a typical signalling system arrangement to provide a background to the discussion.

The system in Fig. 2.1 is composed of the following subsystems:

- The main System Management Centre that provides the operator interface and the operational management interface. This provides a safety-related function.

- Area control centres that act as area controllers covering a number of site controllers. These provide a safety-critical function.

- Site controllers that provide the interface to the wayside equipment. Depending on the amount of wayside equipment there may be a number of site controllers or just one for small sites. These provide both safety-related and safety-critical function.

- Wayside equipment. These provide both safety-related and safety-critical functions.

- External signal systems. This could be an interface with Network Rail for example.

- Vehicle interface via radio link for train control and signalling.
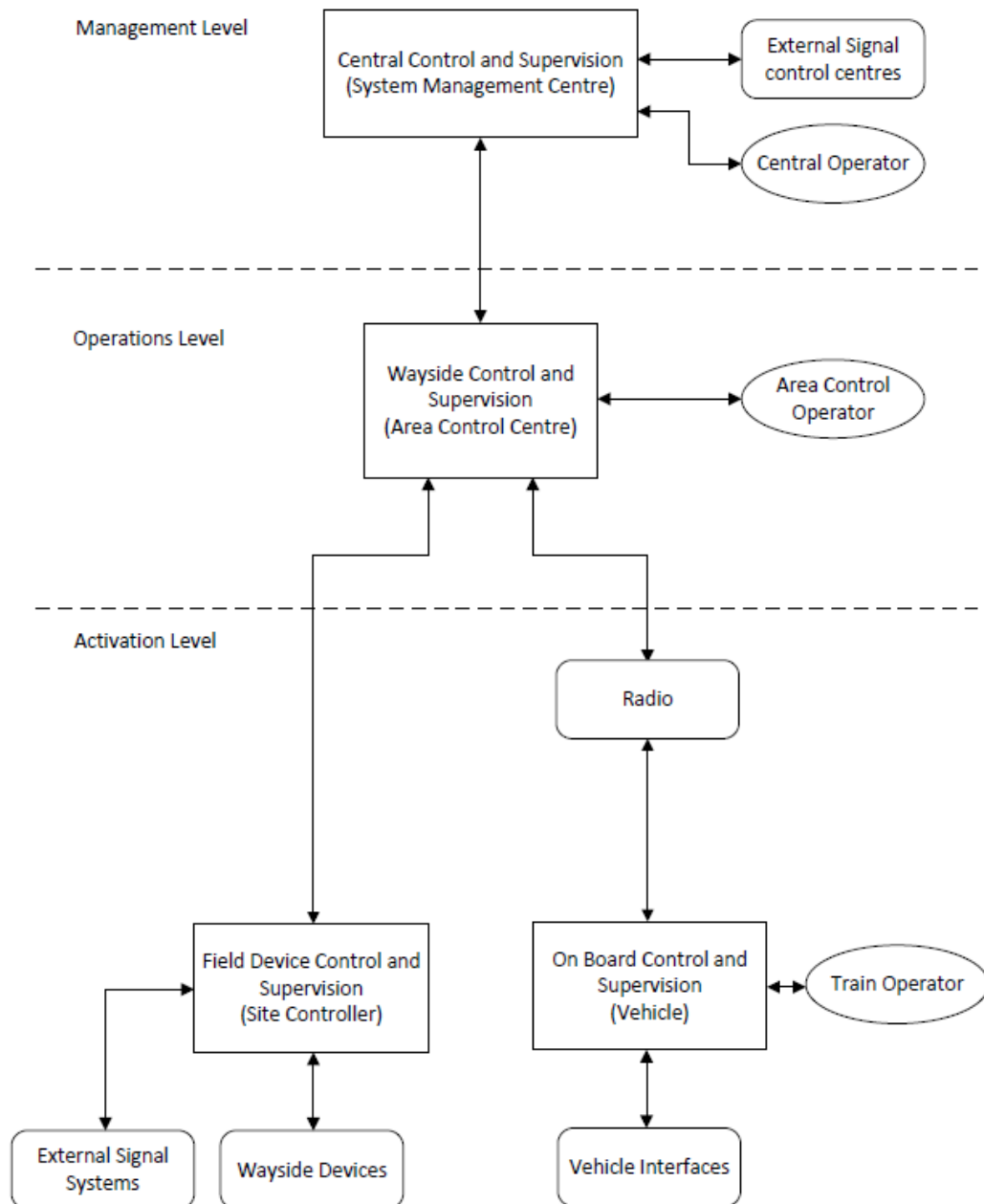
Fig. 2.1 Typical signalling control system levels of control (adapted from Figure 5 in [3])

Communication between System management Centre, Area Controllers and Site Controllers is by data link on fibre networks in most current systems. The output/input between the site controllers and wayside equipment is still in almost all cases for systems installed in the UK over copper cables at power frequency or DC voltages.

The data that is transmitted between controllers is in serial telegram format at various baud rates depending on the hardware used. The site controller provides for control outputs and detection inputs.

In all cases there is a need for the design to be such that faults are self-announcing, as stated in LU standard [2]. This is to prevent dormant failures that could combine with further faults and lead to a wrong side failure. In cases where the fault is not self-announcing then mitigations must be proposed, and risk assessment must be carried out to decide if the mitigations reduce the level of risk to an acceptable level.

A wrong side failure is one such that it directly leads to an unsafe condition rather than a right-side failure where a fault leads to safe condition for the system.

A typical signalling system as illustrated in Fig. 2.1 comprises sub sections that may be many miles apart in the case of the higher level system management centre and the area control centres. There is a single management centre to control a line in almost all cases for urban transit systems. Railways by their nature are dimensionally linear. The area control centres are not necessarily equally spaced along the railway.

They are located based on the system level needs of the operational railway. They have a given capacity to control a certain amount of functions safely and reliably; they are the safety critical backbone of the system.

Site controllers are provided where they are required based on the number of wayside assets they need to interface with. The number of site controllers at a site is based on the number and types of wayside equipment that they are required to interface with. Site controllers have limited amount of inputs and outputs available. When new brown field projects are undertaken in the UK there is a need to keep the operational railway running as near to normal as possible. This means that new signalling equipment rooms must be built, or old unused rooms converted for

the new project. These are costly undertakings and there is an obvious need to limit the amount of new rooms where possible, while still providing an adequate footprint for the new equipment. There is always a drive to reduce the amount of equipment in rooms to reduce civil construction costs on the size of building or conversion works; these need to be considered in proposals to introduce any additional monitoring systems. The maintenance and reliability of any new monitoring system is of obvious concern and safety considerations mean that a non-intrusive monitoring system is essential. The costs of safety assessment and additional design to meet safety requirements make a directly connected monitoring system highly undesirable.

The site controllers in modern signalling systems provide a level of redundancy. This is usually achieved by having two independent systems that can provide input and output functionality. The systems may be active-standby or active-active; Fig. 2.2 illustrates a typical active-active system that provides outputs to interface relays from two possible sources, control card A or control card B. The control cards form part of the site controllers.

The following descriptions are based on the use of the site control and detection equipment in implementing the design requirements.
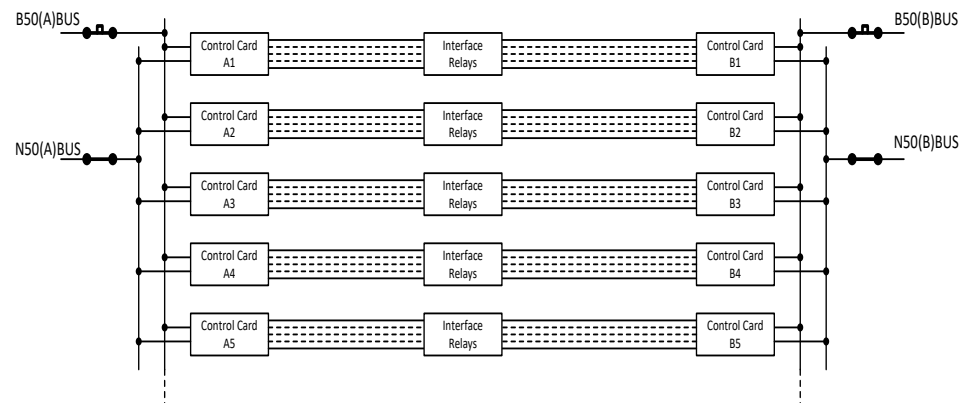
Fig. 2.2 AREMA card layout (adapted from sheet G039 [4])

The Site Controller Power Supply Bus Layout Fig. 2.3 illustrates a typical layout of local supplies to meet the requirements of the overall design.

Comprised of:

- BX/NX110(EXT)(ENX)

This is a 110 volt 50 Hz supply with the NX side of the supply connected to site control room earth. This supply is used with a type of concentric cable that provides for short circuit fault protection.

- B/N50(EXT)BUS

  This is a 50 volt DC supply with both B and N legs floating with respect to earth. This supply is used for circuits external to the site control room earth. This is the supply provided for point detection circuits.

- B/N50(INT)BUS

  This is a 50 volt DC supply with both B and N legs floating with respect to earth. This supply is used for circuits inside the site control room.

- B/N50(A)BUS

  50 volt DC supply used to supply circuits inside the site control room as one half of redundant supply together with the B/N50(B)BUS.

- B/N50(B)BUS

  50 volt DC supply used to supply circuits inside the site control room as one half of redundant supply together with the B/N50(A)BUS.

- BX/NX110(EXT)(SIC)BUS

  Used for control of 110 volt 50 Hz circuits external to the site control room that are driven vie solid state switches; this supply is sub-divided into an A and B bus.

- BX/NX110(EXT)BUS

  Used as 110 volt 50 Hz supply that drives equipment external to the site control room across control relay contacts. The associated control relays are normally contained within the site control room.
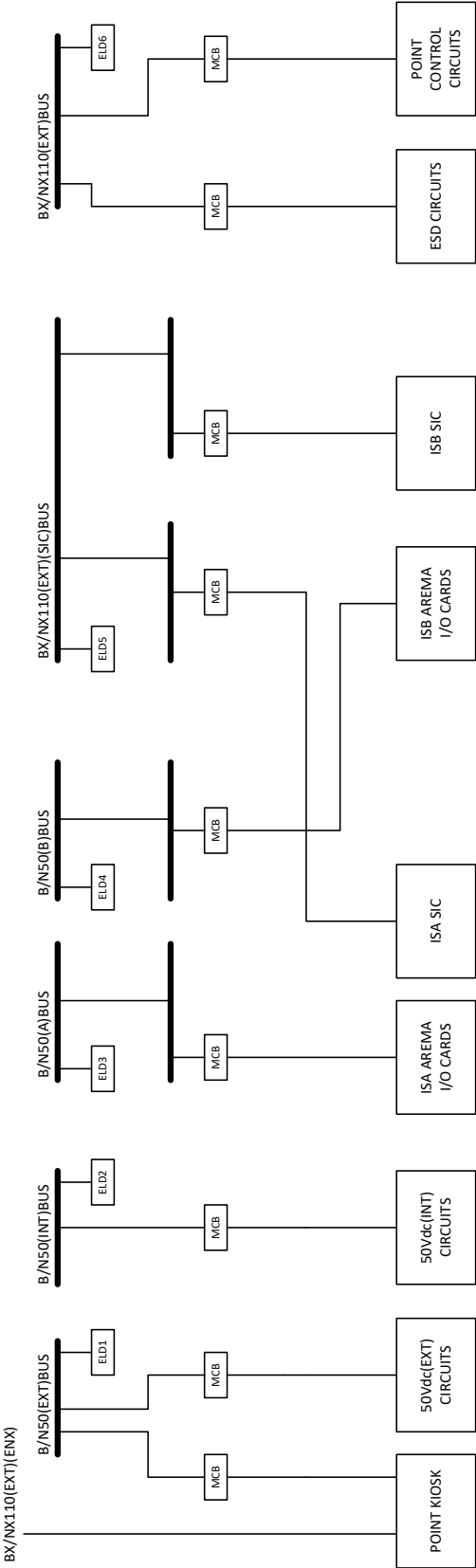
Fig.2.3 Site power supply bus layout (adapted from sheet SCH1[4])

3 LITERATURE REVIEW

The safety critical functionality of the point machine in railway engineering has led to a considerable amount of research being carried out into their safe and reliable operation. The maintenance of point machines has been a major focus of large sections of this research, making use of condition monitoring techniques and developments from other engineering disciplines, notably control engineering. A review of the existing literature has been carried out to investigate the approach taken by others; the questions they have posed and the solutions they have proposed to answer these questions. The work carried out by others provides the basis for any further study into the topic.

Goodall and Roberts [5, p.90] noted that, "There is a variety of benefits that arise from the use of advanced monitoring techniques, all of which contribute to meeting key business drivers for today's railway systems". Although this was several years ago it is still very much the case, albeit that the monitoring techniques and data processing have progressed over the interim period. They make the point on the attributes that the use of monitoring in predicting or detecting critical failures can contribute to system safety. The suggestion is made in [5, p.90] that "Condition monitoring can either be used to enhance safety, or to make the current level of safety more affordable".

Definitions are introduced in [5, p.90] that provide a distinction between fault detection (FD) and fault detection and identification (FDI). These definitions have previously been well developed in the field of control engineering. Within [5] it is stated that "Fault detection only detects that there is a fault, whereas adding identification also attempts to specify what the fault is".

Possibilities for condition monitoring systems and a range of techniques appropriate to applications are discussed. In [5] they make a clear distinction between the control engineering approach to condition monitoring, where system inputs are compares to the outputs, which are known as quantitative process models; and quantitative signal models where only the output is available. This approach assumes that that changes in the signals may be related to faults in the process, actuators or sensors, which can be equated to control and detection subsystems in the case of point machines. Then there is the computational approach, which is problem specific, where real time data is analysed using time- and/or frequency-domain signal processing. These methods are known as signal

analysis and feature detection, and can be considered particularly relevant to the analysis of sensor signals representing measurement of current and vibration.

Maintenance data provided from various sources over a period of time is collected and used to interpret the condition of the point machine in relation to its continued operation in a safe and reliable manner. This is in effect determining the maintenance requirements for the point machine [5].

Asada and Roberts [6] attempt identification and categorisation of faults that can occur to point machines. They use the expected typical fault categorisation to develop tests to identify the fault. They introduce an approach to fault detection for electric point machines based on measuring the current drawn by the point machine motor during its operation, the voltage across the supply, power derived from voltage and current, and the drive force exerted on the mechanical drive rod. A key point that they make is that many condition monitoring systems in use at the time of their study generate alarms close to a failure or after a failure occurs; further that most condition monitoring provides warning of abnormal behaviour but not to a level that would enable specifically targeted intervention by maintenance personnel. They state in [6, p.322] that "A condition monitoring system for point machines which generates an alarm in the early stages of the development of the fault and also diagnoses faults correctly is therefore desired".

Asada and Roberts [6] carried out testing on a set of UK DC point machines at an infrastructure training facility. They measured five fault conditions over one hundred and forty two point operations. As described in [6] the force plot from the load pin provided clear distinction between fault and fault free conditions, however the use of a load pin on the operational railway was discounted as it could introduce additional failure modes to the drive assembly. The use of current and voltage sensors located at trackside was considered non-intrusive and the use of the data sets to distinguish fault modes was pursued in [6].

Asada and Roberts in [6] found that the data obtained from the current and voltage sensors could not be used directly due to problems in handling the amount of data and fluctuations in power supply. To find a solution that enabled the use of the current, voltage and power, data feature extraction methods were explored, in particular using wavelet transforms and support vector machines. One of the simplest types of wavelet is the Haar wavelet and this was used within the paper. As described within [6], cluster analysis was used to mine the data to test for

parameters that give a clear distinction between different fault conditions. The outcome was that the current "…has more useful information in terms of condition monitoring than the power." [6, p.328]. Cluster analysis as a data mining technique as described in Han [7] is used to "…evaluate the appropriateness of parameters (electrical current, electrical voltage and electrical power) for condition monitoring."[6, p.326]. Clear visible distinction between fault conditions is the aim. Classification of the patterns for fault recognition is carried out by using an extension of a support vector machine (SVM) known as a classification support vector machine (C-SVM). An explanation of the theory of SVM is detailed in Bishop [8]. It is demonstrated within [6] that the approach adopted accurately classifies fault conditions and can differentiate the level of severity of the fault using C-SVM as a classifier.

Asada et al. [9] use the same techniques as in [6] to provide condition monitoring to an a.c. points machine rather than a d.c point machine as in [6]. Hall effect current transducer and voltage transducer were used to collect data in both studies, as was a load pin inserted in the drive rod linkage to provide drive force data. Parameter selection and feature extraction were approached in the same manner with the same conclusion that the methods employed provided accurate classification of differing fault conditions.

Hao et al. [10] presents a generic approach to fault detection and diagnosis for a particular type of railway asset with common dynamic characteristics. These assets are known as Single Throw Mechanical Equipment (STME), examples of which are point machines and train stops. One type of point machine discussed is the electro-pneumatic 4-foot design, as used in the London Underground environment, which is to be the focus of the discussion in this thesis. The displacement profile for a typical STME is introduced with a plot of displacement against time.

The methodology used to apply fault detection and diagnosis to an STME is based on a generic model for the class of equipment. The aim of their paper [10] is to present a classification of assets with similar features into groups for development of a generic fault detection and diagnosis (FDD) method based on the common characteristics of the assets.

The discussion in [10] covers several assets, and test beds were set up for each type of asset. Several parameters were then measured for each asset. The

parameters measured for the electro-pneumatic point machine were displacement, airflow and air pressure. The operation of the point machine is described as simple, but the design is complex due to safety and reliability requirements. Precise physical modelling is considered as often not achievable. Hao et al. [10] approach the problem by defining the system in terms of "input, machine and output, with dependant relationships". An attempt was made to produce a device to simulate the loading on point switch rails during the throw operation, however it was considered too simplistic to represent the actual point operation with any degree of realism.

The FDD method developed in [10] considers the power supply as the input. If out of its normal range it is reported as a power failure. Displacement prediction versus time for operation or throw of the device is estimated from comparison of power input and measured output. This was carried out by using Radial Basis Function neural network theory. The conclusion of the study is that further work is required to develop "…the relationship between output displacement and machine parameters…"[10, p.7] The study sets out a basic framework, however within [10] at the stage of development of the framework there is not a detailed discussion of the sensors and data collection that will need to be deployed.

A review into condition monitoring and point detection was provided by Marquez et al. [11] that pulled together the primary concepts that had been studied up to that point. They remind people of the consequences of failures in railway infrastructure by referring to the Potters Bar derailment [12] and the Grayrigg disaster [13] just a few years later. They point out in [11, p.35] " More recent research using data collected from line-side equipment and lab-based test rigs, though, is suggesting that it should indeed be possible to predict failures with sufficient accuracy and notice to be of genuine use to infrastructure maintainers and owners." A number of key statements are made in their conclusions. These include the communication of the fault information obtained to the relevant operational and maintenance staff; and communicating the criticality of the fault in regard to the immediacy in actioning the required maintenance procedures. In some cases, this can obviously mean immediate cessation of traffic operations in the area until the fault is rectified.

The works referenced so far are concentrated on the measurement and feature extraction of certain parameters obtained during operation of the equipment. There

have been other approaches to condition monitoring of point switches. Zwanenburg [14] makes use of the databases of the Swiss Federal Railway to carry out statistical analysis of railway switches and crossings. The method looks at how "The expected lifetimes are attributed to different parameters which influence the speed of geometrical degradation or wear of the material, e.g. total train loads (expressed in cumulative tonnage), axle loads, train type, the quality of the foundation." [14, p.765]. The aim is to produce a model to predict the "…maintenance and renewal needs of switches and crossings." [14, p.765]. Asset databases are used to compare the actual lifetime maintenance tasks with those predicted by the model. The conclusions drawn indicate that there are a number of further parameters that need to be built into the model to give more information on changes in equipment usage, and that weighting of parameters changes throughout the lifetime of the equipment. The modelling presented in [14] would be of use in verifying the advantages or otherwise of other condition monitoring approaches.

A not dissimilar approach is taken by Rama and Andrews [15], although in this work the authors stress the need to have "…the ability to predict problems at component level is needed" [15, p.344]. They use collected field data to derive lifetime failure distributions. The aim is to use the analysis to predict required maintenance activities, including costs of replacement components over specific time periods.

Within [15] the authors discuss modelling carried out in studies by Markine et al. [16], Johansson et al. [17], and Xiao et al. [18] on "…predicting degradation mechanisms and failures of a single element of an S&C unit, i.e. either points operating equipment (POE) or track."[15, p.345].

In [16] the authors discuss the effects of rolling contact fatigue (RCF) causing damage to the crossing nose, this being the discontinuity of the rails to allow the train to pass over points and crossings. Finite element models are developed to predict the failure behaviour to be expected at the point crossing nose. In [16, p.166] "…the relationship between the elastic properties of the turnout substructure and the RCF damage on the crossing points has been investigated."; this study provides an insight into the damage mechanisms of points and crossings. Similar methods are employed to simulate and model the stresses and

resultant deformation of specific rail assemblies experienced by switches and crossovers in Johansson et. al. [17] and Xiao et. al.[18].

Rama and Andrews [15] use the Network Rail (NR) Fault Management System (FMS) database as a source of information on failures. The data is filtered according to switch and crossing subsystem and probability plots for each subsystem are produced. The output from the study "…was to obtain life-time distributions of individual S&C components based on their historical failure data…" [15, p.362]. Salient points from the study conclusions included the observation that larger data samples, attention to different types of equipment carrying out the same functionality, and switch utilisation rates through the observation periods should all be explored in more detail in further studies.

The effort of the research by Jin et al. [19, p.1] is "…the development of the statistical and pattern recognition tools for point machine health monitoring." Towards this aim they constructed an extensive test bed comprising of an electro-mechanical point machine, together with sensors, data collection and data analysis capabilities. The test bed was placed in a climate chamber as temperature was identified as an important variable affecting measured performance. Failure modes were identified, and simulated faults introduced to the test rig. As in previous studies the current and power signals were measured over the period of point moves. In the particular point machine under test, there are built in sensors in the wayside point machine. The information from these sensors is normally taken back to the control room as part of the design and installation phase in "real world" applications. As the aim of the study is to develop tools for field applications then the presence of a sensor and data collection system in already installed equipment makes implementation an attractive proposition for railway asset managers. Plus, they are non-intrusive, therefore no introduced effect on system safety. The diagnosis of the data in [19] compared using SOM-MQE (Self-Organising Map, Minimum Quantisation Error) and PCA (Principal Component Analysis) to "…detect the degradation modes and evaluate its severity levels." [19, p.10]. The study even introduced a re-configurable HMI (Human Machine Interface) platform with a view to future develops in field trials over an extended period. Further reading on SOM-MQE and PCA and their applications can be found in Yin [20]. Similarly, Yu and Xi "…analyse the performance of the MQE chart under the assumption that predictable abnormal patterns are not available." [21, p.5907]. The analysis and findings within [21] would be advantageous for identifying abnormal

patterns that could not be predicted from domain knowledge provided by maintenance staff based on their prior experiences of faults.

The ageing effect is investigated by Sa et al. [22] in an effort to define a criteria for replacement of railway point machines (RPM); the study pursues the ageing effect approach rather than fault diagnosis, fault diagnosis having been the focal point of a number of previous research studies. In [22] they analyse the electrical current drawn by the electric point motor during point movements. They collected "…both before and after-replacement data obtained from the RPM monitoring system…" [22, p.2]. The before- replacement data is labelled into two classes; these being, does not need to be replaced, and needs to be replaced. An off-line training phase is then implemented where "…features minimising the within-class distance and maximising the between class distance are extracted…" [22, p.2]. The shape obtained by each RPM movement is then subject to analysis with the extracted features in an online testing phase. This then is used to detect a replacement condition for the RPM. The shape of the current waveform is analysed using a time series shapelet algorithm to minimise the within class distance and maximise the between class distance. The study made use of ten years of in-field replacement data to provide the offline training data which was available from the maintainer. The results indicate distinct advantages over Dynamic Time Warping (DTW) methods to detect subtle difference to enable RPM replacement decisions by the maintainer.

In Sa et.al [23] a similar approach to condition monitoring of EPMs is taken to that presented by Sa et al. in [22]; that is, "…to developing a strategy that facilitates their replacement at an appropriate time." [23, p.1]. Once again, the data is obtained from a current sensor unit monitoring the current waveform during EPM movement operations. The point machines are labelled Electric Point Machine (EPM) in [23], rather that Railway Point Machine (RPM) as in [22]; they are the same unit as both are electrically driven point machines and the data is obtained from the same maintainer source.

In [23] the approach differs in that only the "after-replacement" EPM data is trained offline. This is carried out using support vector data description (SVDD) methods.

This is stated in [23, p.2] as,

> "Then, only the after-replacement data among all of the labelled
> current signals is trained through SVDD to produce a hypersphere for

classifying the aging effect regarding the EPMs. Using the hypersphere, the before-replacement data can be classified as to whether the data is aging. Finally, the results from this method are directed (as an alarm) to a maintenance staff to consider the aging effect of the EPMs.".

The authors come to the conclusion that using the one-classification SVDD method of data analysis, gives improved accuracy over the two-classification methods that include shapelet and SVM analysis as in their previous study in [22].

Atamuradov et al. [24] assess degradation level assessment by collecting data on the force on an electric point machine actuator rod. This is done by means of a force sensor inserted in the rod linkage. The study is focused on the degradation experienced by the sliding chair plates of the point; the sliding chair plates are that part of the point machine structure that supports the switch rails. The switch rails are the moving parts of the rails that enable the change of direction of the route that a train can take. Contamination was introduced to various sets of sliding chair plates to simulate wear due to ageing. The level of degradation was performed using a k-means algorithm, this identified predicted lifetimes of the point machines based on the machine learning from the key health indicators (HI) obtained in the analysis.

An interesting approach is taken in Hamadache et al. [25] where a model based FDD approach is undertaken. An electric point switch machine is modelled in MATLAB/SIMULINK; the model is based on a conventional switch layout that is used in many proprietary designs. The study has the advantage that the number of sensors gathering data can be increased to look at assessing the sensitivity of the signals obtained and their usefulness in fault detection and diagnosis. This has resulted in the model looking at "… an assessment of several signals, including the motor speed signal, the motor stator current signal, the force signal, and the linear position of the switch rails (i.e., the switch toe position)…" [25, p.1229]. They further state that "Four faulty scenarios (i.e. motor fault, total system overloaded fault, switch blade changes fault due to spring force stiffness changes, and excessive friction or resistance fault) can be considered…" [25, p.1231]. The output of the model under fault conditions was compared to that for the five introduced fault conditions and the residuals between the signals. This was a simple accumulated error between no-fault and fault condition. The modelling

approach employed seems a practical way to explore various fault conditions and the value of using sensor outputs to provide accurate FDD. The work intends to move on to a point machine test bed at the Birmingham Centre for Railway Research and Education (BCRRE). Although the number, type, cost, complexity and deployment of sensors will always make it desirable to limit the number of sensors, this approach does allow for investigation of the sensors most suitable to produce the required data.

The research carried out to date on condition monitoring of railway switches and crossovers use a number of approaches. The data sets use are either obtained from sensors for direct analysis, statistical analysis of the expected usage and operational environment of the equipment, or component level modelling to predict lifetime failure rates for components and mechanisms. In the case of the latter two methods the approach is to predict the optimal replacement time for points equipment. The former method focusses on fault detection and fault detection and diagnosis.

The parameters measured by the sensors include the current drawn by a motor, voltage across the supply to motor, and derived power for electric point machines. Electro-pneumatic point machine sensors include air flow and air pressure to cause displacement of the point tips . The use of load sensors fitted to drive rods has also been used in test rig applications but discounted for practical deployment due to the intrusive nature of changing mechanical parts to provide load sensing.

The data from the sensors is subjected to feature analysis and feature detection by various methods, the authors explore the best means of providing distinction between fault identification and classification of faults. The methods used include wavelet transforms, support vector machines and cluster analysis. These analysis methods are required as the raw data obtained from sensors is subject to power fluctuations that mean simple level or shape comparisons do not provide the appropriate level of feature extraction.

The various approaches to condition monitoring of points equipment have found that it is possible to collect and classify the data to enable decisions on maintenance strategies to be made.

The studies that measure current use the current drawn by the motor in moving the points in electric point types. The equivalent measurement for pneumatic point

types is the air pressure that moves the points. In both cases the effects of faults or lifetime degradation of the equipment on the parameters measured is analysed.

This project will look at using the detection current of the point machines to monitor performance of the point apparatus rather than the parameters relate to drive force. It will also look at means of measuring the acceleration forces on the point tips to provide condition monitoring data.

4   THEORY

There are four main types of powered point machines used on underground rail systems in the UK. There are three electro-pneumatic types and one electric type. Electric driven points use an electric motor to drive the points to the required position, electro-pneumatic points use solenoids to actuate valves to turn air on and off to pneumatic cylinders that drive the point to the required position. Note that the terms point, and switch are interchangeable when referring to the apparatus for changing routes on rail systems.

The two areas of measurement are the point detection current and the acceleration forces acting on the point blades during both the movement of the points and when a train transits the points. The point call function is crucial to the system operation and is subject to a high frequency of maintenance in order to maintain the safe operation of the railway. The point machine under consideration is a four foot electric-pneumatic type but the principles and techniques involved can be applied all or in part to the other types of point machines.

4.1   FOUR FOOT POINT APPARATUS

The generic railway point layout used for mainline underground railway systems is shown in Fig. 4.1. The parts of the points that move are the Point(Switch) blades between the toe and the heel, they move when commanded to allow a train to take whichever of the two routes available is required by central control.
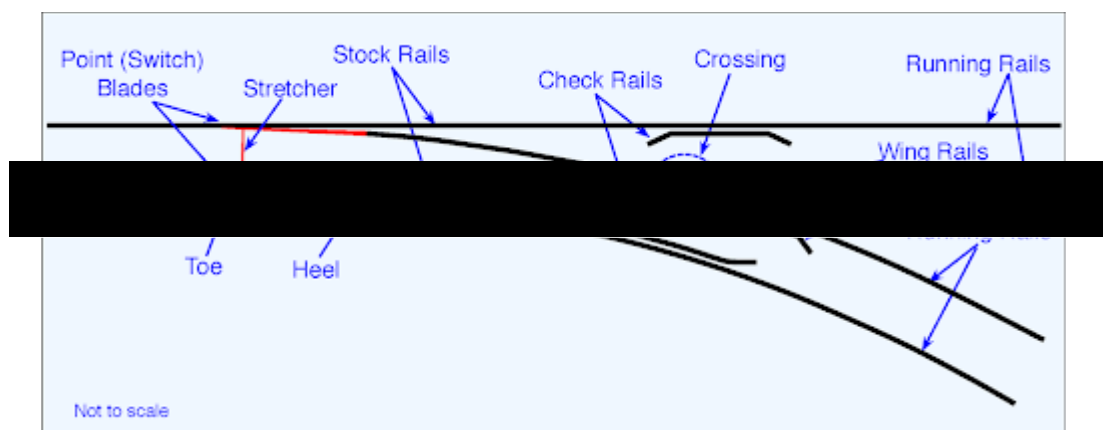
Fig. 4.1 Generic railway point layout [26]

The stretcher is the tie bar that links the two point blades together to maintain the distance between them. This ensures that when one point blade is against its stock rail the other is clear of its stock rail with a sufficient gap to allow the flange wheel

of a train traversing the point to pass cleanly. The check rails, crossing area and wing rails are there to assist in guiding the train wheels through the points

4.1.1 POINT STRETCHER BAR ASSEMBLY DETAIL

The installation and setting up of the points is described in the LU Signals training unit [27] . The key components and their function are now described with enough detail to provide a framework for the discussion on sensor applications. The arrangement for stretcher bar installation is shown in Fig. 4.2; consisting of front and back stretcher bars.
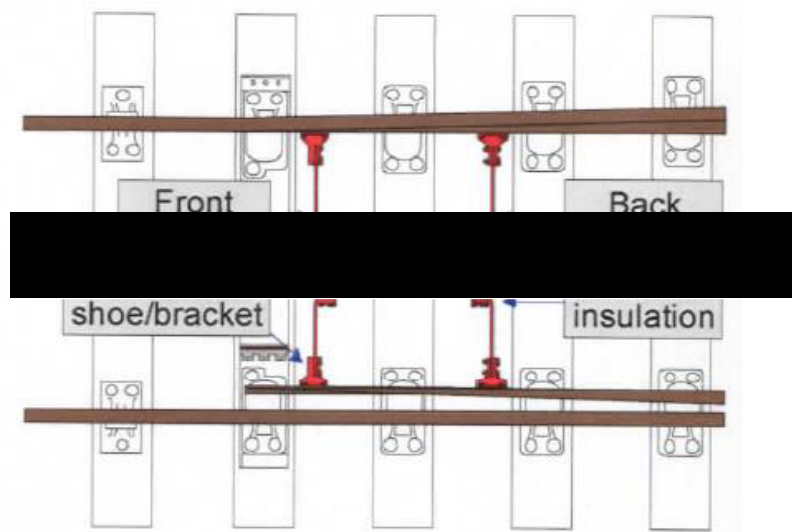
Fig. 4.2 Stretcher bar assembly [27, p.5]

The stretcher bars fitted to the majority of points on the LU system are made from 65mm x10mm flat spring steel, they incorporate an insulation joint, the purpose of the joint is to provide electrical isolation between the running rails. This is needed to allow the use of signalling track circuits that prove occupancy or otherwise of sections of track. The train is detected by the wheel axle effectively shorting out the track circuit, hence the need for the stretcher insulation.

The stretcher bars are supplied to the track maintenance staff with one end pre-drilled to be bolted to the point tip on the pre-drilled end as illustrated in Fig. 4.3. The other end is drilled by the maintenance staff using guides and specialist drilling equipment. The stretcher bar is constructed such that it sits below the level of the sleepers that form the base for the fixed track sections of the point apparatus. When installing point assemble the front stretcher bar is fitted first to enable setting up the flangeway gap. The gap being the distance between the open switch blade and the running rail with the closed switch blade hard against the running rail. The

flange way gap should be 105 mm at a distance of 127 mm from the tip of the point blade according to the LU standard for maintenance of points [28].

Fig. 4.3 Front stretcher in position [27, p.5]

Prior to drilling the blank end, packing shims are added between the stretcher plate shoes and the switch rail. This allows for adjustment of the flange gap if it is not correct after drilling. The back stretcher is drilled and fitted in a similar manner with a check being made again of the flange way gap at a distance of 127 mm from the tip of the point blade and this time checking that here is a minimum gap of 50 mm at the end of the planed length of the point blade. The planed end being the place on the point blade where the machining of the point blade to make it lay flat against the stock rail finishes.

4.1.2   FOUNDATION PLATE AND POINT DRIVE ASSEMBLY

The foundation plate provides the mounting for the remainder of the point assembly, it is mounted on the railway sleepers and the stretcher bars run underneath it.
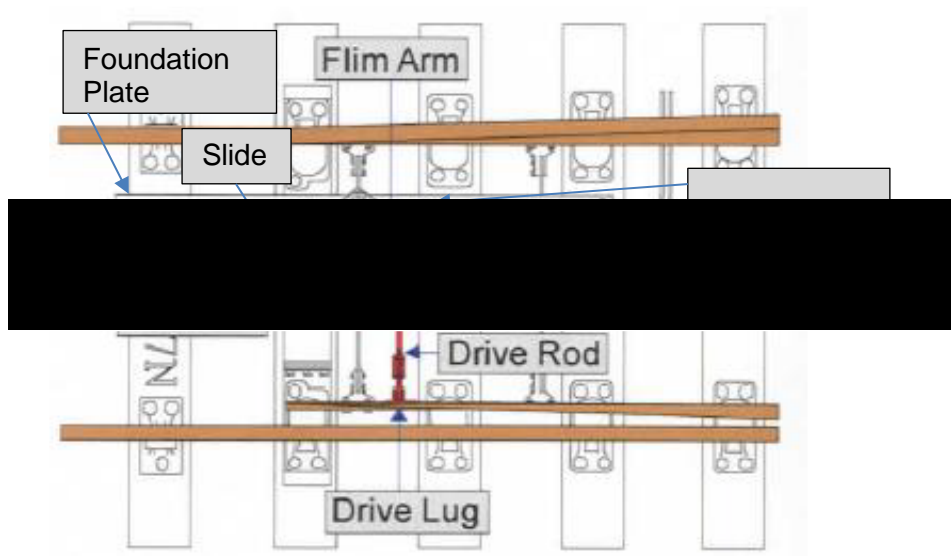
Fig. 4.4 Foundation plate and point drive assembly [27, p.33]

The point motor is a double acting pneumatic cylinder that is mounted on the foundation plate and connected to the point escarpment. The escarpment, including the butterfly crank and flim arm provides for the backwards and forwards movement of the slide in the direction of the red arrow in Fig. 4.4 to be translated to a lateral movement. The flim arm also provides fine adjustment of the distance the point is driven. The drive rod is connected to the point blade in order to move the point blades. Note that the drive function for the point is only provided to one point blade. The other point blade is driven via the front and back stretcher bars.

4.1.3   FACING POINT LOCK ASSEMBLY (FPL)

When a train approaches the point where the route diverges, that is travelling from left to right in Fig. 4.5 it is known as a facing move. This is when the travel direction of the train is facing the open point blade.
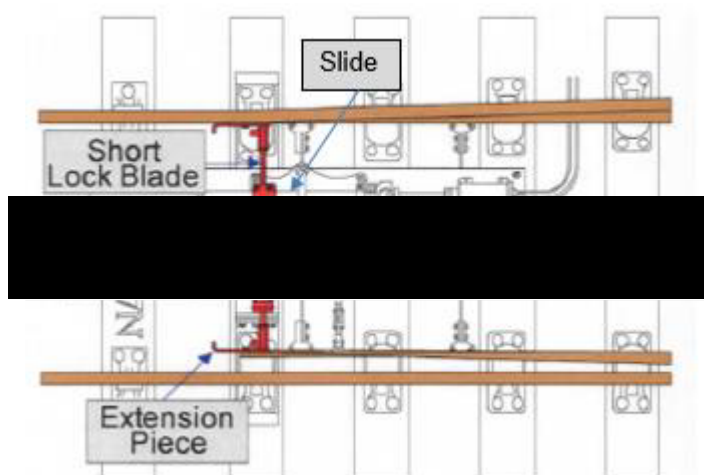
Fig. 4.5 Facing point lock assembly [27, p.39]

Four foot points that have this facing route are required to have a facing point lock as stated in LU Signalling Functional Requirements Section 3.6.3.1.1 [2] "All facing points in signalled routes shall be equipped with a facing point lock that locks the open and closed switches in position.", and Section 3.6.3.1.2 goes on to say that "The facing point lock when engaged shall prevent the closed switch from opening by more than 1.6 mm."

The point lock blades interact with the slide to mechanically lock the closed switch blade in position to meet the requirement to prevent the closed switch opening more than the permitted 1.6 mm. The slide has a top and bottom dab attached to it that engage with slots in the lock blades. The lock blades act as a third stretcher

bar, only they do not form a continuous bar. They are formed of two separate bars in order to allow for expansion and contraction of the point structure with temperature changes, and still meet the requirement to prevent the closed switch from opening by more than 1.6 mm. A single piece construction would be prone to jamming under changes to the point structure caused by temperature changes or changes to the set up tolerances that still fall within the limits for safe operation. There are two lock blades, one connected to the nearest switch blade, known as the short lock, and one connected to the furthest switch blade, known as the long lock. The arrangement for the blades interacting with the top dab is shown in Fig. 4.6 for the case where there is no damage to stretcher bars and the facing point lock is set up correctly.

The top dab engages with the ports on the tops of the lock bars, these ports relate to the case where the right hand switch blade is closed against the stock rail. The bottom dab, that is not illustrated, engages with the ports on the bottoms of the lock bars, these ports relate to the case where the left hand switch blade is closed against the stock rail.
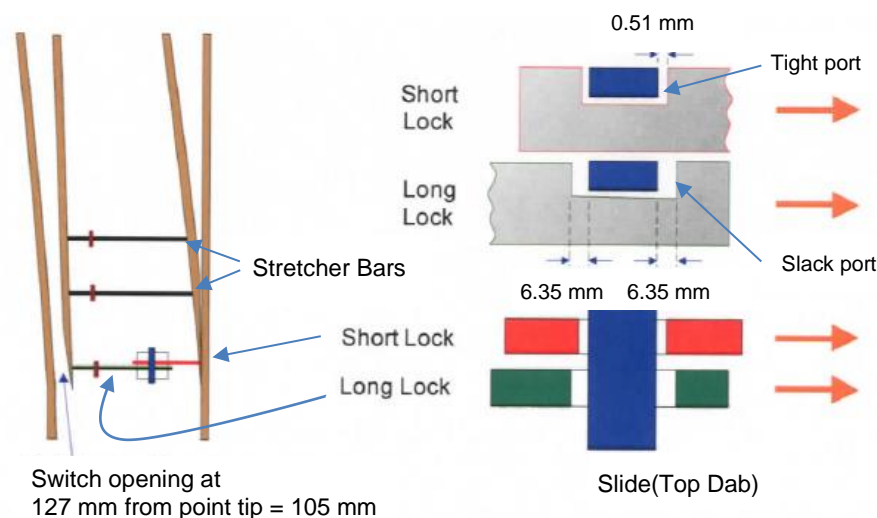
Fig. 4.6 Facing point lock engaged with all stretcher bars intact (adapted from [27, p.43])

The width of the tight port is 39.7 mm and the width of the top dab which is located on the slide is 38 mm. This is known as the tight port; it is set up by the maintainer clamping the point blade against the stock rail with a gap of 0.51 mm. The width of the slack port is 50.7 mm. The long lock is adjusted such that there is a gap of 6.35 mm either side of the top dab where it sits in the slack port. Although the slack port allows for 6.35 mm of movement, the stretcher bars are intact, and the switch

opening is fixed at 105 mm other than slight variation for temperature of within tolerance changes to the point structure.

When the stretch bars are broken or loose as in Fig. 4.7 then the open switch is held in place the engagement between the lock port and top dab. The switch opening can now close by up to 6.35 mm, leaving a gap of 98.65 mm. This is still open such that a train wheel flange can pass through safely.

Switch opening at
127 mm from point tip = 98.5 mm

Open switch held open by 50.7
mm lock port and top dab
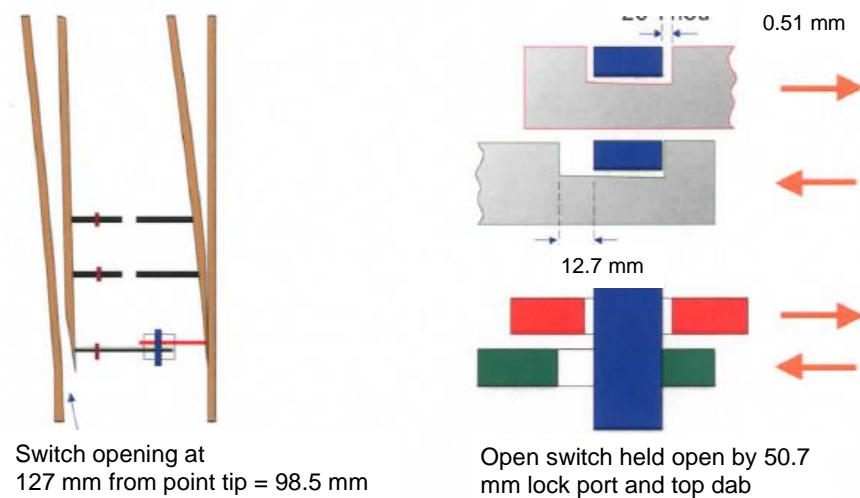
Fig. 4.7 Facing point lock with stretcher bars broken (adapted from [27, p.44])

If the stretcher bars are broken and the facing point lock is only engaged on the closed side as in Fig. 4.8 then the open side switch can close and there is no gap for the train wheel flange to pass through. This is an extremely dangerous position that would likely result in the derailment of an approaching train.

0.51 mm

If no open switch lock and DAB, then above condition would be dangerous

Switch closed
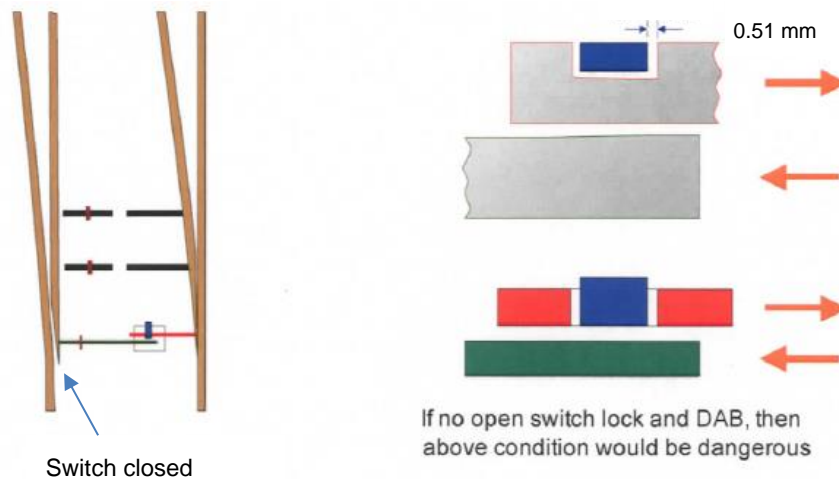
Fig. 4.8 Facing point lock with broken stretcher bars and open switch lock disengaged (adapted from [27, p.44])

The next section discusses the detection of points locked in their commanded position.

4.1.4   POINT LOCK AND DETECTION BOX (P&LD BOX)

The point lock and detection box is mounted further forward of the point tips as shown in Fig. 4.9. It is comprised of three cams and contact assemblies. A central cam interfaces with the slide bar and detects that the dabs described in the previous section have been mechanically engaged with the ports and the facing point lock has locked the point ends in their relative closed and open positions.
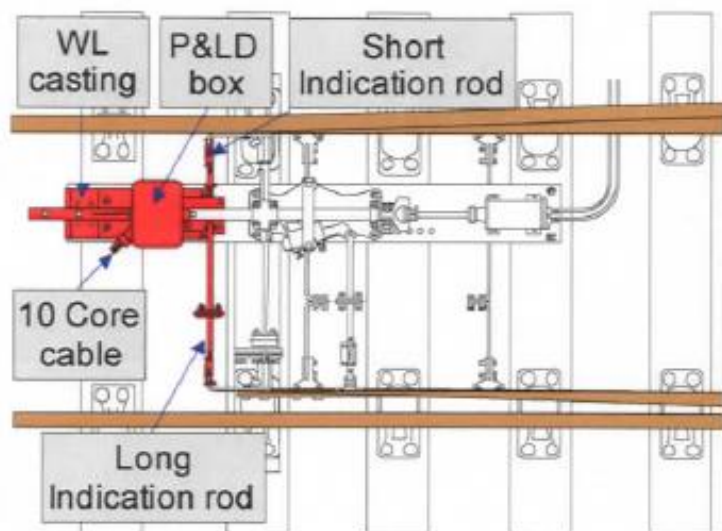
Fig. 4.9 Point and lock detection box assembly [27, p.51]

As the point tips move, they operate the long and short indication rods that are attached to the point tips. This movement is translated into radial movement of the

cams within the P&LD box, which makes and breaks the point detection contacts in conjunction with the central cam. In this way the detection box not only confirms the position of the point tips but also that the FPL is in a locked position.

4.1.5   GROUND LOCK ASSEMBLY (WL)

A secondary lock known as a groundlock is fitted to four foot points when they are used for facing moves with passengers on the train. They are mounted in position as shown in Fig. 4.10 at the end of the slide bar assembly. They are used to keep the points in the last commanded position in case of the air supply being lost and the points starting to creep away from the running rail. The vibration from the passage of a train may cause the points to move as the train is passing over, resulting in a derailment. The ground lock is disengaged from its slot in the slide by energising a solenoid valve, once de-energised it sits on the slide until it again re-aligns with either of the slots depending on which way the point has thrown.
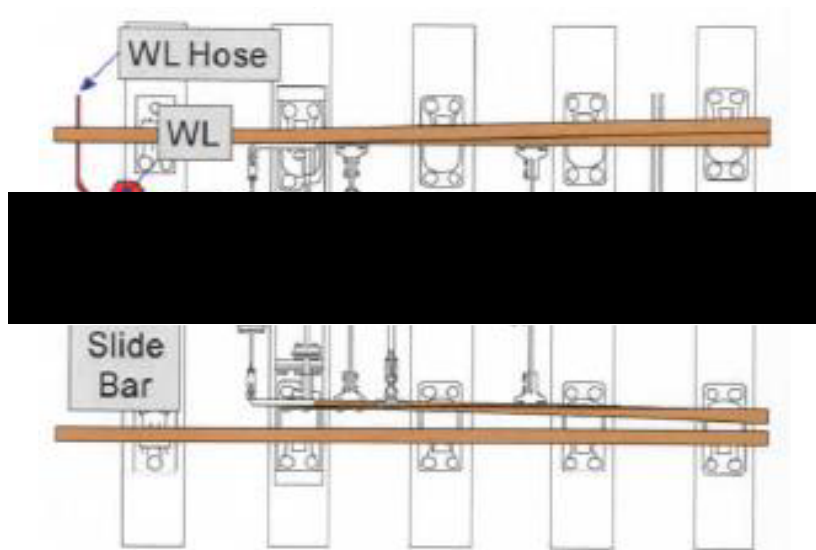
Fig. 4.10 Ground lock assembly [27, p.63]

There is also a set of contacts within the ground lock enclosure that detects whether the groundlock is engaged or disengaged with the slot in the slide bar.

The detection of the groundlock forms part of the point detection circuit and proves the engagement or otherwise of the groundlock. If the groundlock is not engaged and locking the movement of the slide and therefore the points, then the points is not detected locked in the commanded position and the signalling system will not route a train over the points.

4.2   POINT OPERATION

A point move is called by the system to set the desired route. The sequence of events that constitute a point move and the actions that occur during the process are described in the following sections.

This type of point machine has the feature that the point switch blade is continuously driven to the last commanded position. This is to ensure that in the event of a failure of certain components then the potential energy stored in the point system does not lead to an unsafe condition.

In order to move the point, the groundlock valve is energised to release the point lock then the point is driven to the new position and locked in the new position. In railway parlance the point direction is normal or reverse and these correspond to the normal route or the reverse route.

Point control involves energising combinations of three components for a certain amount of time; the action of moving a point may require a number of attempts; this can be due to obstructions such as track ballast or other debris causing the switch blade to not close to the fixed rail, or maybe indicative of components starting to move out of adjustment.

Detection of the point position involves sending a feed out through detection contacts in the point machine P&LD box; in a successful point move, depending on the lie of the points and the points being locked, the feed energises one of two inputs to the sub-system control card, one set for normal and one set for reverse.

4.2.1   POINT CONTROL

The specific point type under consideration for the purposes of this discussion is a four foot electro-pneumatic, as illustrated in and described previously in Section 4.1.
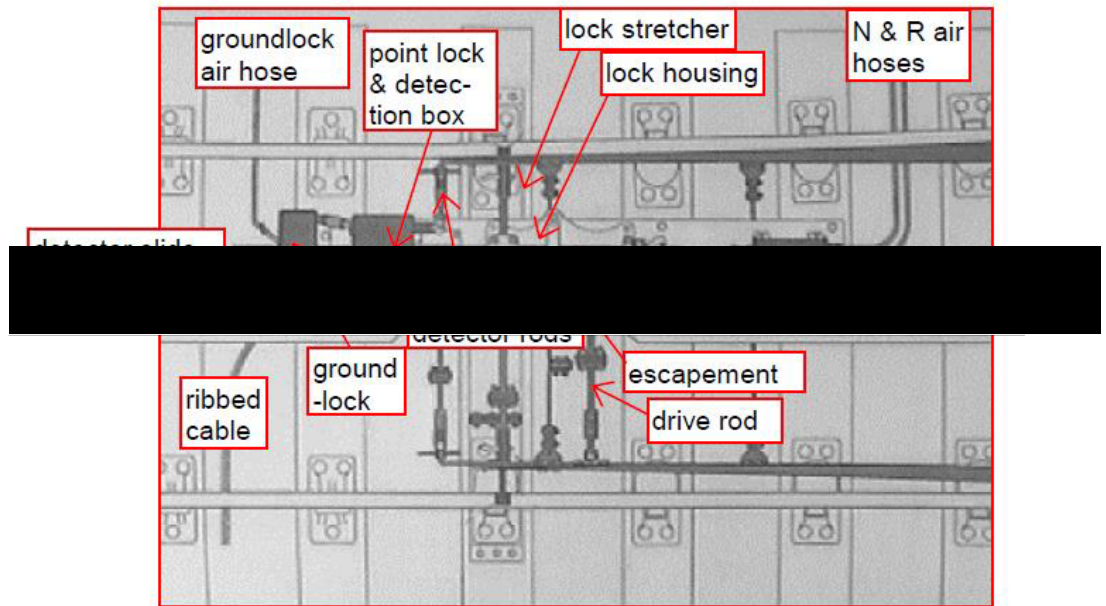
Fig.4.11 Four foot points arrangement [29, p.40]

The complete point apparatus arrangement is illustrated in Fig.4.11, which is taken from the Signalling Design Handbook [29]. The point selection and control circuit diagram is illustrated in Fig. 4.12. They are adapted from typical circuit configurations found in [4]. The acronyms used in the circuit diagram are derived from the elementary signals training document [30], and are known as the signalling alphabet.

The specific acronyms and symbols used in Fig. 4.12 are described in Table 4.1. The set of points is assumed to be locked and detected in the normal position at the start of this description of a point move.

Due to the active/active design of the system the relays P1 WMR, P1 WNR, and P1 WRR are fed from both Input/Output Card A and Input/Output Card B at the same time when the system calls for them to be energised. The relay type used has two coils wound on the same armature and is designed for use in active/active systems.

Sensors and Methods for Railway Signalling Equipment Monitoring

Table 4.1 Point Circuit Acronyms and Symbols

Circuit Acronyms and Symbols	
P1	Point number designation
WMR	Point Move Relay
WNR	Point Normal Relay
WRR	Point Reverse Relay
NLR	Normal Latch Relay
RLR	Reverse Latch Relay
AN	Detection Normal Contact (contact closed when point detected and locked in normal position)
BR	Detection Reverse Contact (made when point detected and locked reverse position)
NW	Normal Point Valve solenoid
RW	Reverse Point Valve solenoid
WL	Point Groundlock Valve solenoid
⌣—•	Front contact (normally open)
⌒—•	Back contact (normally closed)
⊏⊐	Relay coil or air valve
⬛▬•	Point normal contact (contact closed when point detected and locked normal)
•—⊢—•	Point reverse contact (contact closed when point detected and locked reverse)
⊏▲⊐	Latch Relay operate coil
⊏▼⊐	Latch Relay release coil

The initial condition and the sequence of events of the point selection and control circuit to move the points from normal to reverse is now described.

The initial condition is that point P1 is locked in NORMAL position; Latch relay P1 NLR is latched in the operate position, latch relay P1 RLR is latched in the release position. This results in P1 NW valve solenoid being energised as contacts P1 NLR A1:A2 and P1 NLR C1:C2 are closed, the point being driven to the normal position.
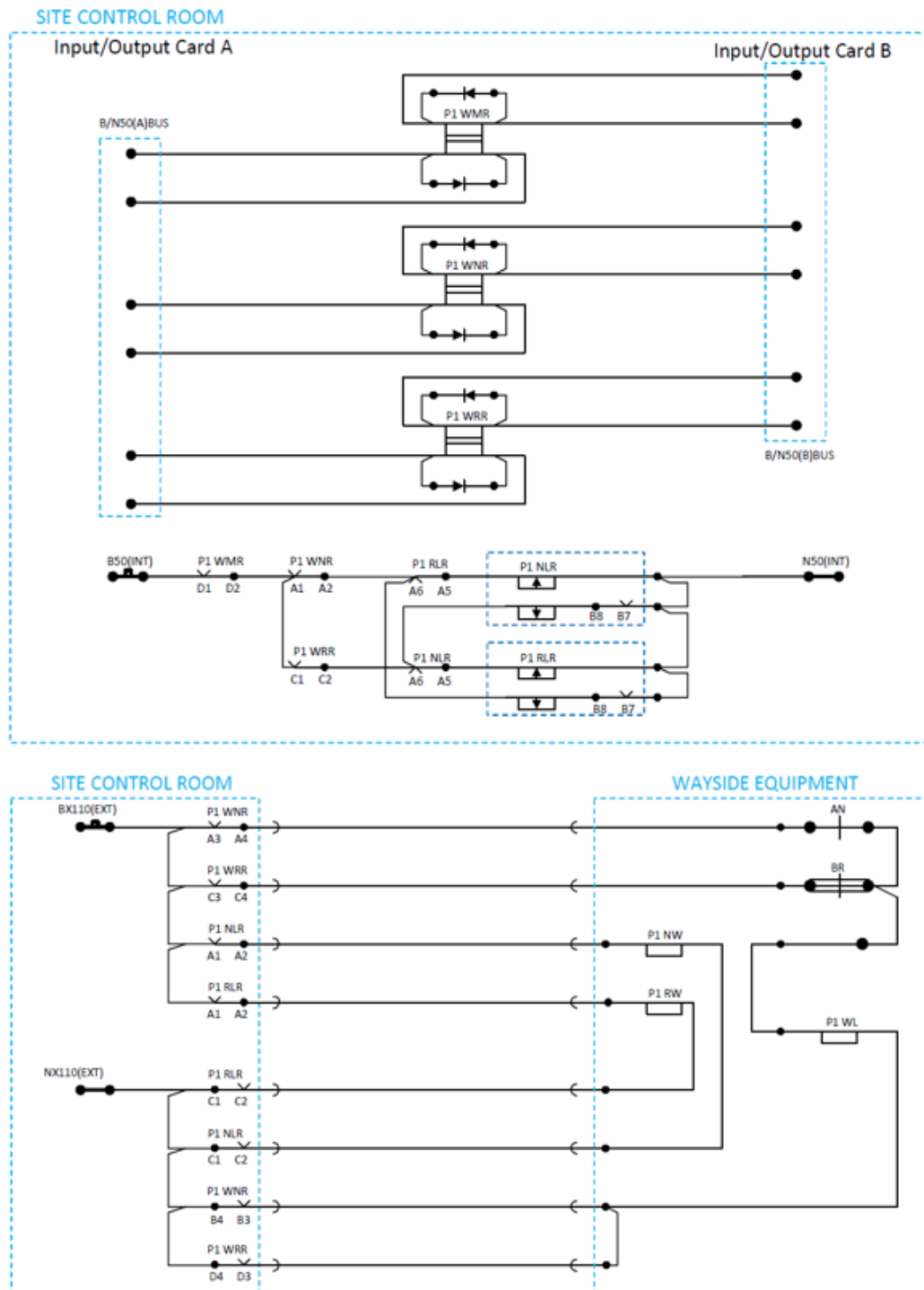
Fig. 4.12 Point selection and control circuit (adapted from [4]).

The point call to the reverse position is initiated by P1 WRR relay being energised. This results in contact P1 WRR C1:C2 in the point selection latch relay circuit closing, at this stage the latch relays do not change state as P1 WMR relay has not been energised. Contacts P1 WRR C3:C4 and P1 WRR D3:D4 are closed, this results in P1 WL solenoid valve being energised because the points being

locked in the normal position means that detection contact BR is in a closed state. This results in the groundlock being disengaged.

The system allows enough time for the groundlock to be disengaged before attempting to drive the point to the reverse position, for this type of points the time allowed is 700 milliseconds. The control voltages are illustrated in Fig. 4.13 that are output from the control cards to the primary point command relays point reverse relay(WRR), point normal relay(WNR) and point move relay(WMR) to achieve the point control sequence.
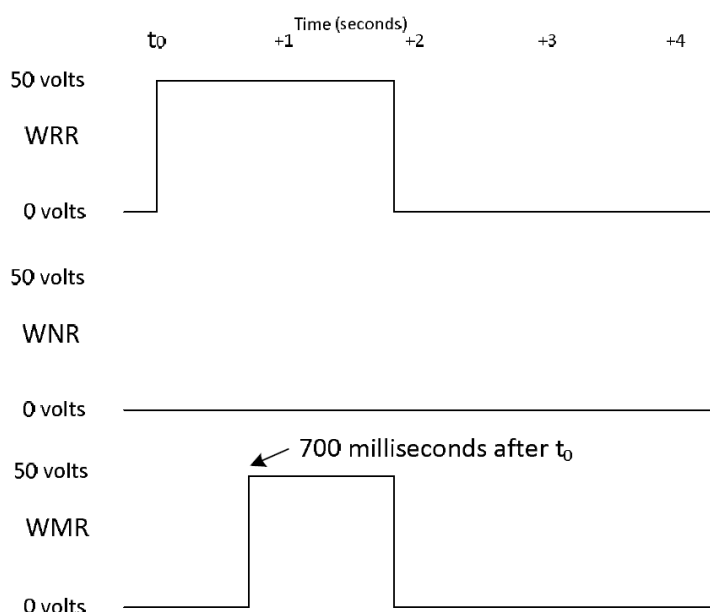
Fig. 4.13 Control voltages from I/O card [31]

After this period has elapsed P1 WMR relay is energised; in the latch relay circuit P1 WMR D1:D2 is closed, which results in P1 NLR release coil being energised causing P1 NLR A5:A6 contact to close resulting in P1 RLR operate relay energising. Also, when P1 NLR release coil is energised contacts P1 NLR A1:A2 and P1 NLR C1:C2 are opened and P1 NW valve solenoid is de-energised, removing the drive to the normal position. The latch relays are now in the latched reverse position. P1 RLR A1:A2 and P1 RLR C1:C2 contacts are closed resulting in P1 RW solenoid valve being energised and the point being driven to the reverse position. When the point moves away from the normal position the detection contact BR is broken and P1 WL solenoid valve is de-energised. The construction of the point slide bar is such that the groundlock drops onto the slide bar until the point has completed its move to the reverse position, then the ground lock drops

into a slot in the slide when it aligns with the reverse position. The point is now locked in the reverse position.

The description of operation goes into detail of how the points are controlled to provide aid in understanding the point move process. However, it is not proposed to measure control current; this is because the requirements detailed in [31] call for the primary point control relays to make use of contacts on the relays to provide status and check-back of the relay to the control card of the associated site controller. In the event of there being a disparity then the system halts the site controller until the fault that caused the disparity is rectified.

4.2.2   POINT DETECTION

The point detection circuit monitors and confirms the position and locking of a point machine. A typical point detection circuit is shown in Fig. 4.14 consisting of a feed from the site control room out to the point lock and detection box which is part of the point arrangement in Fig.4.11. The detection circuit is fed across contacts in the P&LD box and back to the detection inputs in the site control room.

Prior to the move to reverse being called by the system the points are locked in the normal position. Contact P1 WL is closed as the groundlock is engaged in its slot in the slide bar, contacts 1N and 2N are closed as the point is in the normal position providing normal detection input This completes the detection circuit and the points are detected locked in the normal position.

Referring to Fig. 4.12, at the start of a point move from a locked normal position to a locked reverse position, relay P1 WRR is energised, contacts P1 WRR C3:C4 and P1 WRR D3:D4 close. The points are in the normal position, contact BR is already closed therefore groundlock solenoid valve P1 WL is energised and the groundlock moves out of the slide. The effect on the detection circuit Fig. 4.14, is that P1 WL contact is opened as the point is no longer locked in position by the groundlock. As previously described in section 4.2.1 after a 700 milliseconds delay from the start of the point move when P1 WRR was energised then P1 WMR is energised and the point moves to the reverse position.
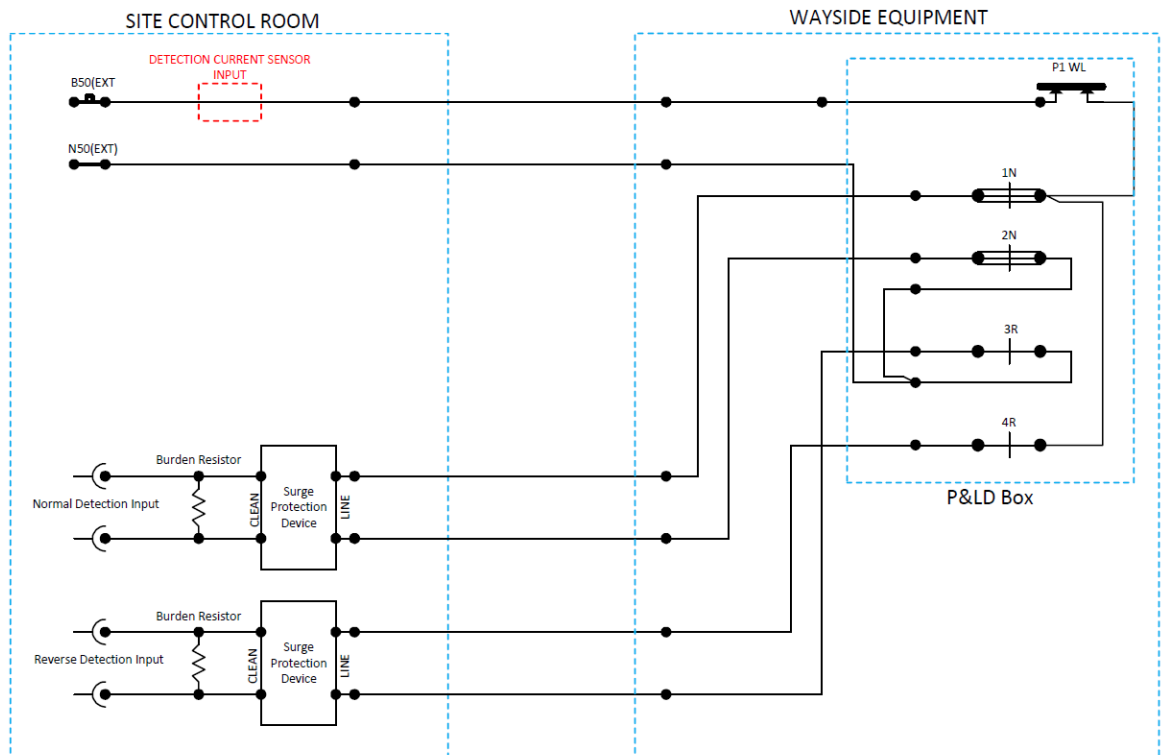
Fig. 4.14 Point detection circuit (adapted from [4])

The move is complete when the point moves fully to the reverse position and the groundlock drops into the slot in the slide bar. When the ground lock is fully engaged, contact P1 WL is closed and the reverse detection contacts 3R and 4R in the P&LD box are closed, providing reverse detection input. This completes the detection circuit and the points are detected locked in the reverse position.

However, if the point does not get detected in the commanded position within a certain time (15 seconds is a typical time [31]); then the sub-system controller drives the point end back to its original position and starts another point move attempt. Note that during this re-attempt at moving the point to the reverse position the groundlock feed is not removed, this is to allow the groundlock to remain energised during the remove attempt when it is in the normal position, this stops the groundlock from re-engaging in the slide bar. The effect on the detection circuit is that the detection input is low for the entirety of the point move, including any re-attempts. After two attempts if the point is not detected in the commanded position then the point move is cancelled, and the point is declared unmoveable at the system control level. The system controller can still set a route over the points if

the point is detected in the position prior to the move being called, but this obviously restricts the routes available to the controller.

The area of track in the vicinity of the points known as the "switch zone" is defined in the system design overview [32] as an area bounded by the toe of the point (see Fig. 4.1) and the fouling points of the branches at the other end the points. The fouling points are the place on the track that if a train were to pass this position then it could come into contact with a train on the other track that had passed the corresponding position on the other track.

The emergency brake on a train is a failsafe system that applies the brakes on a train at the highest braking rate to bring the train to a halt. The emergency brakes are applied when the system detects an unsafe condition as defined in [32].

Once a train enters the point zone then it is considered to present more a risk of derailment if a train has its emergency brakes applied than if it runs at line speed through the points. This is because the distribution of dynamic loads present when a train emergency brakes make it more likely than a derailment would occur under heavy braking.

4.3   DETECTION CURRENT

The monitoring of detection current can be used to determine performance data during point movement operations and during the passage of a train. The system does not permit both of these events to happen at the same time; the movement of the points and the passage of a train occurring at the same time is a highly undesirable event that introduces a high risk of derailment.

The current flowing in the detection circuit from the supply is determined by the supply voltage, the load at the inputs to the detection inputs and the electrical properties of the cable used to implement the circuit design.

The nominal detection supply voltage is 50 volts DC and the load at each of the normal and reverse inputs is 2 kΩ which is the value of the burden resistor across the detection inputs; these values are to meet the requirements [33] for the site controller subsystem to operate as intended. The supply voltage within a control room can vary according to LU standard [33] by +10% and - 20%, giving a maximum voltage of 55 volts DC and a minimum voltage of 40 volts DC.

Fig. 4.14 shows that the circuit consists of an ideal 50 volt DC feed from the control room out to the detection contacts in the P&LD box and then back to the detection inputs for normal and reverse in the site control room. The cable type used is 1.5 mm^2 screened twisted pair as required in the typical design [4]. The cable manufacturer's technical specification [34] states that the cable has the electrical properties shown in Table 4.2.

Table 4.2 Electrical properties of detection circuit cable [34]

Cross Sectional Area of wires	mm^2	1.5
Max. Conductor Resistance @ 20^0 C	Ohm km^{-1}	<12.2
Max. Mutual Capacitance (Core-core)	nF km^{-1}	< 86
Insulation resistance value (Core to core)	MΩ km	>10
Inductance	H m^{-1}	5 x 10^{-7}
Conductance	S m^{-1}	< 0.2 x 10^{-9}

In order to establish the rise and fall characteristics of the detection current levels when detection circuit contacts are opened and closed, the circuit has been modelled using the values from the cable specification in MATLAB SIMSCAPE (Fig. 4.15). The model type used is a lumped parameter L-section transmission line. It is comprised of the following parameters: line resistance per unit length (R), line inductance per unit length (L), line capacitance per unit length (C), line conductance per unit length (G), length of the line (LEN).

The maximum cable run distance from a site controller to a set of points has a maximum value of 2 km as stated in [3] to meet the interface requirements. The feed and return cables each have a length $LEN = 2$ km, giving a total circuit length of 4 km.
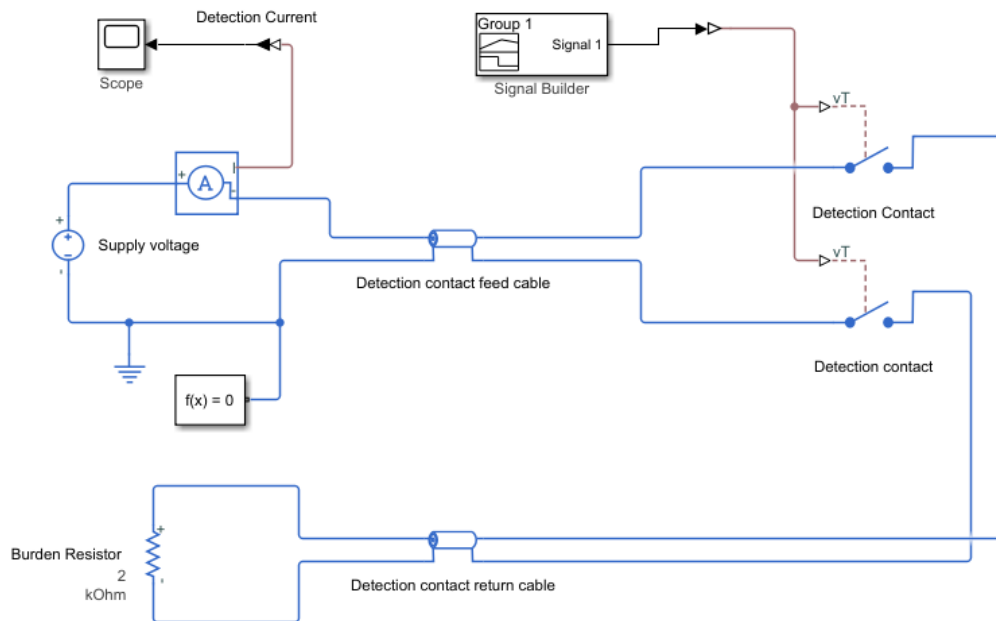
Fig. 4.15 Detection circuit MATLAB SIMSCAPE model

The maximum values of conductor resistance and core to core capacitance per unit length are taken from the manufacturer's data in Table 4.2 and used in the model. The model was run with the maximum supply voltage allowed by LU standards [33], this being 55 volts DC.

The signal builder provided a signal to control the direction current contacts. If the threshold vT applied to the switches is greater than 0.5 volts, then the contacts are closed; if vT is less than 0.5 volts then the contacts are open. At the start of the simulation the signal builder output is at 1volt and the contacts are closed; after 10 milliseconds have elapsed the output drops to zero for 10 milliseconds, opening

the switches, and then 10 milliseconds later the output rises back to 1 volt and the contacts are closed. The effect on the DC current flowing in the circuit is shown in Fig. 4.16. It can be clearly seen that there is an overshoot in the current level when the switches are opened and a considerably larger overshoot when the switches are closed.
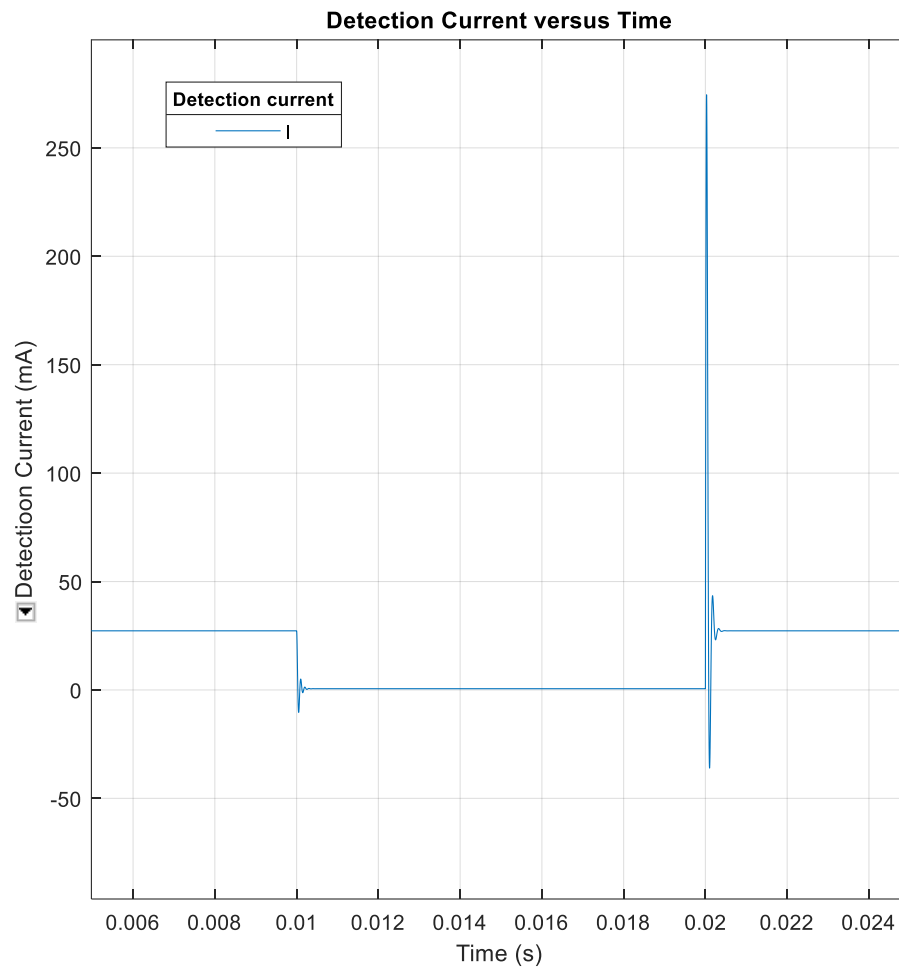
Fig. 4.16 Detection current change when model detection switches are opened and closed

The difference in the amplitude of the overshoot is due to the fact that when the switches open at 10 milliseconds the circuit is composed of the *L*, *R*, and *C* per unit length components between the supply voltage and the switches, which represents 2 km of cable. When the switches are closed at 20 milliseconds the circuit is composed of *L*, *R*, and *C* components representing 4 km of cable.

Fig. 4.17 shows the scope view of the detection current at time 10 milliseconds when the detection switches are opened.
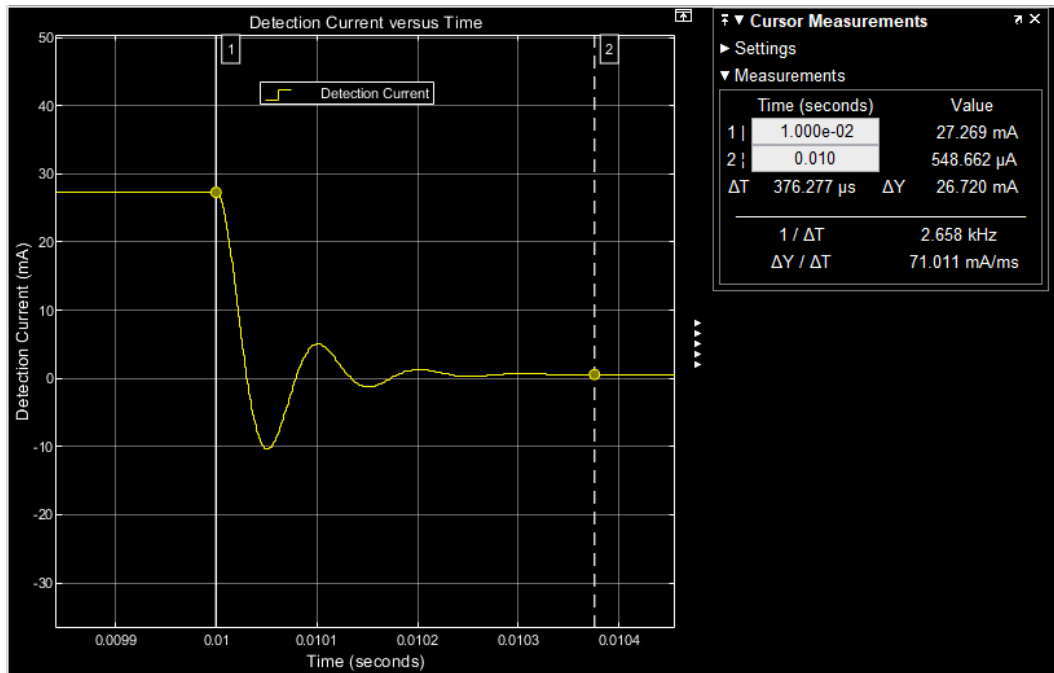
Fig. 4.17 Detection current when detection contacts open – time to steady state.

The cursors have been positioned to measure the time to settle from the steady state when the switches are closed and the steady state after the switches have been opened. The time to settle taken from the cursor measurement is 376 µS. The change in the current is 26.7 mA.
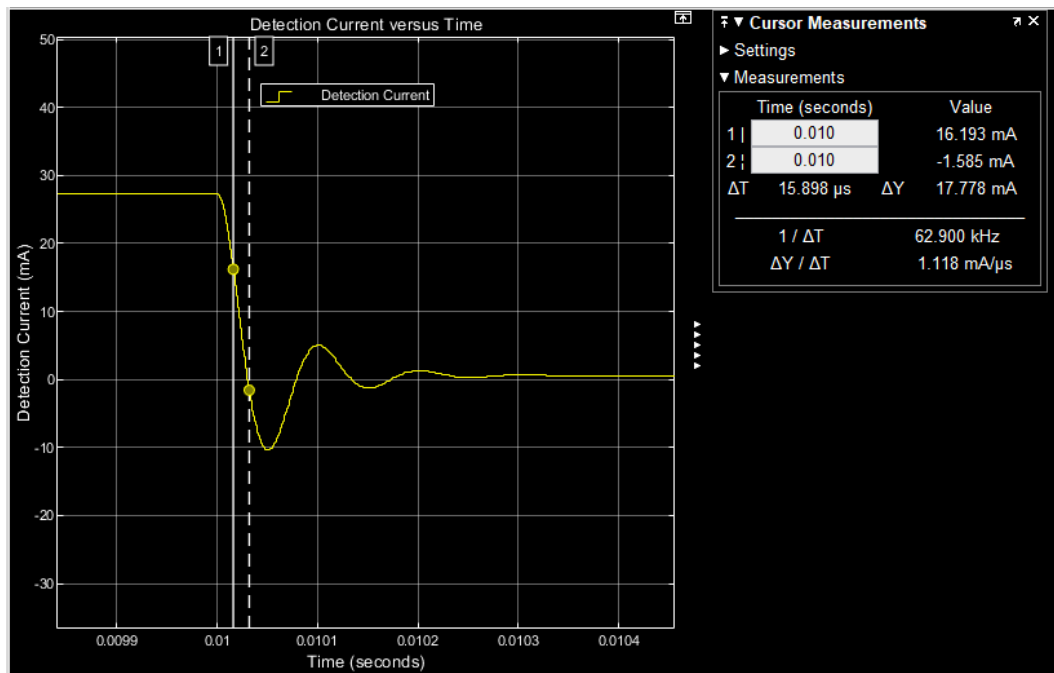
Fig. 4.18 Detection current when detection contacts open - falling edge.

In Fig. 4.18 the cursor position has been changed to look at the rate of change of the detection current art the leading edge of the waveform. The rate of change taken from the cursor measurement is approximately 1 mA/µS.
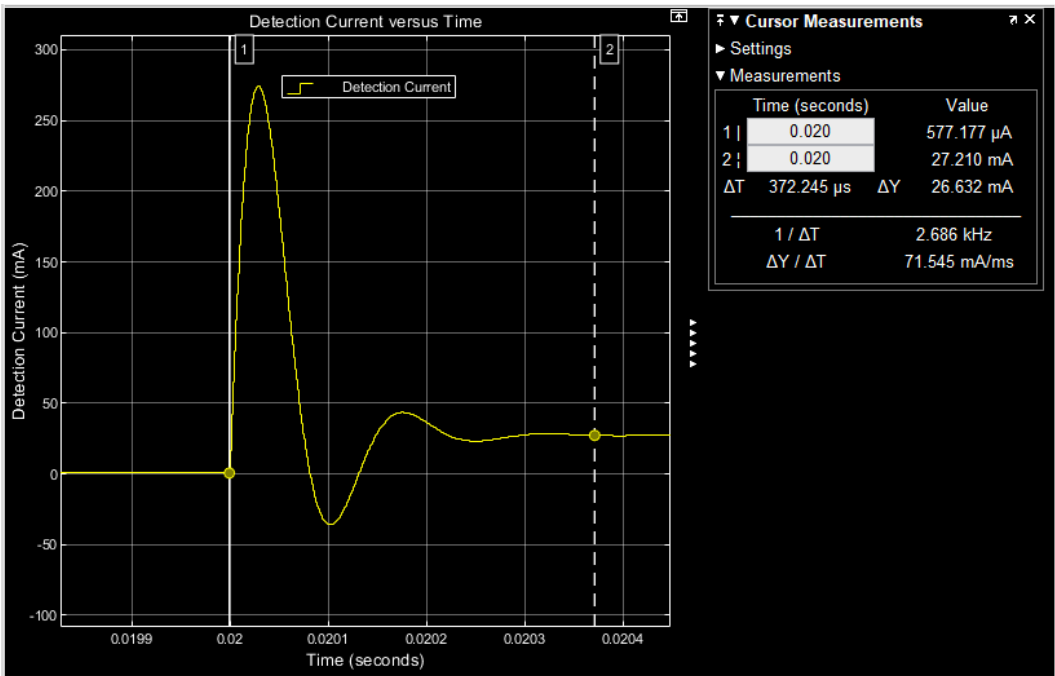
Fig. 4.19 Detection current when detection contacts close – time to steady state.

Fig. 4.19 shows the scope view of the detection current at time 20 milliseconds when the detection contacts are closed. The cursors have been positioned to measure the time to settle from the steady state when the contacts are open and the steady state after the contacts have been closed. The time to settle taken from the cursor measurement is 372 µS. The change in the current is 26.6 mA.

In Fig. 4.20 the cursor position has been changed to look at the rate of change of the detection current art the leading edge of the waveform. The rate of change taken from the cursor measurement is approximately 14 mA/µS.

The time taken for the level of current to settle to a steady state when the detection contacts are opened or closed are 376 µS and 372 µS, respectively.

The rate of change of detection current is considerably different between the opening and closing of the contacts as is to be expected due to the greater amplitude of the current when the contact is closed.
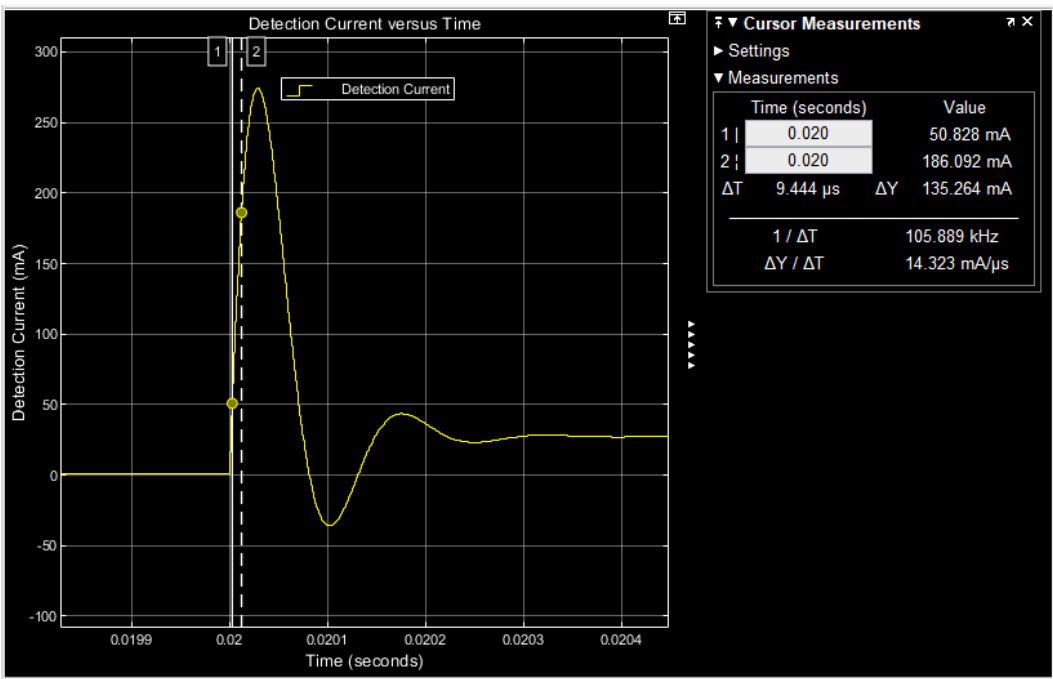
Fig. 4.20 Detection current when detection contacts close - rising edge.

4.3.1   POINT MOVE ATTEMPTS

The detection current drops to zero as soon as the groundlock is energised and the detection is lost. If the point move is successful at the first attempt, as should be the case for the majority of point move attempts then the detection current should rise to a value equivalent to a single input being fed. This happens within approximately one second. However, if the point move is attempted multiple times (up to two for this application) then the waveform of the detection current provides information on how many attempts were made, the end position of the points and the timings of the point move attempts.

The inputs to the controller from the detection contacts are anti valent and as such if the current was measured at a value approximately twice that of a single input then this would indicate that both inputs were being fed. Irrespective of the non-intrusive current monitoring under discussion the safety critical design of the control system would react to this invalid input pair by declaring the points as disturbed and not allow trains to be routed over them.

The load of each of the two inputs to a detection circuit is 2 kΩ resistive, with a nominal 50 volt DC supply voltage. This gives a 25 mA DC current flowing when a single normal or single reverse input is fed. The waveforms for three scenarios of

attempted point moves are illustrated below in Fig.4.21. Note that the groundlock detection contact remains open circuit until the point is detected in the last commanded position when the groundlock engages the slot in the slide at its commanded position. If the groundlock does not engage with either its normal or reverse slot, then the points are declared unlocked by the control system and neither route is available for the passage of a train.
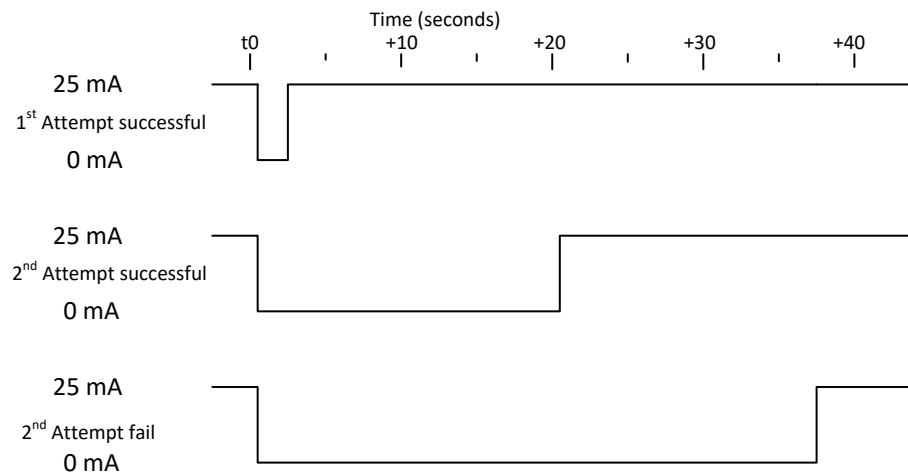
Fig. 4.21 Detection current timing diagram for multiple attempts at point throw with nominal 50 volt DC supply and 2 kΩ burden resistor as load.

The three waveforms illustrated in Fig. 4.21 shows the ideal detection current levels that can be used to determine if the operating parameters of the points have changed and would then warrant an intervention by maintenance personnel.

The key elements of interest are:

1. Did the point move result in a locked point with detection in either of the normal or reverse positions?

2. Did the point move prove successful in its requested move from normal to reverse or reverse to normal to provide the intended route selection?

3. How many attempts did it take to achieve its final position?

4. How long did it take between any changes of state between high and low amplitude of the point detection current?

An ideal detection current ≥ 18 mA represents "high" and an ideal detection current of ≤ 5 mA is represented as "low". The value 18 mA is based on the minimum supply voltage requirement defined in LU standard [33] as 40 volts DC. Taking into account the resistance of the cable in the circuit and the 2 kΩ burden resistor at the detection input.

The start of the data gathering for a point move event is when detection is lost and the detection current goes from high to low, a time stamp is to be attached to this event. A timing count is then initiated to determine the time until the detection current goes from low to high, if this time is less than 5 seconds the point throw is classed as successful at the first attempt.

If the detection current is low for longer than 10 seconds, then this indicates a second attempt is being made to move the points to the commanded position. If the time to attain a high state is between 10 and 25 seconds, then the point move was successful at the second attempt.

If the point move does not attain a high state for a period longer than 30 seconds, then the second attempt has failed. If the high state is attained in a period between 30 to 40 seconds, then the second attempt to move the points has failed but the point has been returned to its original position then locked and detected in its original position.

Depending on the time taken for the current to change to a high state determines if the second attempt has been successful or has failed and the detection current going high is an indicator of the original point position and locking being attained, in this case the point is declared not-moveable.

After a period exceeding 40 seconds the current remains low then the point has not achieved a locked position in either of the normal or reverse positions. This would be reported by the site controller to the operational management centre as a disturbed point and no passage of trains would be allowed over the set of points. These events are depicted in Fig. 4.22
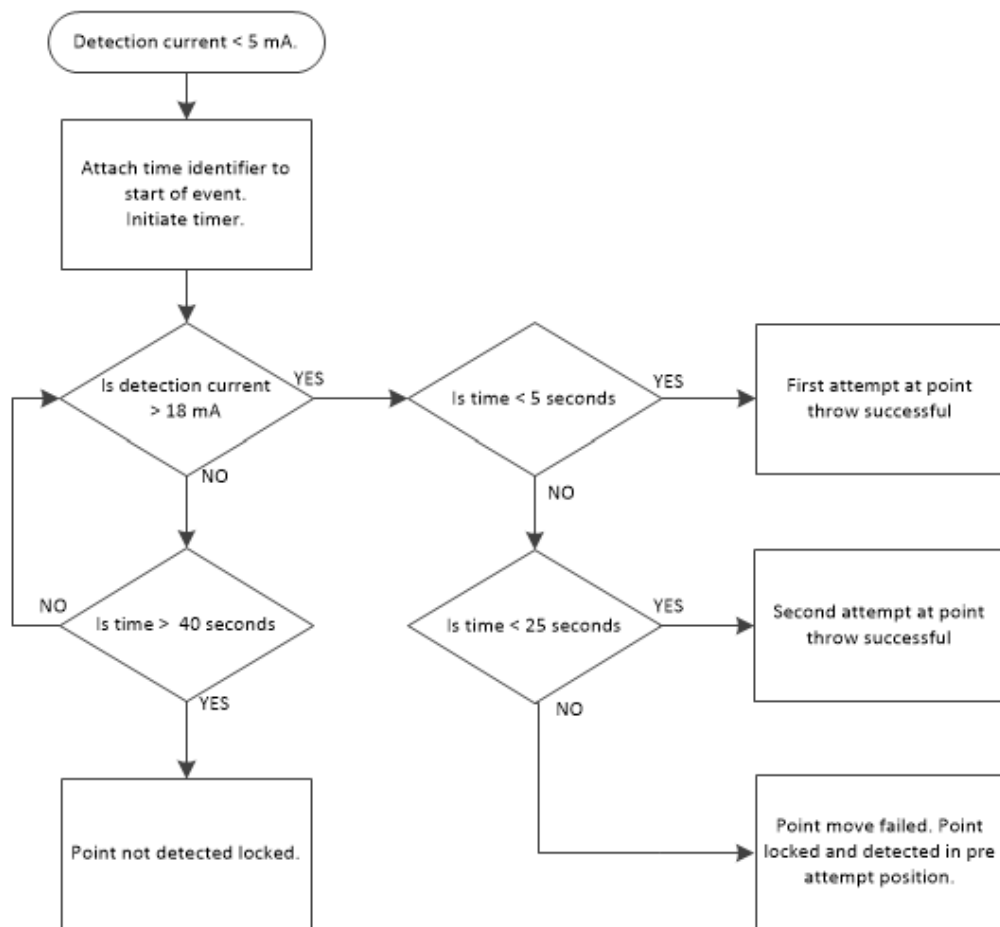
Fig. 4.22 Flowchart depicting point move attempts

The data output from the activity illustrated in Fig. 4.22 is a timestamp and a classification as; first attempt successful, second attempt successful, point move failed, or point not detected locked.

4.3.2 INTERMITTENT DETECTION

There is a further point detection event that is of interest when monitoring performance; this is when detection is momentarily lost when a train passes over the points. The loss of detection happens due to the vibration caused by the passage of the train; this may mean that the point equipment is moving toward the limits of its adjustment, or that linkage mechanisms have started to become worn or that fixings have started to work loose. There may be a single occurrence or multiple loss of detection as the train transits the point. This is different to a loss of detection due to the point moving away from a locked position. In the case of automated signalling systems there is a persistency built into the software that determines the difference between the events based on the duration of the time that the detection input to the system is lost.

The station controller subsystem software architecture design [35] requires that a change at the input be read for two application cycles to be recognised as a change at the input. An application cycle being 100 milliseconds, thus the input must change state for longer than 200 milliseconds. This feature is to take into account the effects of relay bounce and momentary detection contact open circuits when trains pass over points.

The loss of detection in this type of event does not result in any emergency brake application, by the signalling system. If the loss of detection persists for a time in excess of the software persistency time (200 mS), then the system considers the point to be unlocked; the system would then apply emergency brakes in all other trains in the vicinity to reduce the chance of multiple collisions in the event of a derailment.

As can be seen in Fig. 4.23 the loss of detection during the passage of a train may be a single instance or multiple losses of varying duration. The transition from high to low and back high for a single loss of detection is similar to the waveform for a successful first attempt at a point move as illustrated in Fig.4.21; except that the length of time to complete a point move is longer than the momentary loss of detection, so any measurement technique needs to be able to differentiate between the two events.
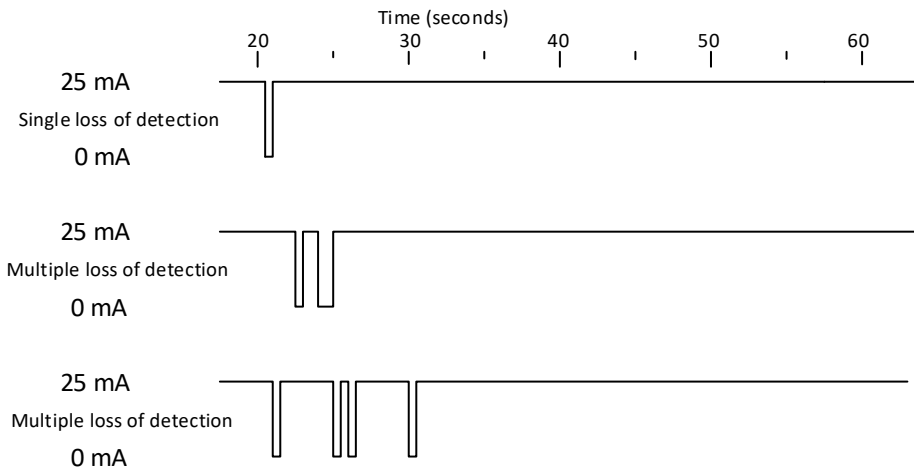
Fig. 4.23 Momentary loss of detection during the passage of a train

Loss of detection can be monitored over a twenty four hour period as a set of times that detection is lost. This will include point moves, which by their nature will have much longer times between loosing and regaining detection.

The data recorded will be a set of times that represent the time that each loss of detection event lasted over a twenty four hour period. This data set can then be analysed to separate the momentary loss of detection from the point moves using data classification techniques.

4.4   POINT THROW ACCELERATION

The measurement of the acceleration forces experienced by point tips when they are moved and during the passage of a train can provide data on point performance over a period of time.

The London Underground standard S1195 Signalling-Functional requirements section 3.6.3.3.4 [2] states "At open switches the flangeways shall be proved clear to prevent derailment and damage to the switch toe". To achieve this, the open switch is set up such that the flangeway gap is 105 mm at the lock stretcher position (127 mm) from the end of the point tip [28]. In Fig. 4.24 point tip A is closed, and point tip B is open.
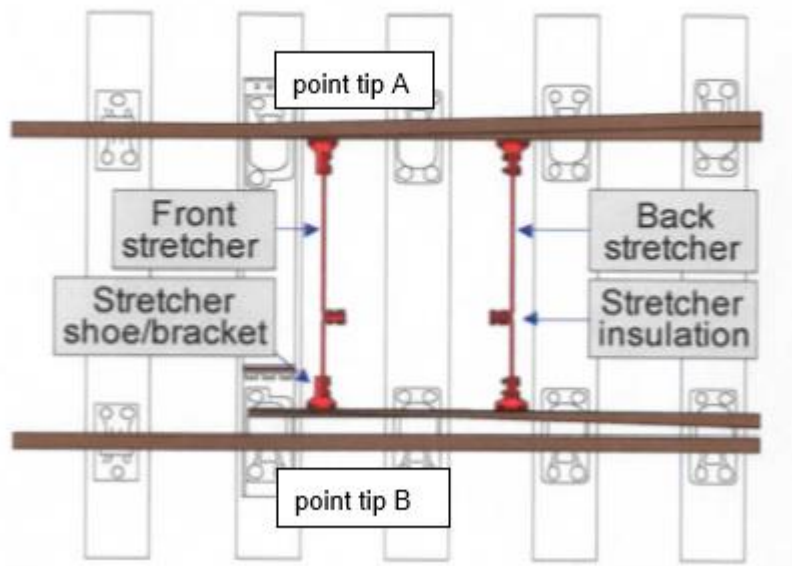
Fig. 4.24 Four foot point layout (adapted from [27])

The front and back stretcher bars are key components in maintaining the mechanical integrity of the point machine. This is discussed further by Rama and Andrews [15], who provide a compilation of mean time to failure and failure rates for railway point components based on Network Rail assets, from this they build reliability models. In addition, Reffye and Dersin proposed models for stress analysis of failure modes in their paper on mechanical reliability of a point system [36].

The addition of accelerometers to the point tips can provide information on the point move operation and the integrity of the mechanical linkages of the point during the passage of a train. Note that an obviously key attribute of safe point

operation is that the points do not move during the passage of a train, so the nature of both scenarios is considered.

The accelerometers to be used can measure acceleration in three axes.

It is to be expected that for a correctly adjusted point machine the amplitude from the accelerometer measurements from the point move operation will be predominantly higher in one axis for normal operation. It is expected that as point machines start to approach the limits of correct adjustment that the amplitudes of the other two axes will increase. In the vertical axis the higher amplitude will be that from wheel impact across the rail discontinuity between the stock rails and the point tips. It is the combination of information from all three axes that provides the performance signature for the individual point machine under operating conditions over an extended period of time.

One of the main parameters of interest will be the time between initial movement of the point and the time when the point comes to a rest at the completion of the point move attempt. There should be a correlation between the point move accelerometer readings and the detection current sensor readings. The point move accelerometer reading will themselves give indications of linkage set-up or mechanical wear problems.

Once the point is locked in position and a train is routed over the points then the accelerometer readings can provide data on the vibration and movement of the point tips when under the stresses of a train passing over them. As for the case when the point move is carried out it is expected that this would be in the form of a "signature" in all three axes of movement. Interpretation of the changes in signature and their relevance to the mechanical integrity of the point requires multiple data sampling techniques.

Although this work is exploring using accelerometers placed near the point tips, if field trials were successful then the possibility arises of using further accelerometers placed at other positions on complete point assemblies. It can be seen from Fig.4.11 that the point assembly consists of many mechanical assemblies and interpretation of multiple sensors may prove for an interesting future work stream.

4.5 SENSOR SELECTION

The discussion in the previous paragraphs describes the current waveforms expected for the various behaviours of the point circuit. The following describes the characteristics of the current to be measured; type of sensor to be used to measure the current, together with its ancillary equipment; the environment in which the measurements are to take place and the data gathering techniques and infrastructure to be employed. The idea is to use a single sensor for each detection circuit mounted within existing cable termination frame cabinets. There is no intention to mount current sensors at the point machines at the trackside, in this way the amount of equipment to be added to the infrastructure for monitoring of points may be limited and localised to equipment rooms. The accelerometer sensors and ancillary equipment would have to be mounted on the point apparatus to provide monitoring data.

4.5.1 CURRENT SENSOR

The intention is to use a single sensor to measure the detection current. The location of the sensor for each circuit is within the termination frame cabinets in the site control rooms. The point detection circuit of Fig. 4.14 shows the single detector at the input to the circuit.

The nominal current to be measured is 25 mA for the case where the detection feeds a single normal or reverse control card input which has a 2 kΩ burden resistor as a load with a 50 volt DC supply.

The magnetic field produced by the test values of current flowing in a conductor is now considered. The test range of the current flowing in the current conductor is chosen to be -120 mA to +120 mA; this is to provide for possible future applications of the sensor in other signalling circuits.

The magnetic field arising from a steady current flowing in a single conductor can be calculated by use of the Biot-Savart law, Grant and Phillips summarise that "The Biot-Savart law gives an expression for the magnetic field that arises when currents flow in thin wires in free space, or, for most practical purposes, in air" [37, p.137].

Ampere's Law may also be deduced from the Biot-Savart Law [37, p.141] and allows determination of the magnetic field around a long straight wire.

Ampere's Law is given as:

$$B = \frac{\mu_0 I}{2\pi r} \qquad (1)$$

Where:

B = magnetic flux density in Webers/metre^2

$\mu_0 = 4\pi.10^{-7}$ (permeability of free space)

I = current flowing in conductor = 0.025 Amps

r = distance from centre of conductor to point of measurement = 2.6mm

$$B = \frac{(4\pi \times 10^{-7}) \times 0.025}{2\pi \times .0026}$$

$$= 1.92 \times 10^{-6} \text{ Teslas}$$

This result is the value of the magnetic field density at a point 2.6 mm from the centre of a conductor with 25 mA of current flowing through it. This applies for a long straight wire.

A graphical representation of the relationship between the current in the conductor and the magnetic field at a distance is provided by using a numerical Toolbox found in MATLAB for the numerical integration of the Biot-Savart law, it is known as BSMag Toolbox [38].

The toolbox contains an example that calculates the magnetic flux density at incremental radii from the centre of a filament representing the flow of current. In this instance the magnetic flux density at a given point on the radius is the resultant of contributions from segments of the filament along the length set as a parameter within the model.

The model is set up with the following parameters:

- Value of current in filament is set at 25 mA.

- Length of filament is set at 100 mm; this represents the internal length of the enclosure described in section 5.1.1.3. The measurement point is set at the centre of the enclosure to represent the position where the sensor is placed within the enclosure.

- The distance at which the magnetic flux density is measured is 2.6 mm; this represents the distance from the centre of the conductor to the centre of the sensor as described in section 5.1.1.1.
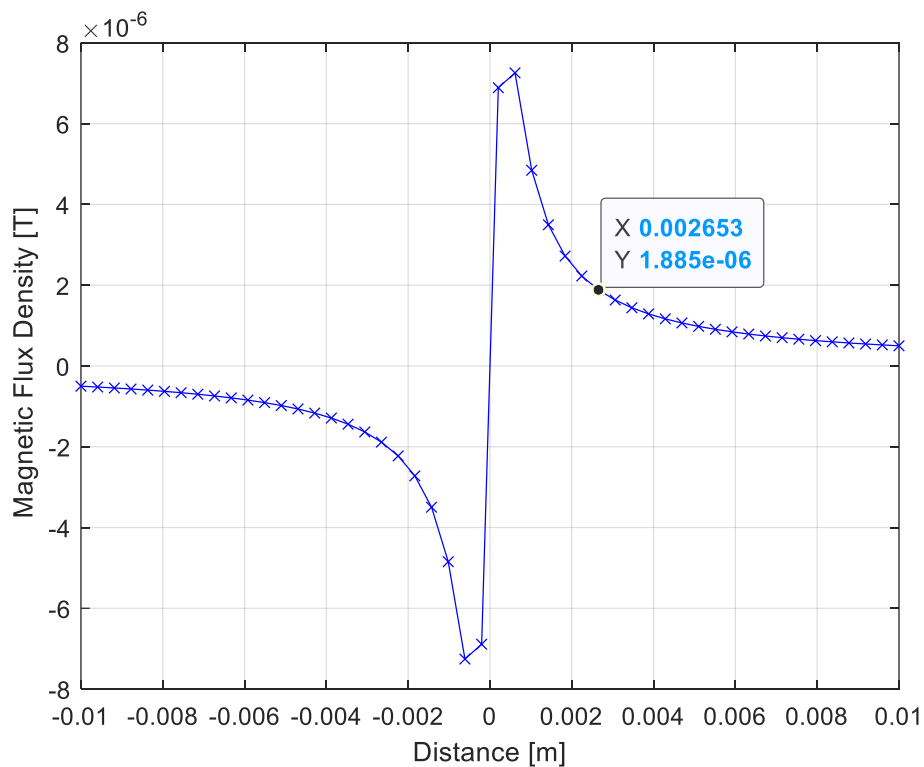
Fig. 4.25 MATLAB toolbox magnetic field solver output

The figure obtained from the output of the MATLAB toolbox is illustrated in Fig. 4.25. The value for a distance of 2.65 mm is given as:

$$B = 1.89 \times 10^{-6} \text{ Teslas}$$

The decision making for which type of sensor to use is based around the requirement for the sensor to be non-intrusive and have the ability to measure low

values of current. The value of conductor current to be measured is in the range of milliamps (10^{-3} Amps) direct current for detection circuit current measurement.

The need for the sensor to be non-intrusive immediately discounted the use of shunt resistors in series with the load and sensing the voltage drop across the load with precision operational amplifier circuits. This could be considered as a means of condition monitoring at early system design stages, but as stated in the introduction the concept that is the focus of this study is for cases where monitoring has not been considered early in the system design stages. There is also the question of safe failure modes where circuitry is directly connected to safety critical circuits; shunt resistors and associated circuitry would introduce more components to the safety critical circuit that did not have galvanic isolation.

Hall Effect sensors were considered for the application but discounted as the low values of current to be measured and the need for the sensor to be non-intrusive did not seem to be mutually characteristic with the comparatively low cost requirement of the sensor to be used for the investigation.

A review of types of sensors led to a decision to test the application of solid state magnetic field sensors using the anisotropic magnetoresistive properties of Permalloy materials to provide current sensing for detection current circuits. There are a number of manufacturers producing such sensors including Analog Devices, Measurement Specialities and Honeywell. A decision was made to choose a device produced by Honeywell; the main factor in this choice was the extensive application notes provided by the manufacturer and the author's familiarity with using Honeywell sensors and on-line application tools from previous projects.

The sensor chosen for the current sensing measurements is the Honeywell HMC1021 single axis magnetic sensor.

The particular type of sensor utilises Anisotropic Magnetoresistive (AMR) technology. As noted by Maguire and Potter [39] in the introduction to their paper, anisotropic magnetoresistance was first discovered by William Thompson (Lord Kelvin) in Glasgow in 1857. The development of applications for the effect was not fully explored until the middle of the twentieth century when manufacturing techniques were refined for production of thin Permalloy layers. The basis of the sensor application is that the resistance of the sensor element changes in the presence of a magnetic field dependant on the direction of the field relative to the magnetic axis of the material.

The extract from application note [40], shown in Fig. 4.26 illustrates the magnetic domains within the Permalloy magneto-resistive element of the solid state sensor.

The devices have the property due to their manufactured structure that the magnetic domains can be aligned by the application of a strong uniform magnetic field. The presence of a magnetic field in the easy axis then results in a change to the resistance of the element. According to the information supplied in the manufacturer's data sheet [41], as long as the device is not subject to a high magnetic field in the easy axis in excess of approximately 20 gauss, then the elements react lineally to changes in magnetic field within the operating range.
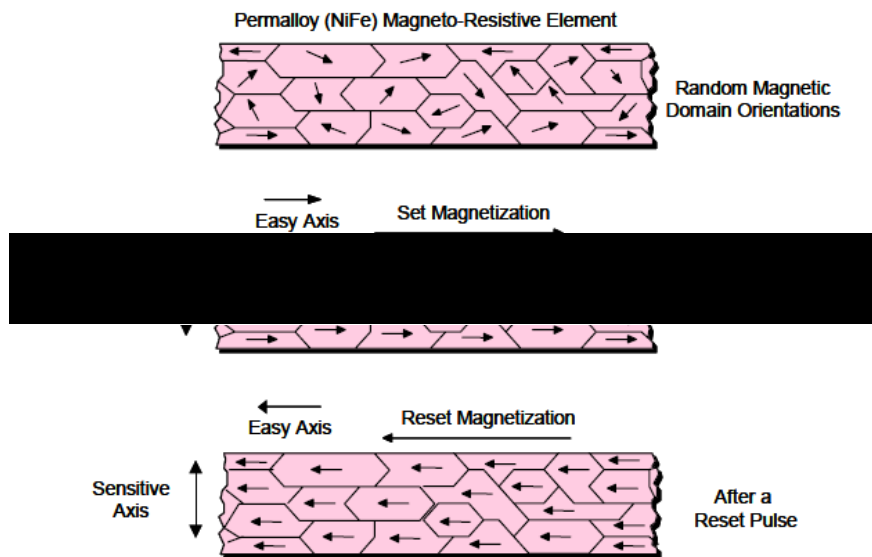
Fig. 4.26 Magnetic orientations [40]

The sensors are described within the manufacturer's data sheet [41, p.1] as "They are extremely sensitive, low field, solid state magnetic sensors…" they have been designed with the capability and sensitivity to measure the Earth's magnetic field, in both direction and magnitude. The range they can measure is from tens of micro gauss to 6 gauss with a typical sensitivity of 1.0 mV/V/gauss from the resistance element bridge. Note that the data sheet values are provided using gauss as the unit of magnetic flux density from the CGS measurement system, in SI units the Tesla is used.

$$1 \text{ Tesla} = 10{,}000 \text{ gauss} \qquad 1 \text{ gauss} = 10^{-4} \text{ Teslas}$$
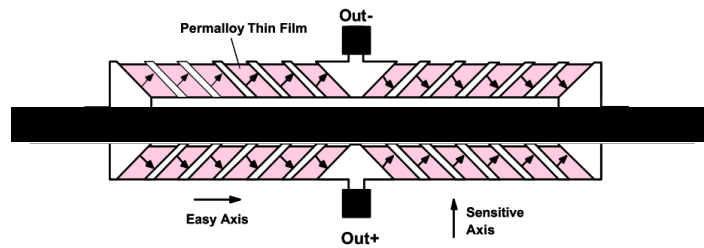
Fig. 4.27 Magneto-resistive Wheatstone bridge elements [41, p.6]

The sensor is made up of four magneto-resistive elements made of a nickel-iron (Permalloy) thin-film that is deposited on a silicon wafer that forms a resistive strip element; these are configured to form a Wheatstone bridge. The other on-chip elements are a set/reset strap function and offset straps. The basic structures of the resistive elements that form the Wheatstone bridge are illustrated in Fig. 4.27. The offset and set/reset features are not shown.

The manufacturer states in [41, p.6] that the offset straps are formed of a metallised spiral that is coupled to the sensor elements sensitive axis. They are used to compensate for incident stray magnetic fields on the sensor. They are not used in the application described in this document; other means of offset correction are used and discussed in further sections. According to the manufacturer's literature the heating effect of these offset straps over a long period can cause degradation of the device performance.

The set reset straps are further metallised straps that are coupled to the sensor's easy axis, these provide for realignment of the magnetic domains when the sensor has been subject to a large magnetic field that has caused the domains to move out of uniform alignment. The set/reset function is used in this application.

The environment where the sensor is to operate is subject to magnetic fields other than that from the current flowing in the supply conductor being measured. Indeed, the bench test environment is subject to fields produced by test equipment, mains supplies, the earth's magnetic field and focussing of any of these fields can happen due to metal objects in the vicinity.

This means that testing in a shielded environment is desirable for the test bench investigation. This will provide data on the effects of shielding on the sensor operation prior to any future field testing. The effects of shielding for low frequencies are investigated; this is because noise sources described in the

previous paragraph are predominantly low frequency in nature. There is also the effect of the trailing test load supply circuit to consider, as the leads are necessarily in close proximity to the sensors under test.

In the discussion on shielding of magnetic fields [42, p.179] Ott comes to the conclusion that it is difficult to shield low frequency magnetic fields. At low frequencies, the main shielding effect is absorption and not reflection; "The primary loss for magnetic field is absorption loss" [42, p.179]. Effective shielding for magnetic fields is provided for by a low-reluctance path to shunt the magnetic field around the equipment to be shielded. In this case the equipment is the sensor. The material chosen for shielding the sensor must provide a low reluctance shunt path for the external magnetic field. Such material as steel or mumetal, which is a nickel iron alloy can be used.

Consideration of which material to use for bench testing must take into account:

- the cost of the material

- how easily can it be shaped to fit enclosures

- Availability of the material

A material that meets these considerations is mumetal, which has a much lower reluctance than that of cold rolled steel of the same thickness at low frequencies [42, p.183]. A source of mumetal was found with a thickness of 0.1 mm that could be purchased in small batches, details of which can be found in the manufacturer's data sheet [43]. This material was found to meet the criteria for providing shielding for the prototype sensor.

4.5.2 ACCELEROMETER SENSOR

The accelerometer has to be able to measure the acceleration forces at the point tips during a point throw from normal to reverse or vice versa. It also has to be capable of measuring acceleration forces during the passage of a train.
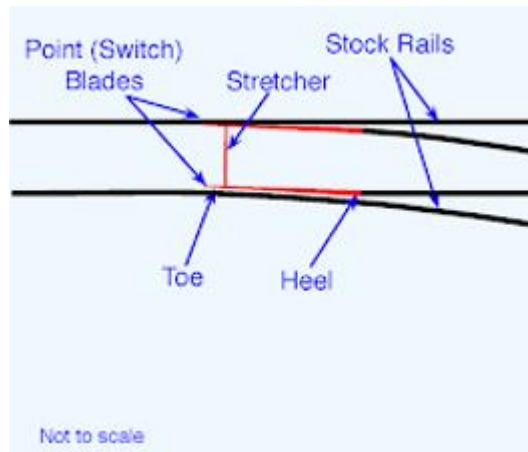
Fig. 4.28 Point layout (adapted from [26])

The acceleration forces to be encountered by a point mounted sensors are discussed by Hamarat et al [44] in their paper on turnout systems under impact loads. They use existing literature to obtain a figure from field testing for vertical acceleration of stock rails caused by the passage of a wheel train of 214.05 m/s^2. A similar study on rail crossing degradation by Liu and Markine [45, p.3] found that maximum value for vertical acceleration did not exceed 150 g (approx. 1500 m/s^2). The first study had sensors mounted on the stock rails and was primarily concerned with the effects of the complete rail structure including sleeper beds. The second study had sensors mounted at the nose of the points where the discontinuity in the rail produced a higher measured acceleration due to the higher forces experienced.

4.6   SENSOR CABLING

The current sensors and sensor data collection unit are to be mounted inside control cable termination frame (CCTF) cabinets in site equipment rooms as shown in Fig. 4.29.
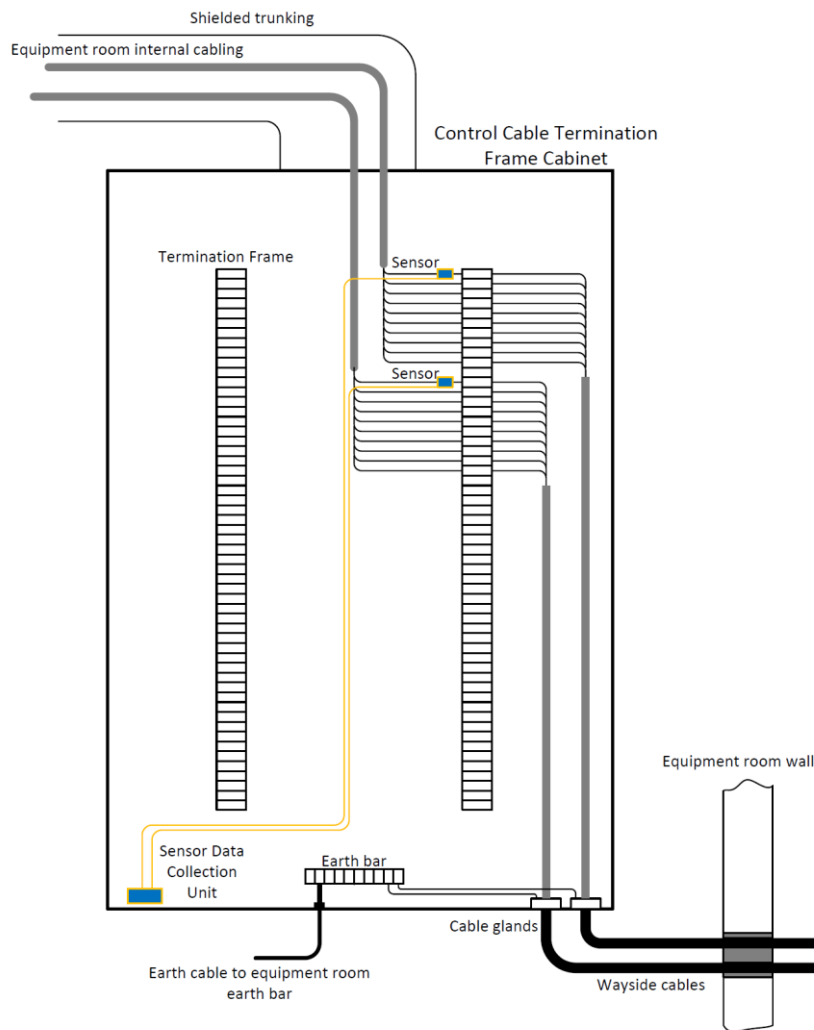
Fig. 4.29 CCTF cabinet showing position of sensors relative to termination frame

The cables from wayside equipment, including points, are brought into the signalling equipment room and terminated within the CCTF cabinet. The cable termination frame provides the interface between the external wayside cabling and the internal control room cabling. The electromagnetic compatibility (EMC) requirements for signalling system assets are laid out in LU standard S1193 [46] and British Standard on railway applications [47]. The sensor, data collection unit, and the cabling between them have to electromagnetically compatible with the CCTF environment.

The cabinet itself has been specified to meet the requirements of the LU standard [46] for electromagnetic interference shielding. The cables attached to the frame that run internally within the equipment room run through shielded trunking to racks that house relays, miniature circuit breakers, and connectors that interface to the

input/output terminals of the site controller as detailed in the typical design [4]. The wayside cables that terminate in the cabinet are connected to wayside equipment that can be up to 2 kilometres from the equipment room. In a single cabinet there could be tens of kilometres of external cabling connected to the termination frames. The internal control cabling consists of single 1.5 mm^2 PVC insulated cable running from the termination frame to the relay rack. The external cable consists of three cable types; multicore, concentric and screened twisted pair. The multicore is constructed with an overall screen surrounding the conductors, the concentric is screened by the nature of its construction, the screened twisted pair has a screen over each individual pair and an overall screen. The cables all carry voltage at either DC or a frequency of 50 Hz AC.

The internal and external cables have both been subject to an induced voltage study [48] to ensure that the specification of the cables, and the final design of the application of the cables is compliant with LU standard [46] for electromagnetic interference. There are still induced noise voltages and currents in the cables in the CCTF cabinet which mean that the cabling used for the sensors and sensor data collection unit need to neither cause nor be subject to electromagnetic interference.

The cable from the data collector to the sensor has to carry the set-reset positive and negative polarity, short duration, high current pulses signals to the set-reset straps, and the power supply and signal return to and from the resistive bridge on the sensor. The maximum length of cable from a data collector to a sensor is two metres, this allows for routing around a cabinet following existing cable routes to the position of the sensor adjacent to the termination frame.

A single cable is to be used between the sensor and data collection unit that carries the signals to and from the sensor as shown in Fig. 4.30. A three pair screened twisted pair with each twisted pair individually screened and an overall screen for the three pairs is chosen to provide protection from electromagnetic interference.
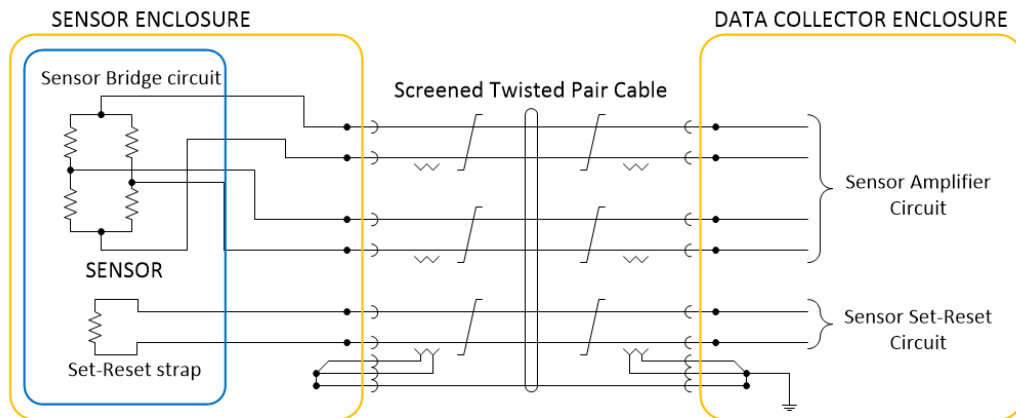
Fig. 4.30 Sensor cable between sensor and data collector

The sensor enclosure consists of a highly permeable shield to prevent low frequency magnetic fields such as the 50 Hz power frequency present in many of the cables in the cabinet causing interference with the sensor. This shielding will need to have an overall non-conducting cover to prevent short circuits in control cabling due to its close proximity to terminations. The data collector enclosure will require similar shielding and covering to prevent interference to the sensor amplifier and data collection circuitry.

In his book on noise reduction techniques in electronic systems Ott [42] analyses and discusses the effects of choice of various cable types on interference in electronic circuits. Further analysis is provided by Paul [49] where he develops lumped parameter models of twisted pair cables to analyse inductive and capacitive coupling, together with the effects of cable twist on crosstalk between cables. Ott summarises [42, p.70] that "The use of nonmagnetic shields around conductors provides no magnetic shielding", and that "a shield grounded at one or more points shields against electric fields".

The screened twisted pair cable chosen for the sensor application has shielding around each individual twisted pair to prevent crosstalk due to electric coupling between the pairs of conductors. The overall screen provides protection against electric field interference from other sources in the CCTF cabinet. The screens are only to be connected at the data collector unit to prevent noise induced in the shield circulating via a ground loop to any common earth introduced by connecting the screen at both ends of the cable.

The way in which the twisted pair reduced magnetic field coupling is described by Paul [49, p.677] as,

"Consider the magnetic flux from the generator wire current. This flux threads the loops of the twisted pair, inducing emfs in each loop. But because the loops alternate in polarity, the induced emfs tend to cancel in the adjacent loops. Thus, the net induced emf induced in the receptor circuit (the twisted pair) is that of one half twist. (A loop is referred to here as a half-twist.)."

The magnetic shielding effectiveness increases with the twists per metre there are in the cable due to the reduction in the area of the loop incident to the magnetic field produced by the interference current. Equal twist rates in adjacent twisted pairs can reduce the overall effectiveness of the shielding as the pairs laying adjacent to each other can produce a net interference field and a resultant induced emf. If adjacent pairs have different twist rates, then there is a greatly reduced chance of there being a net interference field.

The cabling used in the sensor application must also take account of the requirements for fire safety performance as detailed in LUL standard 1-085 [50], with regard to combustibility, smoke emission and toxic fume emission.

4.7   SENSOR NETWORK

The data from the sensors needs to be collected and made available to users. The users will normally comprise the first responder maintainer making use of local data in the equipment rooms and the system reliability engineers using data collected for the overall system. The system engineers may make use of the information in the room location when carrying out investigations, but the information should be available within a networked database.

The detection current sensors are to be attached close to the detection circuit incoming supply circuit breaker. These circuit breakers are mounted in the control cable termination frames (CCTF) that are enclosed within cabinets in the signalling equipment room. The cabinets and ancillary equipment that makes up the CCTFs are modular in nature and this should mean that a uniform design is achievable for detection current sensor assemblies. There may be a number of point circuits within each cabinet and in future the sensor system may be expanded to monitor other types of circuits. Assuming a maximum eight point detection circuits in each CCTF then this would mean a local data collection unit would need associated circuitry to interface with the eight sensor assemblies and say two spare sensor

interfaces for future expansion. This local data collection unit will have a microprocessor to provide for local data analysis; the intention of this is to reduce the amount of data and data sets being transmitted around the data collection system. It has already been said that one of the aims of the project is to limit the amount of data where possible.

The data collection unit then needs to interface with an equipment room level data collection unit. This can be achieved by a number of methods, one such possible method is to set up a wireless network within the equipment room, and another would be to use a physically linked network such as fibre or Ethernet.

The wireless network would involve antennas being mounted on each cabinet and room data collection unit. Within the equipment room there is a comprehensive cable management system (CMS) of trays and trunking to manage the cabling between the various panels and sub-systems. This room CMS would provide routing for a physical room sensor network.

There is also the question of power to the sensor system to be addressed; the CMS can provide routing for power cables to the local date collection units that were based in the CCTF cabinets.

The point acceleration sensor units are to be mounted in a position close to the tips of the switch rails, one on each switch tip. The output of the accelerometers is a voltage signal relative to earth for each of the three axes. These voltages can be fed to the inputs of a microprocessor unit with analogue to digital converter functionality. The intention would be to carry out as much processing of the accelerometer data as possible on the switch tip mounted units. The output from the switch tip data collection units can then be serially transmitted to a local point data collection unit. It is not considered practical to run any cabling in the area of the point machines as it is highly likely to be damaged by operation of the point machines themselves or maintenance activities in what is an area of many moving heavy mechanical parts. The proximity of point machines to each other would determine the number of point data collection units that are required.

The data would then need to be transmitted back to the data collection unit in the equipment room. In cases where wireless masts are already mounted in the area then consideration should be made to transmitting the data to the local wireless network if capacity and data security concerns can be met. If there is no local wireless network available, then there will probably be a need for wireless repeater

stations to get serial data transmitted from point data collection units back to the equipment room data collection unit.

There could be a separate maintenance terminal in the equipment maintenance room, or the data could be interfaced with existing room maintenance terminals. There could even be a mobile phone application for part or all of the diagnostic capabilities of the sensor system; this could be useful where maintainers want to observe the movement of the points while monitoring the sensor data. The internet of things could provide first maintainer interfaces, particularly as the sensor network is for non-intrusive data gathering and analysis. In all such instances the safety of staff would need to be considered in relation to their proximity to moving equipment.

The logging of data and information presentation can be considered based on the following estimate of number of operation and quantities of information.

The number of point operations in an equipment room has already been estimated for a typical signalling equipment room as 4000 per operational day based on 400 operations of 10 point ends.

The data sets can be broken down into one for each accelerometer per point tip; the data from each point tip unit can be transmitted to the local data collection point. The post local processing data then gets transmitted to the equipment room data collection unit. This data is analysed to enable performance monitoring trends to be established. At a local level it would be useful to the first response maintainer to be able to view detail of the last few point operations. There would be an element of maintainer interpretation of the traces available based on experience and training, but there should also be a level of analysis data available to aid the maintainer in diagnosis and any corrective maintenance actions required.

The data set for point detection sensors in combination with the point accelerometer data should provide for convergence of establishing causes of problems with point operation that need to be addressed. It is expected that as the metrics provided by analysis of the data sets become more mature then they will aid in the decision making on corrective maintenance activities. There are comprehensive training facilities available to test the sensor arrangements and identify failure modes prior to deployment in the field for further proof testing of sensor units.

5 MEASUREMENT OF SENSOR OUTPUT

Monitoring of the current flowing into and out of point detection circuits at every point call operation provides information on point operation against an expected behaviour. The expected behaviour is baselined during commissioning or post maintenance check of the circuit when the integrity of the point call operation is verified by test personnel.

Field testing is not within the scope of the project, the aim is to provide an investigation into the suitability of the components and methods to justify field testing as future works.

In order to demonstrate the suitability of the methods, hardware and processing that are proposed for future field testing; benchtop simulation testing is performed on some of the hardware to gain insight into their performance.

The sensors have to be able to be attached to the existing control room and wayside infrastructure with minimum disruption. They can have no effect on the operation of the system, either the safety related or safety critical functionality of the circuits. The data will primarily be the output of the current sensors and the accelerometers. The intention is to use MATLAB and Excel to record and analyse the bench testing data.

A highly desirable attribute of the sensors to be used is that they are non- intrusive and not directly connected to the circuits within the control room. This project explores the use of magnetoresistive sensors to meet the current measurement requirements.

Data provided by measurement of accelerometers mounted on the point switch tips near the tip is similarly baselined at commissioning or post maintenance check.

Current measurements for detection current conductors are investigated using magnetoresistive magnetic field sensors.

- Detection circuits' measurement is of the magnetic field produced by a direct current of tens of milliamps. This is in the form of a pulse train providing information on point operation.

The output of the accelerometer indicates the acceleration profiles of the point move operation and during the passage of a train over the point machine.

Differences between the profiles in combination with the other sensor outputs over a number of operations provide data on the performance of the point end.

- The accelerometers mounted near the switch tips are to measure the proper acceleration of the moving parts during point moves and during the passage of a train. This includes any acceleration caused by parts fixings coming loose or misalignment of point mechanisms.

It is the combination of the current traces and accelerometer outputs for the event of a point move that are to be tested in the event of the project moving to a field testing stage.

The bench testing undertaken at this stage is to be used to inform a decision on the suitability of the sensors and associated analysis methods to be used for field testing.

5.1 TEST APPARATUS

5.1.1 DETECTION CURRENT TEST APPARATUS

5.1.1.1 Magnetoresistive Sensor
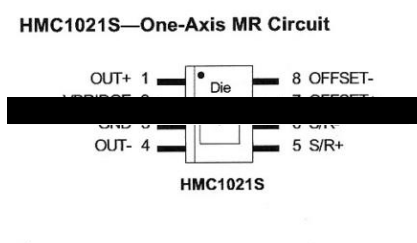
Fig. 5.1 HMC 1021S one axis MR sensor [41, p.5]

The sensor provided is an 8-Pin SOIC package which is soldered to a break out board for the purposes of testing as illustrated in Fig. 5.1. The arrow shown on the face of the chip in Fig. 5.1 indicates the direction of the field that when applied generates a positive output voltage when a set pulse is applied.

For the purposes of testing a number of sensors are attached to breakout boards, for used in testing configurations and spares. There is a consideration to be made as to the effects of the breakout board and header pins on the measuring

capabilities of the sensor test configurations. This is discussed as part of the general discussion on measurement error and offset later in this document.
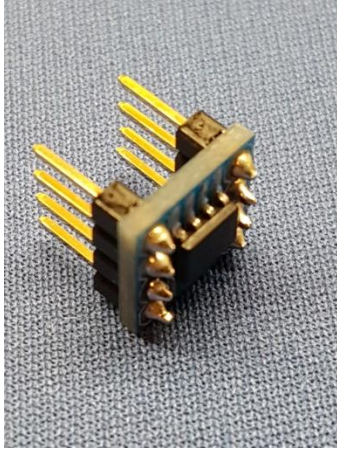
Fig. 5.2 AMR Sensor on break out board

It is noted from data sheet [41, p.3], that the resistance of each of the four elements that make up the sensor bridge is typically 1100 Ω, there are minimum and maximum values for element resistance of 800 and 1300 Ω respectively. Application note AN218 [51] describes how the resistive elements are precision matched to within an ohm of each other with no magnetic fields present when they are manufactured. The AMR elements in the sensors are not perfectly matched and this results in bridge offset voltages, it is also stated in the application note [51], that any mismatch in the resistive elements is fixed for the lifetime of the sensor and therefore offset techniques can be applied to the measurement process.

5.1.1.2 Multiple Sensor Array

The description in the introduction to this section noted that the sensors are manufactured to be as close as possible to matched elements, but that the elements are not perfectly matched. In order to test the variation in the output of the different sensors for a given similar application a test bed was set up as illustrated in Fig. 5.3. The thought behind this layout is that the sensors are in close proximity to each other and would be subject to similar variation in the magnetic field due to the earth's magnetic field and any focussing due to local metalwork.

The distance between each leg of the circuit is approximately 120 mm and the distance between the sensors in each leg is approximately 60 mm.
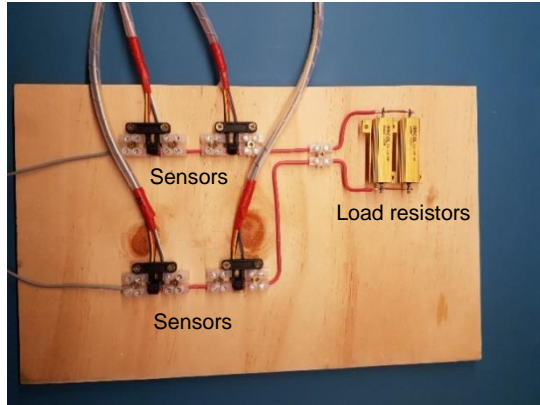
Fig. 5.3 Multiple sensor test bed

Fig. 5.3 shows four sensors set up to measure the current through the load resistors.

5.1.1.3 Sensor Test Enclosures

In order to implement a more uniform approach to the interface between the HMC1021 chip and the cable, a guide was made up from a cable connector strip plastic base. The breakout boards were attached to the plastic cable guides using nylon cable ties, the stages of attaching the sensor chip together with break out board are shown in Fig. 5.4. Using this method, the sensor and cable guide assemblies were all uniform in nature. The cable connector strip was chosen to provide a sliding but not loose fit with the cable used to provide a current carrying conductor through the test enclosure. The cable used for this part of the circuit was 1.5 mm^2 solid single core PVC with an overall outside diameter of 3.2 mm. This size of cable was chosen as it is the same size as that used in [4] to meet the functional requirements [2].   The distance between the centre of the conductor and the face of the sensor chip was measured to be 2.6 mm.

A total of four sensor heads were made up for test purposes. The finished unit is shown in the picture on the right hand side of Fig. 5.4. The current to be passed through the conductor is DC and represents the current flowing in a detection circuit.
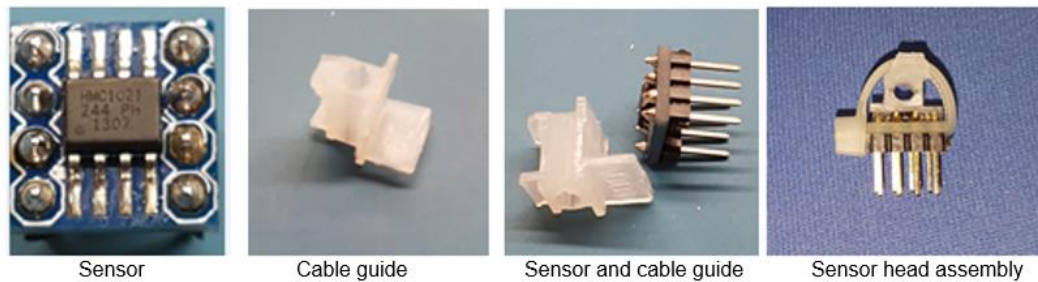
Fig. 5.4 Sensor and cable guide assembly

The next stage was to find a uniform means of mounting the sensor heads where they were not in close proximity to metal parts. To accomplish this, the units were mounted centrally in ABS enclosures. The enclosure external dimensions are 119 x 100 x 45 mm. The holes to accommodate the passage of the cable through the box are drilled 20 mm from the base of the box centrally along the long axis; they are 2 mm in diameter. There is also a hole drilled to the side of box to allow for the sensor head cables to pass through. The current conductor cable is passed through the holes as shown in Fig. 5.5 and through the hole in the sensor head assembly. A length of 100 mm of conductor cable was left either side of the enclosure for connection purposes.
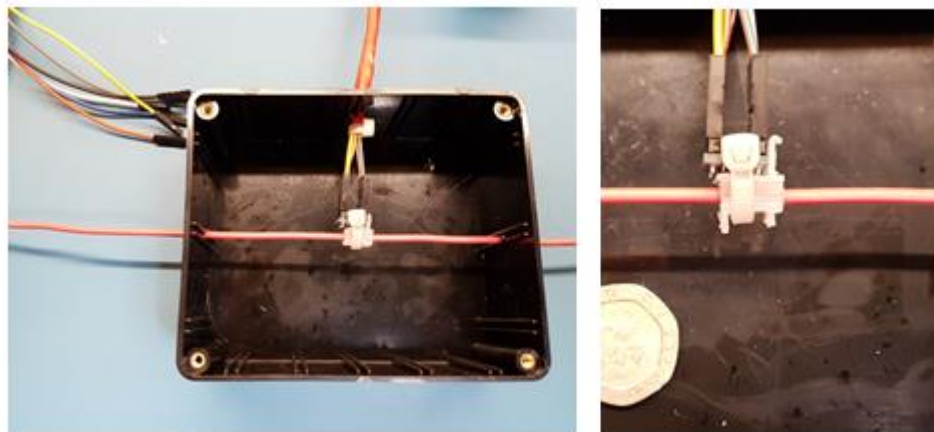
Fig. 5.5 Non screened test enclosure

The description of the initial testing described previously in this section makes it clear that it would be desirable to carry out testing using some form of magnetic screening. The enclosure shown in Fig. 5.5 is not screened but it is required for

testing against a screened version of the same size and type of enclosure with a screen around the enclosure.

When deciding what type of screening would be most suitable a number of factors were considered. The suitability of material was not just based on magnetic shielding properties, but also the suitability of the material to be cut and formed to fit the enclosure. The testing of the effects of the screening was expanded to include an enclosure with two layers of material to test the change in sensor performance.

Fig. 5.6 Single screen enclosure

The screened version of the enclosure Fig. 5.6 used the same size and type of enclosure as the non-screened version with holes drilled in the same positions to accept the cabling for both the current carrying conductor and the sensor cables.

The shielding material had to be capable of being easily formed and cut to the desired size and shape. This meant it needed to be a comparatively thin material. Shielding for low frequency magnetic fields requires a material with a high permeability and ability to not become magnetically saturated when carrying out its shielding function. One such material is Aaronia Magnoshield, which is a Nickel/Iron alloy sheet with a high shielding efficiency. The sheet is 0.1 mm thick and able to be cut with small metalworking shears. The product description in [43] describes it as being developed for shielding during prototyping activities where local radiation sources are present.

5.1.1.4 Bridge Amplifier Circuit

The offset from the AMR resistive bridge is in the order of millivolts when used in this particular application. This signal needs to be amplified in order to provide a useful input to a measuring device or analogue to digital converter.

The AMR manufacturer data sheet [41], suggests a relatively standard inverting operational amplifier circuit for current sensor applications as illustrated in Fig. 5.7. The diagram also shows a set/reset circuit configuration that is described later in the next sub-section.
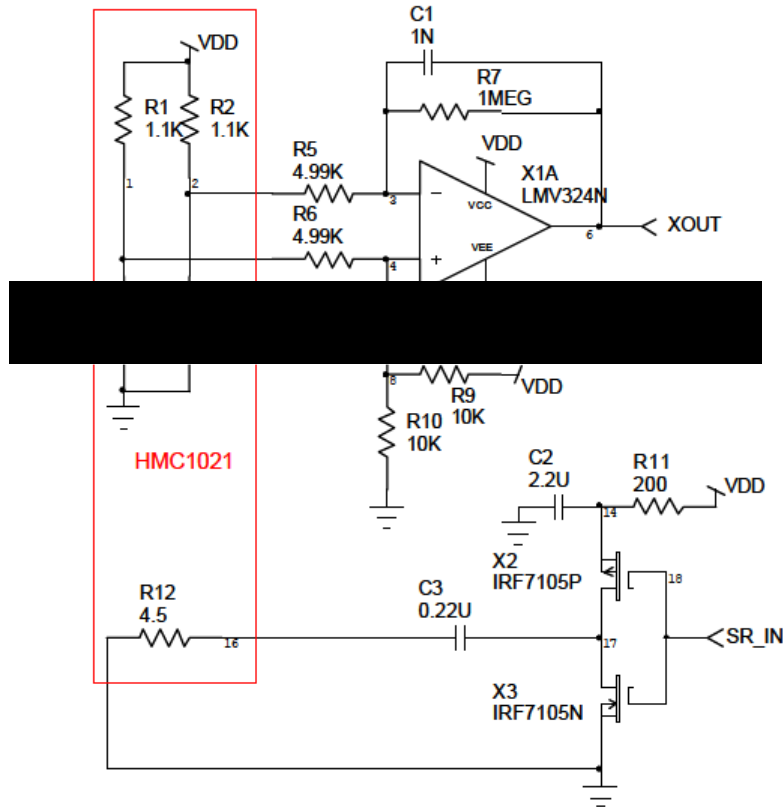
Fig. 5.7 Typical AMR bridge amplifier circuit [41, p.13]

The detection circuit under normal circumstances gives rise to currents varying between 0 and 50 mA flowing in the detection circuit, typical waveforms for point move operations are as shown in Fig.4.21.

The test range of the current through the load conductor was chosen to be +/-120 mA to provide for an extended range if in future other circuits are monitored with the sensor and to confirm the response of the sensor for currents flowing in the opposite direction.

5.1.1.5 Set-Reset Circuit

The set-reset circuit provides the relatively high current pulse for a short duration that is required to realign the magnetic domains in the magnetoresistive material in the sensor; this is necessary in the event of them becoming misaligned to one another.

The circuit was built using a breadboard at this prototype stage and is illustrated below in Fig. 5.8.

Arduino digital output providing set-reset pulse to opto-isolator

Opto-isolator

N and P channel MOSFET in dual package
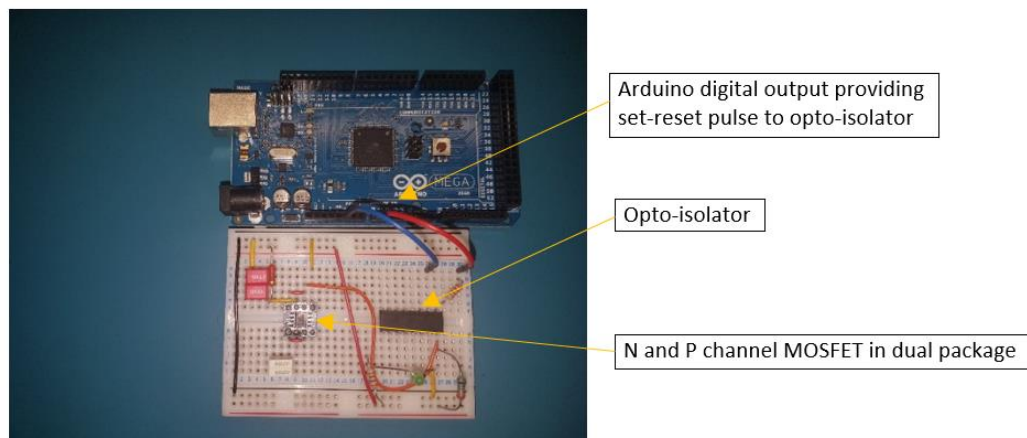
Fig. 5.8 Set-reset bench test layout

After modelling a number of possible circuit configurations suggested by the manufacturer within their application notes [40][41] with circuit simulation tool LTspice, the circuit was implemented using a variant suggested by the sensor manufacturer in application note [40]; as shown in Fig. 5.9.

The digital output of an Arduino Mega2560 microprocessor drives the input of an optocoupler. the output of the optocoupler provides the input logic voltage source V_{SR} in Fig. 5.9 which provides the control voltage between the gate and source of the two complementary N and P channel enhancement mode MOSFETs. The P-channel device is labelled X1 and the N channel device is labelled X2.

The P channel MOSFET X1 has the properties that a voltage V_{SR} >= 4.5 volts results in it being effectively open circuit ("off") between the gate and source; and V_{SR} <= 0.5 volts between the gate and source in it being effectively short circuit ("on") between the drain and source.

The N channel MOSFET X2 has the properties that a voltage V_{SR} >= 4.5 volts between the gate and source of the results in it being effectively short circuit ("on") between the drain and source; and with V_{SR} <= 0.5 volts effectively open circuit ("off") between the gate and source.
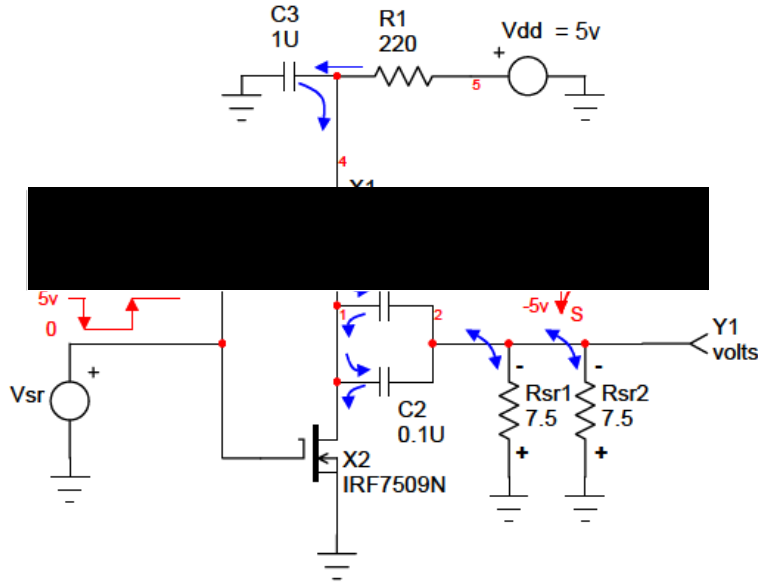
Fig. 5.9 Set-reset circuit for HMC1021 MRS [40]

The input control voltage source V_{SR} is initially at 5 volts X2 is fully "on" and effectively grounding the series circuit comprising of C1, C2, $R_{SR}1$, and $R_{SR}2$.

$R_{SR}1$ and $R_{SR}2$ are the set/reset resistances that form part of the magnetoresistive sensor chip. It is through these resistances that the set reset current pulses needs to be driven to realign the magnetic domains in the sensor.

The input control voltage V_{SR} transitions to a low level (V_{SR} <= 0.5 volts), MOSFET X2 turns "off" and MOSFET X1 turns "on". This results in the series circuit of C1, C2, $R_{SR}1$, and $R_{SR}2$ being pulled suddenly towards the Vdd level held at the C3, R1, and X1 source node. Due to C1 and C2 having near zero voltage initially, the sudden change from ground to Vdd results in all of Vdd to be present at the negative pins of $R_{SR}1$ and $R_{SR}2$ minus the series resistance voltage drop across MOSFET X1. Current flows into the negative pins of $R_{SR}1$ and $R_{SR}2$ and becomes the reset pulse.

The reset pulse now decays, and this causes capacitor C3 to start dumping its charge through MOSFET X1 into C1, C2, $R_{SR}1$, and $R_{SR}2$. Capacitors C1 and C2 accumulate a full charge that is very near to Vdd and C3 also starts to recharge.

The set pulse function is initiated when the control voltage V_{SR} transitions to a high level (V_{SR} >= 4.5 volts), MOSFET $X2$ turns "on" and MOSFET $X1$ turns "off". Capacitors $C1$ and $C2$ are now connected to ground, this creates a negative voltage across $R_{SR}1$ and $R_{SR}2$. Current flows out of the negative pins of $R_{SR}1$ and $R_{SR}2$ and becomes the set pulse.

The traces in Fig. 5.10 were captured on a PicoScope 2406B PC oscilloscope 4 Channel 50 MHz bandwidth.

.
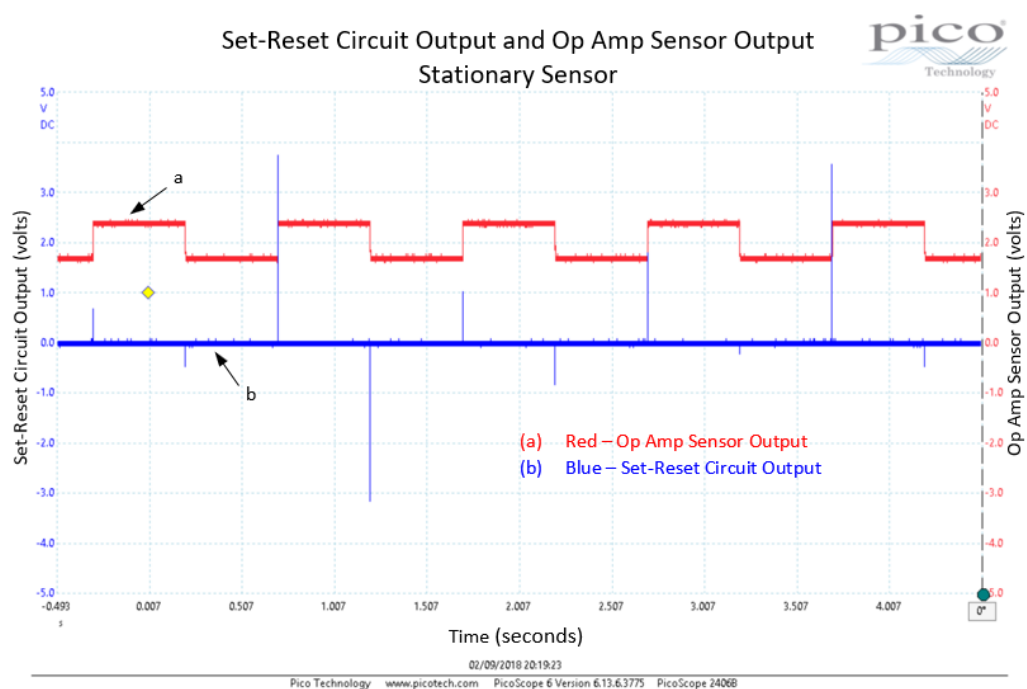
Fig. 5.10 Set-reset circuit output and op amp sensor output-stationary sensor (a) op amp sensor output (b) set-reset circuit output

The red trace illustrates the output of the operational amplifier used to condition the magnetic resistive sensor balanced bridge arrangement. The output of the op-amp is in alignment with the set-reset pulses as expected. This is due to the domains in the magnetic material being realigned by the effect of the pulses applied to the set-reset straps of the magnetic resistive sensor (MRS). The set/reset circuit was connected to drive a single HMC1021, this type of MRS requires a very short duration pulse of above 0.5 amperes in order to realign the magnetic domains. A typical resistance for the set/reset strap is 7.5 ohms. With the pulse duration output from the Arduino digital pin set at 1 second a pulse train

was obtained as illustrated in the scope trace of Fig. 5.10. The positive and negative pulses illustrated by the blue trace are the set-reset pulses; which are not uniform due to the capture rate used to accommodate viewing the two traces with the desired resolution of 500 mS/division on the x-axis.
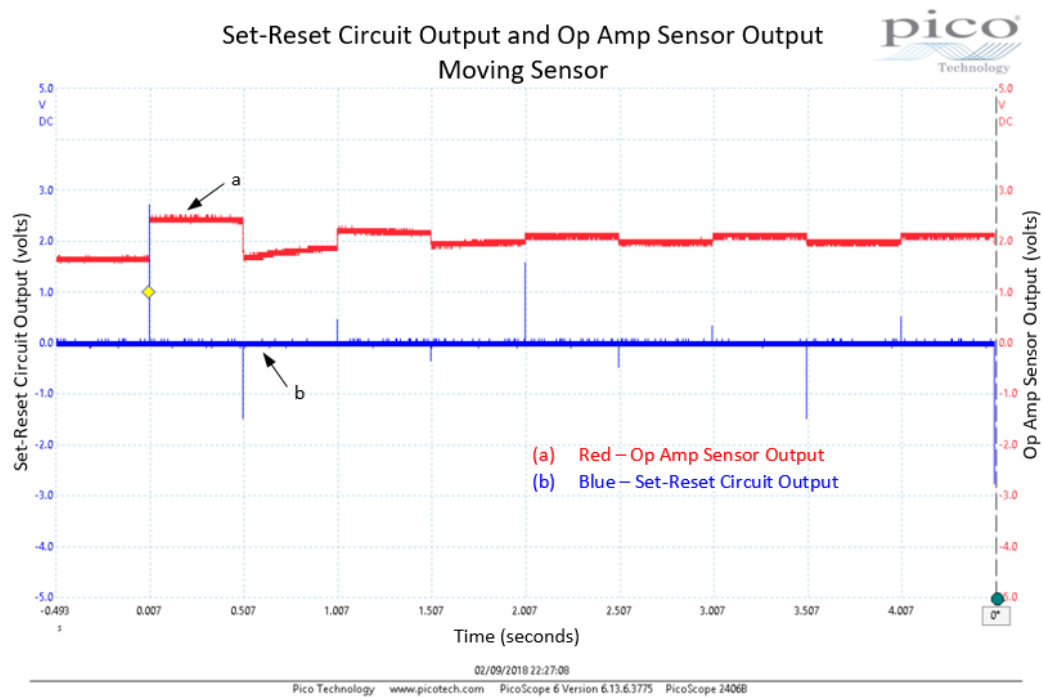
Fig. 5.11 Set-reset circuit output and op amp sensor output-moving sensor (a) op amp sensor output (b) set-reset circuit output

The red trace in Fig. 5.11 illustrates the effect of turning the sensor through 90^0 in the same position in space. This is close to the supply leads for the prototyping boards and is probably picking up the localised field, including the effects of the earth's magnetic field. It does give an indication that the sensors are operating as expected when their sensitive axis is changed relative to the local magnetic field. The curve in the red trace between 0.507 seconds and 1.007 seconds is due to the op amp sensor output changing as the sensor was rotated in space over the half second time taken before the set reset pulse changed the orientation of the magnetic domains in the sensor. The noise in the trace is due to the cables being used to connect between the sensor assembly and the operational amplifier circuit not having any shielding or twisting to protect against noise pickup.

When the scope settings were changed to check that the set-reset pulses were uniform the resultant trace of a positive pulse is shown in Fig. 5.12. The peak is in excess of 3 volts and is only a few microseconds in width. It clearly indicates the decay of the voltage on its trailing edge. The negative pulse is shown in Fig. 5.13, it was observed to be of the same form but negative polarity.
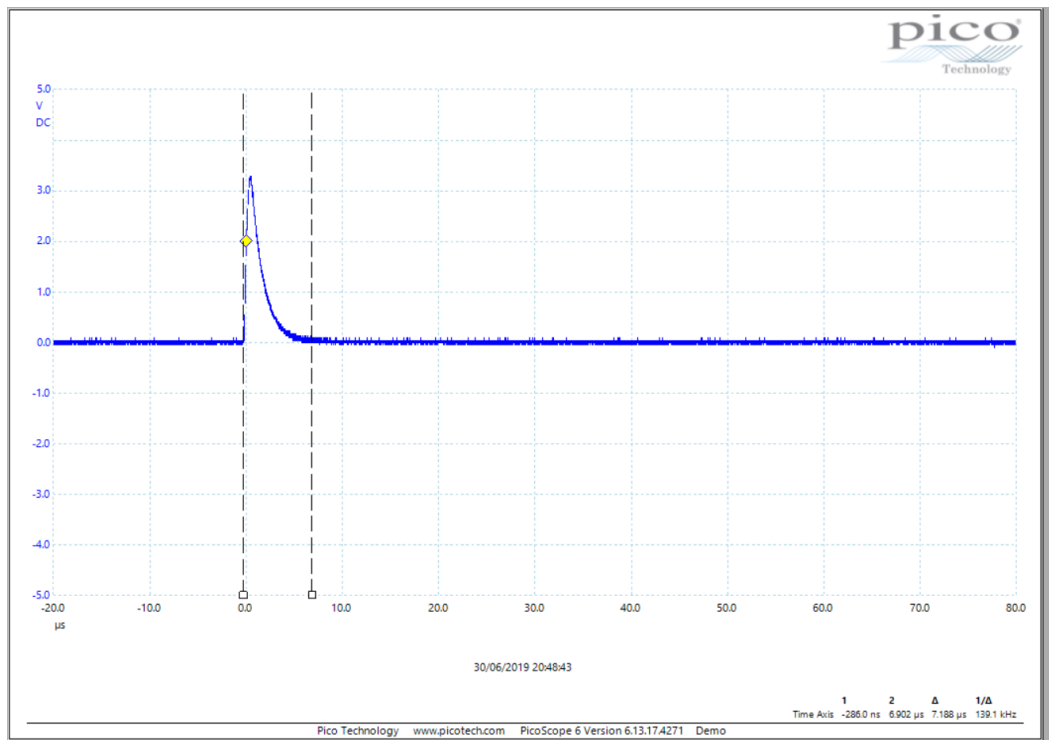
Fig. 5.12 Positive Set-Reset Pulse

The risetime of the waveform is defined by Nise [52, p.181] as "..the time for the waveform to go from 0.1 to 09 of its final value".

The scope used to measure the waveform in Fig. 5.12 has a feature to measure the rise time, this was measured as 440 ns. The fall time of the waveform in Fig. 5.13 was similarly measured using the scope feature as 1.528 μs. The difference in the values is due to the different time constants in the RC legs of Fig. 5.9 used in the set-reset circuit.

Williams and Taylor in [53, p.33] derive an approximation to relate rise time to bandwidth as:

$$T_r = \frac{0.35}{f_r} \tag{2}$$

Where: T_r is the rise time in seconds and f_r is the *3-dB* cut off in hertz.

T_r = 440 ns for the rise time of the positive set-reset pulse

$$f_r = \frac{0.35}{440.\,10^{-9}}$$

$$= 0.79 \text{ MHz}$$
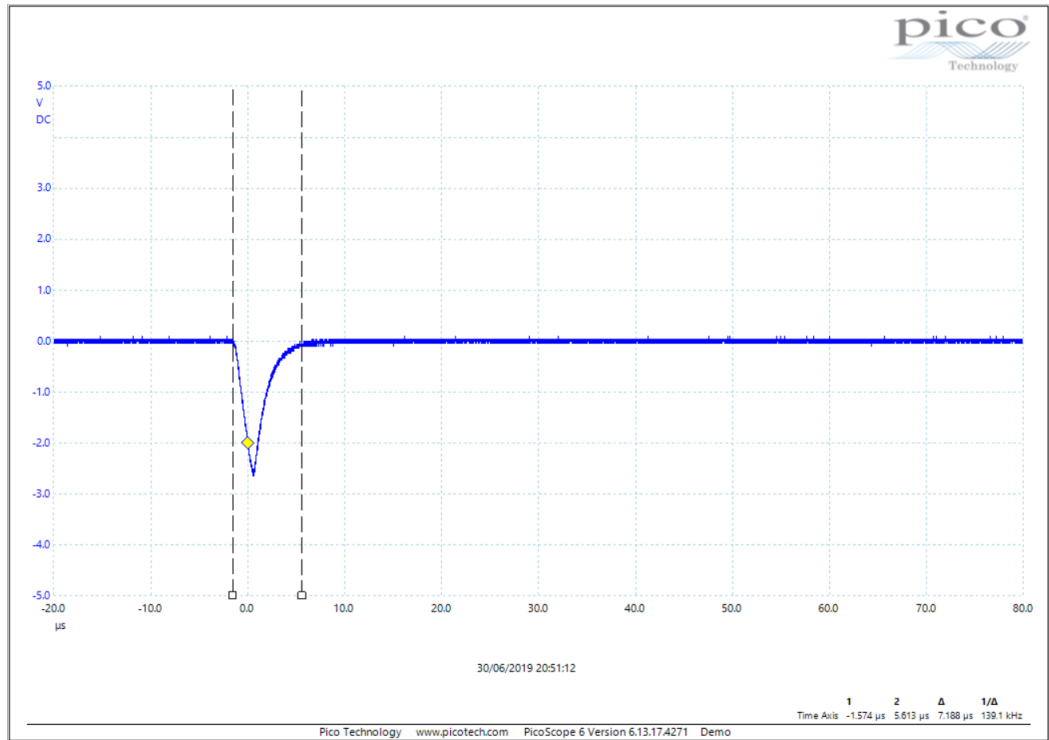
Fig. 5.13 Negative Set-Reset Pulse

T_r = 1.528 µs for the fall time of the negative set-reset pulse

$$f_r = \frac{0.35}{1528.\,10^{-9}}$$

$$= 0.23 \text{ MHz}$$

The oscilloscope used to take capture the waveforms has a bandwidth of 50 MHz. Although equation (2) is an approximation, the figures obtained for the cut-off frequency are well within the limits of the oscilloscope bandwidth and can be considered an accurate representation of the set and reset pulses produced by the circuit implementation.

5.1.1.6 Relay Module

This is to comprise an 8 channel 5 volt relay module to be driven by an Arduino Mega 2560 microprocessor that will drive relays via its input/output ports to simulate the detection operations that take place during normal operation of the circuits.

The relays are driven via optocoupler from the Arduino board. A separate supply is provided for the relay coil circuit which is a simple transistor drive circuit.

5.1.1.7 Test Loads

The test loads consist of 100 Ω 50 Watt aluminium housed axial wire wound panel mount power resistors. They are mounted in parallel to provide loads of 50 Ω with 100 watts power rating. These values were chosen to allow bench power supply voltages to drive the DC current values required for testing.

The loads are resistive to reflect the loads that the site controller detection inputs provide in the real world system.

5.1.2 ACCELEROMETER TEST APPARATUS

The test bed consists of a linear actuator with a stroke length of 100mm and a maximum no-load speed of 18 mm/sec; it is controlled via a linear actuator control card providing an interface to a microcontroller. The position of the actuator is controlled via the RC (Radio Control) input to the linear actuator control card. The position of the actuator is proportional to the width of an electrical pulse applied to the RC input, although this is a form of pulse width modulation, it differs in that the position of the actuator is not proportional to the percentage duty cycle of the PWM signal. The body of the actuator is fixed by its clevis and clamps to the test bench, the accelerometer is attached to the actuator rod.

The position pulse for the linear actuator control card is provided by an analog output pin from an Arduino Mega 2560 microprocessor board.

The output from the accelerometer is in the form of a voltage relevant to ground for each of the three axes. These outputs are connected to three analog pins of an Arduino Uno microprocessor board.

The bench testing aims to give an indication of the signals that are produced by the accelerometer output for the various points throw scenarios.

5.1.2.1 Accelerometer

The accelerometer to be used for bench testing is the Analog Devices ADXL335. It is a low power 3-Axis +/- 3 g accelerometer mounted on a breakout board. Its main applications according to the manufacturer's data sheet [54], are in measuring dynamic acceleration resulting from motion, shock or vibration. When considering its use for future field testing it has a shock survival rating of 10,000 g.

However, Liu and Markine [45, p.3] in their work on rail crossing degradation found values of up to 150 g measured at point cross-overs. Although the accelerometer is suitable for bench demonstration of acceleration forces when the point tips move it only has a range of +/- 3 g so would not be considered for future field testing applications. It has a high survival rating but would not provide the range for measurement of acceleration forces for both point moves and during the passage of a train.

The data sheet states that the device construction as, "The sensor is a polysilicon surface micro-machined structure built on top of a silicon wafer." [54, p.10]. It goes on to describe the operating principle as being a suspended moving mass; the movement of this mass due to acceleration unbalances the output of differential capacitor plates. This results in the sensor output being proportional to acceleration. The sensor output is then subject to phase-sensitive demodulation techniques. The functional block diagram of Fig. 5.14 illustrates the system layout.
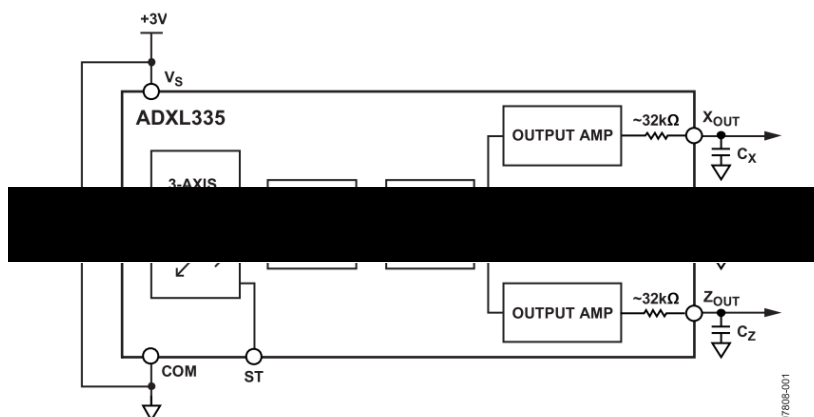
Fig. 5.14 Manufacturer functional block diagram of ADXL335 [54, p.1]

The bandwidth of the unit is chosen by making use of Cx, Cy and Cz capacitors at the Xout, Yout and Zout pins. These capacitors are added to provide low-pass filtering for antialiasing and noise reduction purposes. The bandwidth is selected depending on the application. The accelerometer used for the bench test is mounted on a breakout board and has capacitors of 0.1 µF mounted on the breakout board; according to table 5 in the manufacturer's data sheet this value of capacitor results in a bandwidth of 50 Hz. The filtering is to improve measurement resolution and helps prevent aliasing [54, p.10], the bandwidth is suitable for the comparatively slowly changing acceleration forces encountered in the point move bench top demonstration, but would not be suitable for measuring the quickly changing acceleration forces encountered from rail discontinuities during the passage of a train in the field.

5.1.2.2 Linear Actuator

The device used for the test bed is a miniature linear actuator. They have position feedback from an internally mounted potentiometer. The test bed application does not drive any load other that the accelerometer mounted on the moving clevis. This load can be considered to have no effect on the no-load maximum speed of the device quoted as 18 mm/s in the manufacturer's data sheet [55].

The actuator was controlled by an Actuonix Linear Actuator Control card which is a 'stand-alone closed-loop control board specifically designed for Actuonix actuators' [56].

5.2   DETECTION CIRCUIT CURRENT MEASUREMENT

The first attempts at setting up bench testing of the AMR sensors involved fixing a current carrying conductor to a sensor head and using a bridge offset amplifier to provide an output voltage corresponding to the DC current flowing in the conductor. The sensitivity of the sensor meant that varying the orientation of the sensor in space provided variation in the output, even where the sensor was oriented provided for change in the output voltage. Placing a fridge magnet on the sensor sent the output to the operational amplifier rail voltage. This indicated that the sensor was working, but that the measurement techniques and circuits in the application notes might not be as straightforward as expected. The variation in observed output was changed in orientation relative to the earth's magnetic field

and the variation with position due to the change in flux density caused by focussing of the magnetic field by local metalwork such as the test bench metal frame or power supplies on the bench above the test bench. Early apparatus set up used a sensor attached to a conductor in a fixed position just to develop the amplifier circuits and try variations on sensor and operational amplifier rail voltages. Based on these early attempts the test equipment and application was then developed and built as described in the following sections.

5.2.1 MULTIPLE SENSOR TEST BED

The test was carried out with the multiple sensor test bed as shown in Fig. 5.3 within section 5.1.1.2. Only one sensor was tested at any one time. The test layout is represented in Fig. 5.15.

The test bed was placed in the same position on the test bench for the different sensors under test. The first test on sensor 1 was carried out with the AMR sensor bridge amplifier as illustrated in Fig. 5.16; note that the values of *R5* and *R6* are not as recommended in the manufacturer data sheet [41], which is 4.99 kΩ. the resistors were changed to 2 kΩ to provide a larger gain at V_{out}. A 10 kΩ potentiometer represented by *R11-R12* in the circuit is used to offset the input to the amplifier stage to produce an output voltage of 2.5 volts with zero current flowing in the test conductor circuit. This is used to offset the fact that the bridge resistive elements are not perfectly matched.
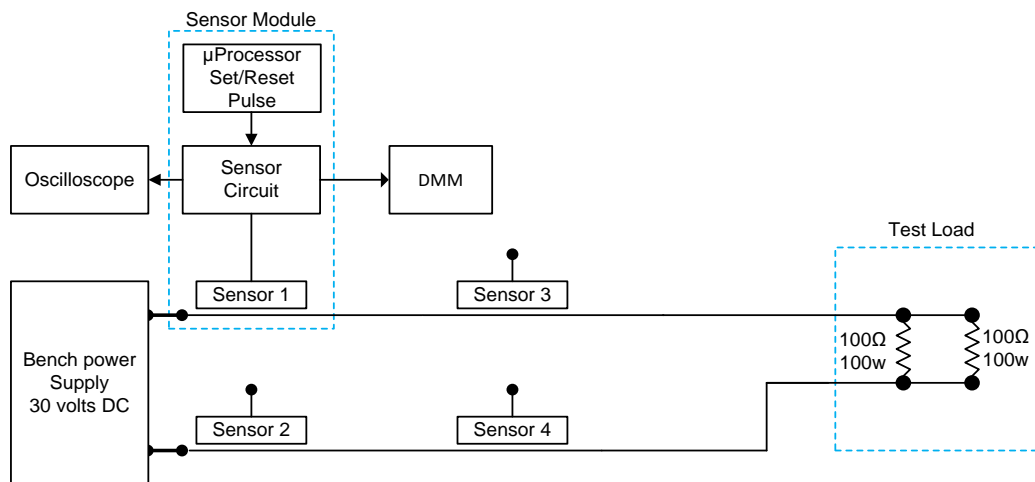
Fig. 5.15 Multiple sensor array test layout

Table 5.1 Multiple Sensor Test Equipment

Equipment	Description
Power Supply-Single 0-30 V DC 0-3 Amps	ISOTECH303DD DC Power Supply
Sensor Circuit	See Fig. 5.16
Sensor	HMC1021 1-Axis magnetic sensor
Set-Reset Timing Circuit (µProc)	Arduino Mega2560
Oscilloscope	PicoScope 2406B PC oscilloscope 4 Channel 50 MHz bandwidth 500 MS/s
Voltmeter (DMM)	RS Pro IDM99 IV digital multimeter
Load	50Ω (2 x 100Ω) 50 W resistors in parallel)

A DC current range from -120 to 120 milliamps in steps of 10 milliamps was passed through the conductor and the output of the sensor circuit measured. This was with a voltage of 5 volts applied across the bridge and a rail to rail voltage of +/- 5 volts applied to the operational amplifier circuit.

The results were recorded in Table A.1.1 and are plotted as the "Low Gain" series in Fig. 5.18.
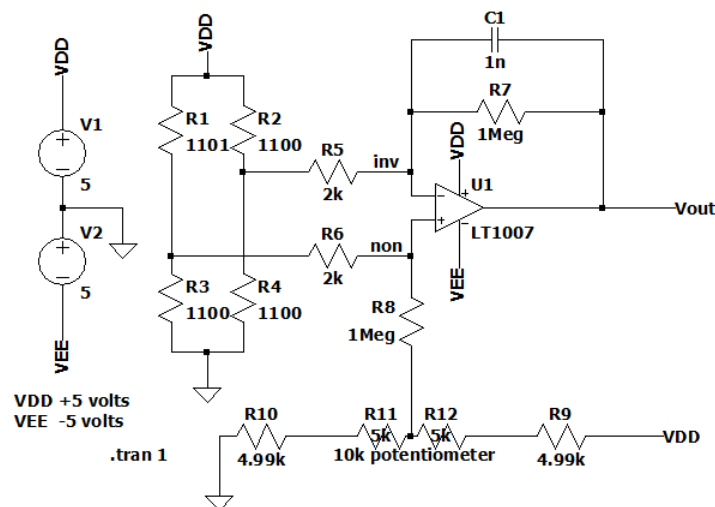
Fig. 5.16 Multiple sensor test bed test 01 amplifier circuit

A second test was carried out on sensor 1 but this time the values of *R5* and *R6* were both changed to 1 kΩ to provide for a larger gain at V_{out}. The test method used was identical other than the change to the input resistors *R5* and *R6* of the bridge amplifier circuit and the resolution of the DMM used as a voltmeter to record the amplifier output was changed, this was to enable measurement of the voltage to 3 significant places. The output was a voltage approximately in a range between 2.300 to 2.750 volts DC.

The results were recorded in Table A.1.1 and are plotted as the "High Gain" series in Fig. 5.18.
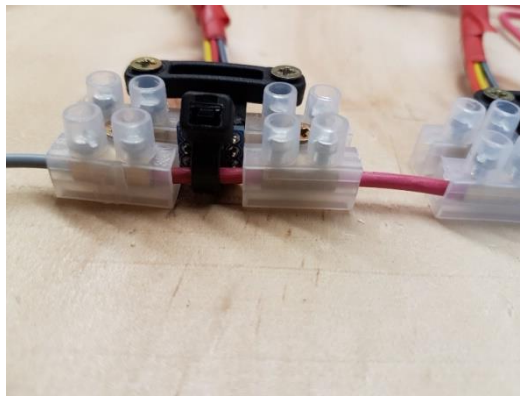
Fig. 5.17 Sensor Head

The close up of the sensor head shown in Fig. 5.17 showing the proximity of the fixings to the sensor head, which is located just left of centre between the terminal connectors. All sensor units for this test layout were fixed in the same manner. Their location in relation to each other is shown in Fig. 5.3 in section 5.1.1.2.
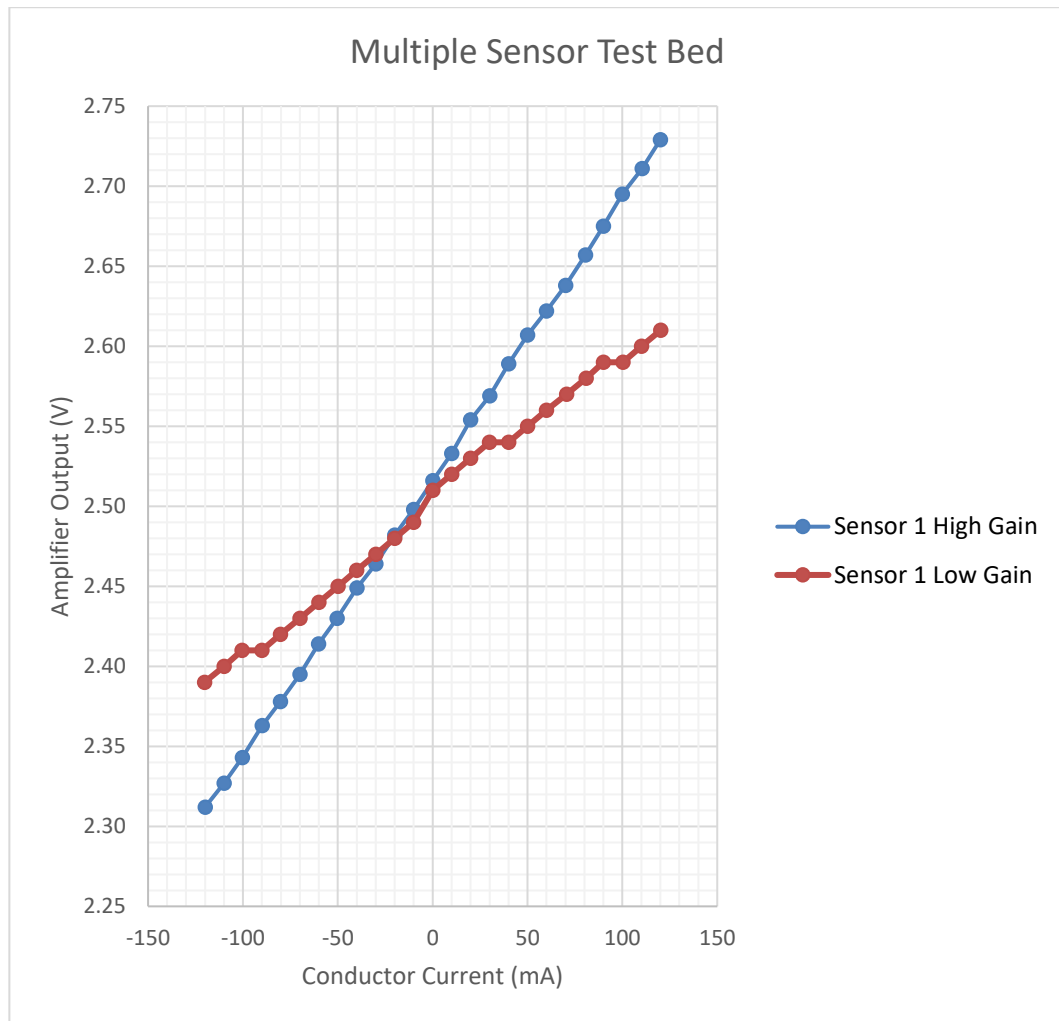
Fig. 5.18 Multiple sensor 1 test bed results

The multiple sensor test bed results for sensor 1 are illustrated in Fig. 5.18. The two traces consist of a high gain bridge amplifier configuration and a low gain bridge amplifier configuration. The current flowing in the conductor that forms part of the test circuit is plotted against the resistive bridge output voltage *Vout*.

The input to the bridge amplifier circuit was adjusted to 2.5 volts at the non-inverting amplifier input by use of potentiometer (*R11*, *R12*). This was to allow for the offset in resistive bridge values of resistance due to limitations in producing exactly equal resistive elements at the manufacturing stage.

The tests for high gain and low gain were then repeated with sensor 3 connected to the bridge amplifier circuit in place of sensor 1. Once again the non-inverting input to the amplifier was adjusted to 2.5 volts which is half of the 5 volts across

the resistive bridge. The results were recorded in Table   A.1.2 and are plotted as "High Gain and "Low Gain" in Fig. 5.19 Multiple sensor 1 and sensor 3 test bed results.
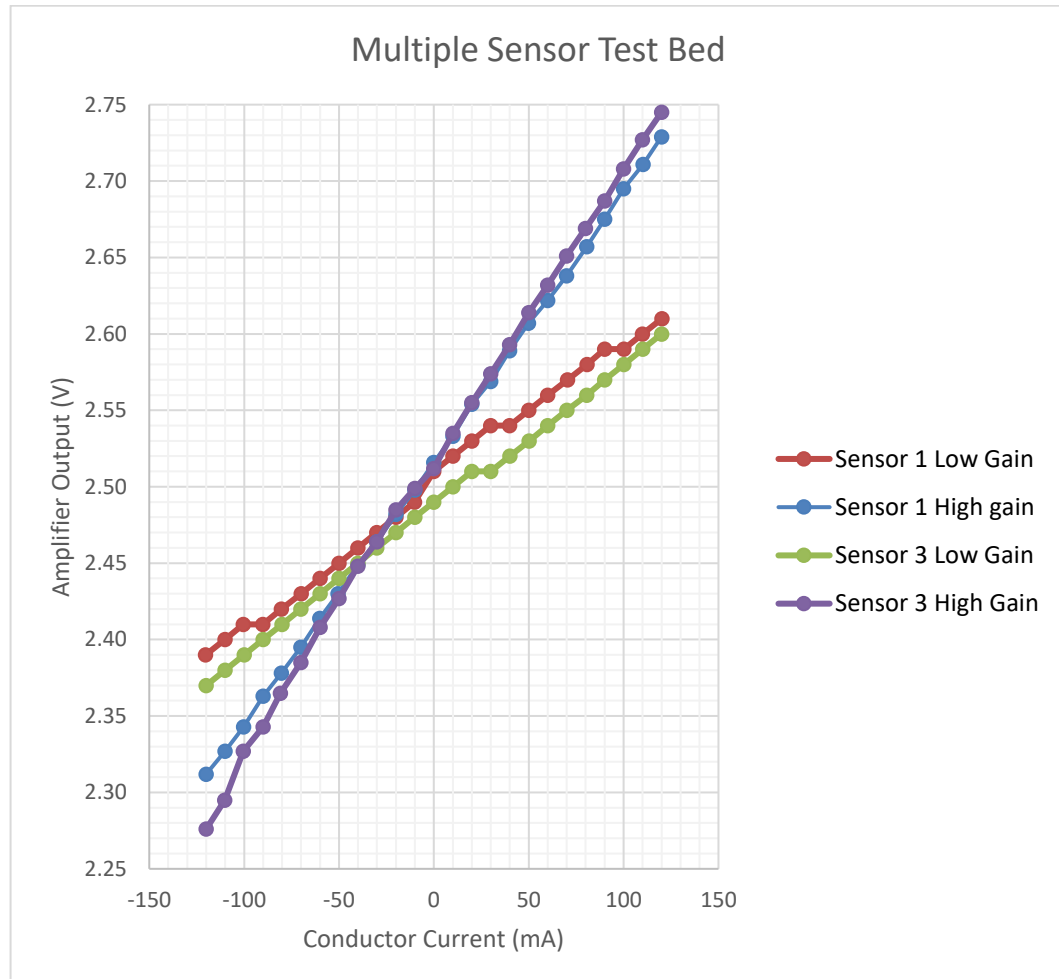
Fig. 5.19 Multiple sensor 1 and sensor 3 test bed results

The plots in Fig. 5.19 are those for sensor 3 combined with the results from sensor 1. They show the results for high and low gain circuit configuration for both sensors.

It can be seen from the plot for sensor 1 shown in Fig. 5.18 that there is a difference in the gain of the bridge amplifier circuit between high gain and low gain as expected.

The amplifier part of the circuit of Fig. 5.16 is a classic differential operational amplifier circuit [57, p.184]; such a basic circuit is shown in Fig. 5.20.
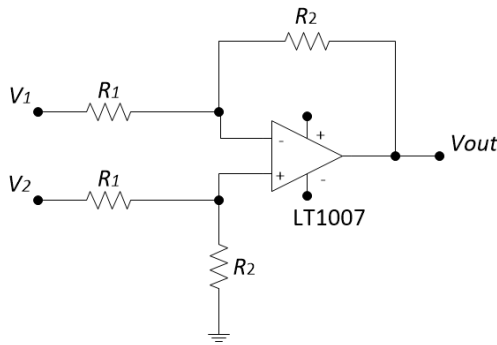
Fig. 5.20 Differential operational amplifier circuit

$$V_{out} = \frac{R_2}{R_1}(V_2 - V_1) \tag{3}$$

The expression for V_{out} is given by:

With values of resistance R_1 = 4.99 kΩ and R_2 =1 MΩ the value of V_{out} is:

V_{out} = (1 x 10^6) / (4.99 x 10^3) = 200($V_2 - V_1$)

These values of resistance result in any differential voltage appearing across the input (V_1 and V_2) of the operational amplifier will have a gain of 200 at V_{out}.

When the value of R_1 is changed to 2 kΩ the value of V_{out} is:

V_{out} = (1 x 10^6) / (2 x 10^3) = 500($V_2 - V_1$)

This results in the operational amplifier circuit having a gain of 500 at V_{out}.

The resistive element bridge circuit of Fig. 5.16 indicates the values of R1, R2, R3 and R4 as being 1100 Ω as stated in the manufacturer's data sheet as the value of a perfect resistive element. In practice the value of resistive element can be up to 1 Ω different to another element.

If the elements were exactly equal then the differential inputs to the operational amplifier would be equal. The value of the output V_{out} would be set by the bias circuit composed of R9, R10 and potentiometer represented by R11-R12 would not be required if resistors R9 and R10 were high precision resistors.

The resistive elements are not equal and the resistive bridge elements are not equal. Potentiometer represented by *R11-R12* is required to adjust the input voltage at the non-inverting terminal of the op-amp to a voltage of 2.5 volts at Vout with respect to ground.

The range of sensor 1 for the low gain circuit is:

Range of current flowing in conductor = 120.2 – (-120.3) = 240.5 mA

Range of amplifier output volts = 2.610 – 2.390 = 220 mV

Giving a low gain sensitivity for sensor 1 of: 220 / 240.5 = 0.91 mv/mA

The range of sensor 3 for the low gain circuit is:

Range of current flowing in conductor = 120 – (-120) = 240 mA

Range of amplifier output volts = 2.600 – 2.370 = 230 mV

Giving a low gain sensitivity for sensor 3 of: 230 / 240 = 0.96 mv/mA

The circuit components *R5* and *R6* were then changed to increase the gain while still being able to adjust the offset for the nominal zero current flowing in conductor to be 2.5 volts.

The range of sensor 1 for the high gain circuit is:

Range of current flowing in conductor = 120 – (-120) = 240 mA

Range of amplifier output volts = 2.729 – 2.312 = 417 mV

Giving a high gain sensitivity for sensor 1 of: 417 / 240 = 1.74 mv/mA

The range of sensor 3 for the high gain circuit is:

Range of current flowing in conductor = 120 – (-120) = 240 mA

Range of amplifier output volts = 2.745 – 2.276 = 469 mV

Giving a high gain sensitivity for sensor 3 of: 469 / 240 = 1.95 mv/mA

From Fig. 5.18 it can be seen that the plots are linear over the test range, the plot for the high gain being considerably straighter than that for the low gain. This is accounted for by the use of a meter capable of only measuring to two significant places for the low gain plot. The meter was changed out for one with resolution to three decimal places.

The amplifier voltage output with no current flowing in the test conductor is above 2.5 volts (approximately 2.515 volts) for both plots. The apparent difficulty with adjusting for an offset closer to 2.5 volts is due to the limited number of turns over the range of the 10 kΩ potentiometer used in the offset branch of the amplifier circuit.

It was noted that when sensor 3 was set up that the potentiometer need considerable adjustment to produce a value of 2.5 volts at V_{out}.

The test was repeated for the other three sensors, and the output was linear for each sensor. It was noted that the different amount of offset adjustment require for each sensor. Even when considering the offset to be expected from the resistive elements of the sensor being mismatched slightly at point of manufacture the offset adjustment was considerable.

When choosing a fixing method for the sensors to the test circuit cable the aim was to get consistency as far as possible without using a bespoke fixing at this stage of testing. Cable connector blocks were used to clamp the cable to the test bed and a cable tie used to fix the cable to the sensor centrally in relation to the face of each of the chips. It was noted that when removing the screws that fixed the connectors to the test bed that there was a lot of variation in the op-amp output voltage when the screwdriver head was moved around in the vicinity. Even moving one of the small fixing screws (10mm long) close to the sensor caused notable variation in the output.

The fixing methods were consistent for each of the four sensors but the fixings in close proximity to the sensors appear to have been focussing the local ambient magnetic field such that the position of each sensor on the bench produced very different offsets in the results.

This was a first attempt at fixing the sensor to the cable and indicated issues with this approach to obtaining test data. The range of results was such that a different approach to sensor attachment and orientation to the ambient magnetic field was

required. What was encouraging was that sensitivity of the sensor was meeting expectations and that linearity of the sensor output was maintained, even with comparatively high offset values given at the output of the op-amp circuit.

5.2.2 NON SHIELDED ENCLOSURE

The test configuration for non-screened enclosure was set up as shown in Fig.5.21. There are two distinct circuits that make up the configuration: the load circuit and the detection circuit.
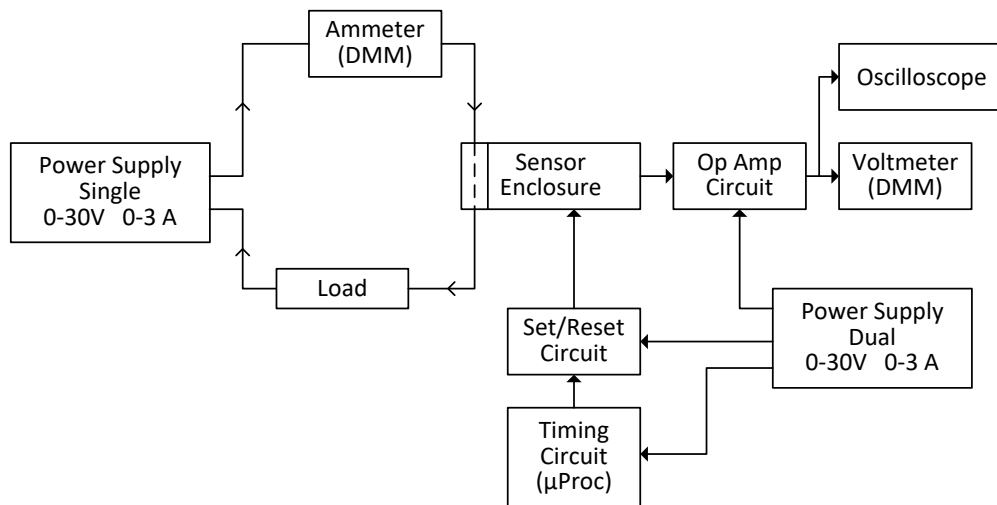
Fig. 5. 21 Sensor enclosure test layout schematic

The load circuit is comprised of a DC power supply supplying a resistive load via a digital multimeter set up as an ammeter to measure milliamps. The conductor supplying the load is connected to the sensor enclosure. The conductor passes through the sensor as described in section 5.1.1.3. There is no electrical connection between the load circuit and the detection circuit.

The detection circuit consists of the sensor enclosure containing the HMC1021 AMR sensor; the leads from the sensor resistive bridge are brought out to the input stage of the operational amplifier circuit, the sensor set/reset leads are connected to the circuit that provides the pulses that enable the sensor set/reset process. The timing for the set/reset circuit is provided by a pulse provided from the digital output pin of a microprocessor board. The output from the operational amplifier is fed to a digital multimeter set to read down to a millivolt level. The operational amplifier output is also fed to an oscilloscope in order to observe the correct operation of the set-reset pulses when they are applied. The feed to the sensor application circuits is provided by a dual output power supply to enable the operational

amplifier circuit to operate with a negative rail supply. The circuits are implemented using breadboards and jumper wires.

Table 5.2 Non screened enclosure test equipment

Equipment	Description
Power Supply-Single 0-30 V DC 0-3 Amps	ISOTECH303DD DC Power Supply
Power Supply-Dual 0-30 V DC 0-3 Amps	Velleman LABPS23023 DC Power Supply
Ammeter (DMM)	RS Pro IDM99 IV digital multimeter
Sensor Enclosure	Non screened HMC1021 AMR Sensor Enclosure
Op Amp Circuit	See Fig. 5.16
Set-Reset Circuit	See section 5.1.1.5
Timing Circuit (µProc)	Arduino Mega2560
Voltmeter (DMM)	RS Pro IDM 99 IV
Load	50Ω (2 x 100Ω) 50 W resistors in parallel)
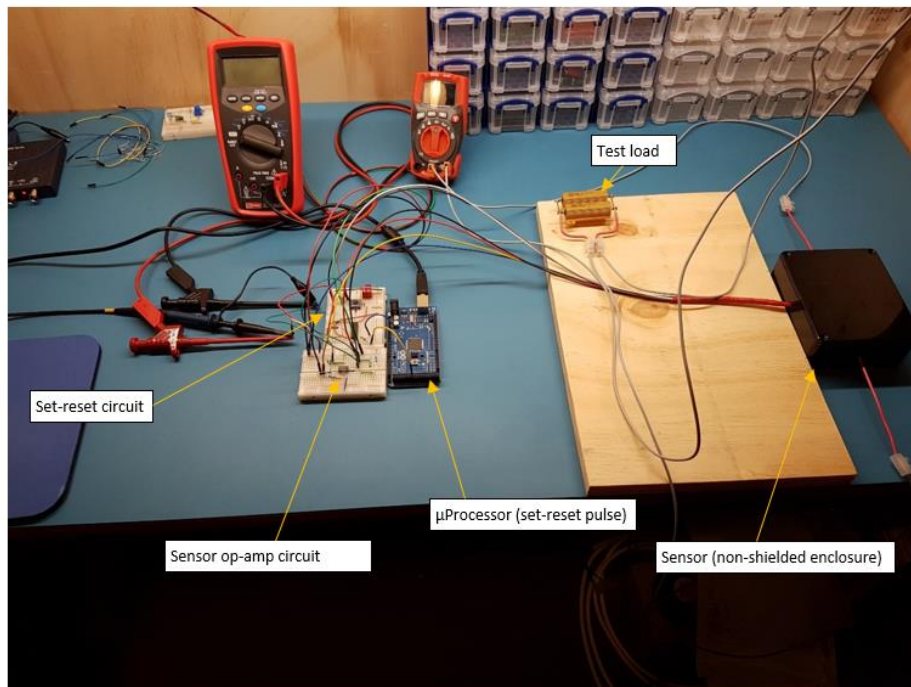
Fig. 5.22 Sensor enclose test layout

The positioning of the sensor was marked and kept consistent for all testing involving the enclosure cases. The bench above the test area did not have any equipment, consisting of power supplies and meters, moved or added during the testing. This was done to attempt to provide consistency in the test environment with regard to stray magnetic fields.

The resistive bridge and operational amplifier circuit are as shown in Fig. 5.23 for this set of tests. The values of components are as recommended in manufacturer's application sheet [41]. The circuit has sensor resistive elements (*R1*, *R2*, *R3* and *R4*) with values of 1100Ω each, which is the typical value given in the product data sheet. In practice a key part of the AMR sensor production is matching of the bridge elements to within 1Ω of each other. This test did not use a potentiometer network at the non-inverting amplifier input.

There has been no attempt at balancing the input offset for this test. The *R9* and *R10* resistors set the non-inverting input at 2.5 volts within the limitations of the 1% tolerance resistors used for the circuit implementation.
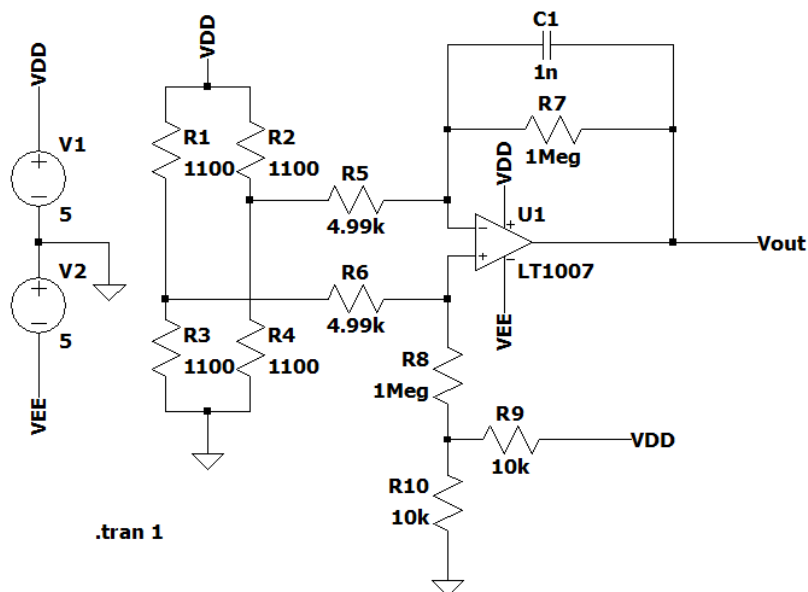
Fig. 5.23 AMR Bridge and Op Amp Circuit 01 (adapted from [41, p.13])

Two sensors were used for the test; they were marked as sensor 1 and sensor 2. The design of the enclosure made for easy swapping out of the sensors while

maintaining the comparative uniformity of the sensors in relation to the conductor. The position and orientation of the enclosure was maintained throughout the tests.

The test involved varying the voltage applied in order to vary the conductor current between -120 mA to +120 mA in approximately 10 mA steps using the power current supply display as the indicator for the steps in the circuit current; this was considered sufficient to provide the stepped input as the parameters being plotted were the conductor current and the operational amplifier output. These were both measured using digital multimeters. The power supply output leads were reversed to observe and record the measurements for reverse conductor current.

The current in the load circuit was observed and recorded against the output voltage of the operational amplifier at each 10 mA step. The results are recorded in the appendices in Table A.2.1 for sensor 1 and Table A.2.4 for sensor 2. The results were plotted in Fig. 5.24.
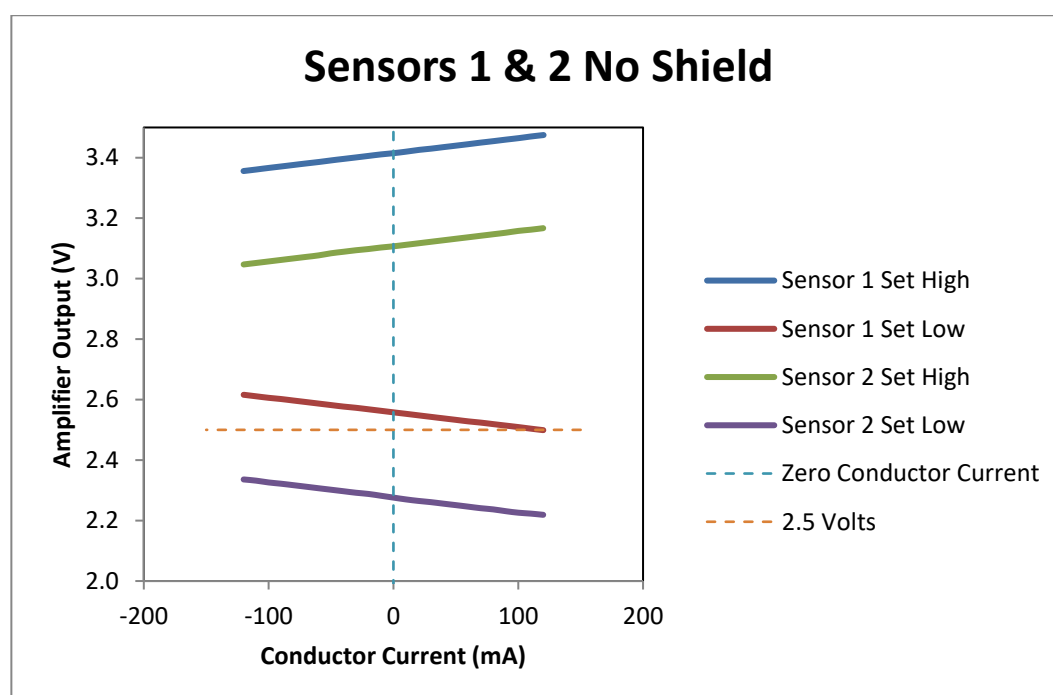
Fig. 5.24 Sensors 1 & 2 no shield

The set high and low refer to the set-reset being applied to the sensor and the readings taken when the operational amplifier output was low or high after application of the set-reset pulse. The levels low and high were maintained at their respective level to obtain the test results for each state.

Initial observations are that the sensors provide a linear output whether they are set high or low. The "set high" plots for sensor 1 and 2 appear to be parallel and indicate that the sensitivity in mV/mA appears to be the same for each sensor. The same applies to the "set low" plots. As can be seen from the plots the slope of the plots is inverted for set low and set high, this is as expected due to the reversal of the magnetic domains in the magneto-resistive elements as described in section 4.5.1.

The plots indicate neither of the sensors produces an operational amplifier output voltage of 2.5 volts for zero current flowing in the conductor. If the sensor resistive elements were perfectly matched; the operational amplifier resistors were of very close tolerance and there was no effect from external magnetic fields incident on the sensor then the output would be 2.5 volts for zero current flowing.

The "set high" plots and the "set low" plots appear to have the same linear response but with a different offset.

In order to investigate whether the response of each sensor was the same considering the offset; the values of the sensors were multiplied by their difference at a value of zero conductor current flowing in the test conductor.

Taking the value of V_{out} for sensor 1 set high from Table   A.2.1   is 3.415 volts with zero current flowing in the test conductor; and the value for sensor 2 set high from Table   A.2.4 is 3.107 volts at zero current.

Offset for set high condition between sensor 1 and sensor 2 at zero test conductor current is:

3.415 – 3.107 = 0.308 volts

This value of offset is then added to the values of V_{out} obtained for sensor 2.

The same exercise was carried out for the set low results and for set low condition the offset between sensor 1 and sensor 2 at zero test conductor current is:

2.558 – 2.276 = 0.282 volts

The results of these additions are shown in Table   A.2.6.

They have been plotted in Fig. 5.25 and show clearly the gain of the response is the same for the range of measurements undertaken between -120 mA and +120 mA. This applies to both the set high and set low conditions.
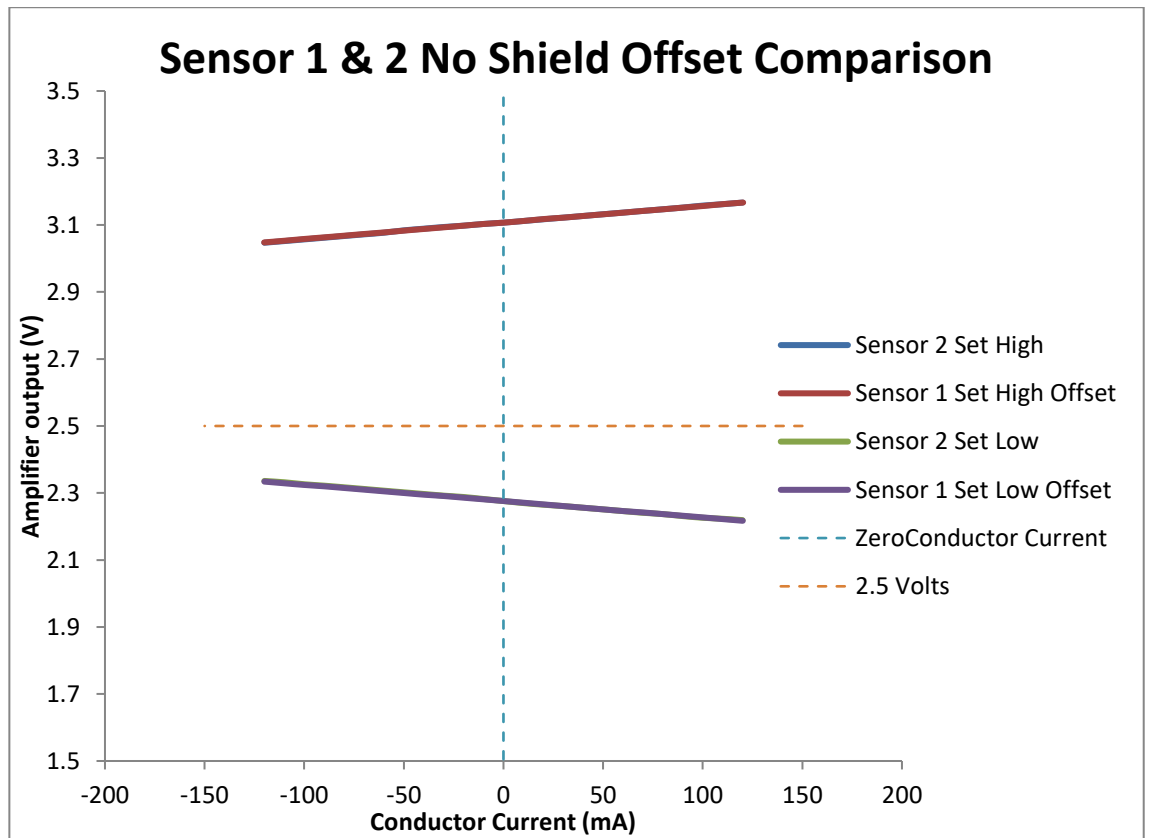
Fig. 5.25 Sensor 1 and sensor 2 non-shielded offset comparison

5.2.3   SHIELDED ENCLOSURE

This test method was identical to the tests for Sensors 1 and 2 with no shield described in previous section, except that the sensor enclosure was swapped for one with a single layer magnetic shield. The results are recorded in appendix A in Table   A.2.2 for sensor 1 and Table   A.2.5 for sensor 2. For this set of tests, the results have been plotted for the individual sensors in Fig. 5.26 and Fig. 5.27.
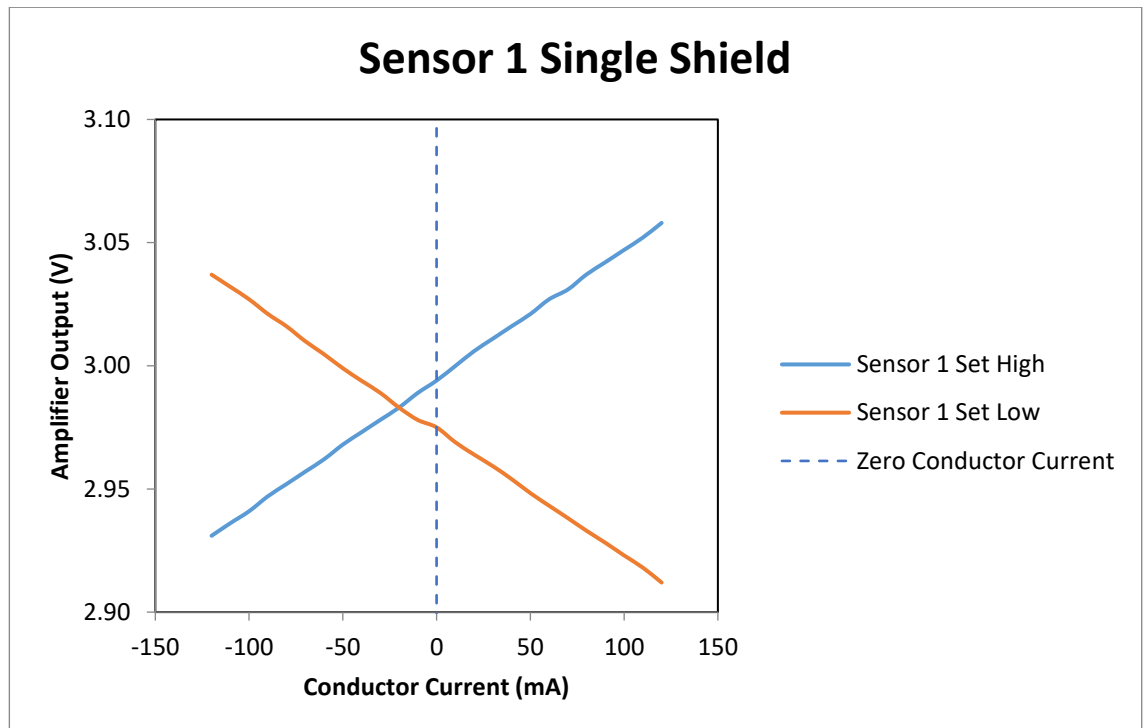
Fig. 5.26 Sensor 1 single shield

The plots of Fig. 5.26 show the set high and set low values for sensor 1 in a single shielded enclosure. A plot for a value of zero conductor current has been constructed to provide a reference.

It is apparent from the plots of Fig. 5.26 that the addition of a single shield has had an effect on the magnetic field measured by the sensor. In comparison with the plot for sensor 1 with no shield in Fig. 5.24 the values of amplifier output voltage with no current flowing in the conductor are much closer together after the set and reset pulses have been applied.

This indicates that the strength of the field measured by the sensor is less with the single shield in place. Note that the application of a set or reset pulse will align the magnetic domains in the sensor resistive elements in one direction or the other, but as soon as the pulse is removed the effect of any incident field on the sensor results in the output of the sensor reflecting the value of the applied field.
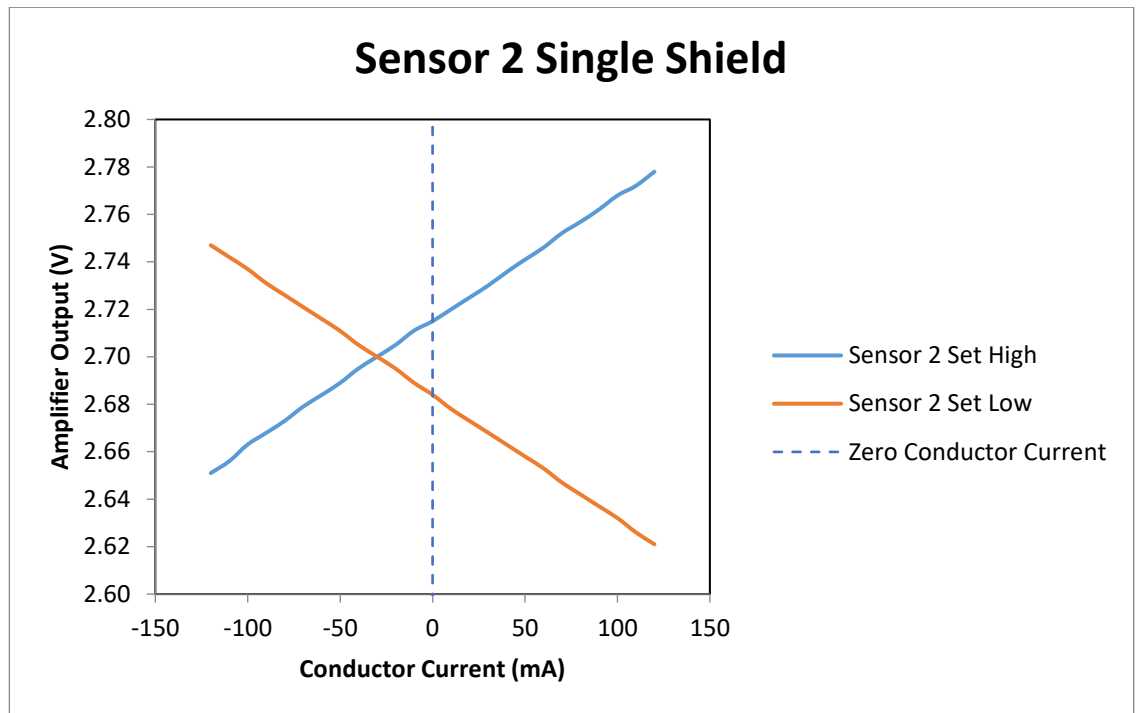
Fig. 5.27 Sensor 2 single shield

The plots of Fig. 5.27 show the set high and set low values for sensor 2 in a single shielded enclosure. A plot for a value of zero conductor current has been constructed to provide a reference.

The result for sensor 2 is similar to that for sensor 1 except that the offset output voltage is different. This is to be expected due to the manufacturing tolerances of the sensor resistive elements as described in section 4.5.1.

The single shield enclosure was swapped out for a double shielded enclosure and the test was repeated for sensor 1 only. The results are recorded in the appendix A in Table   A.2.3. The results have been plotted in Fig. 5.28 alongside the results for no shield and a single shield.
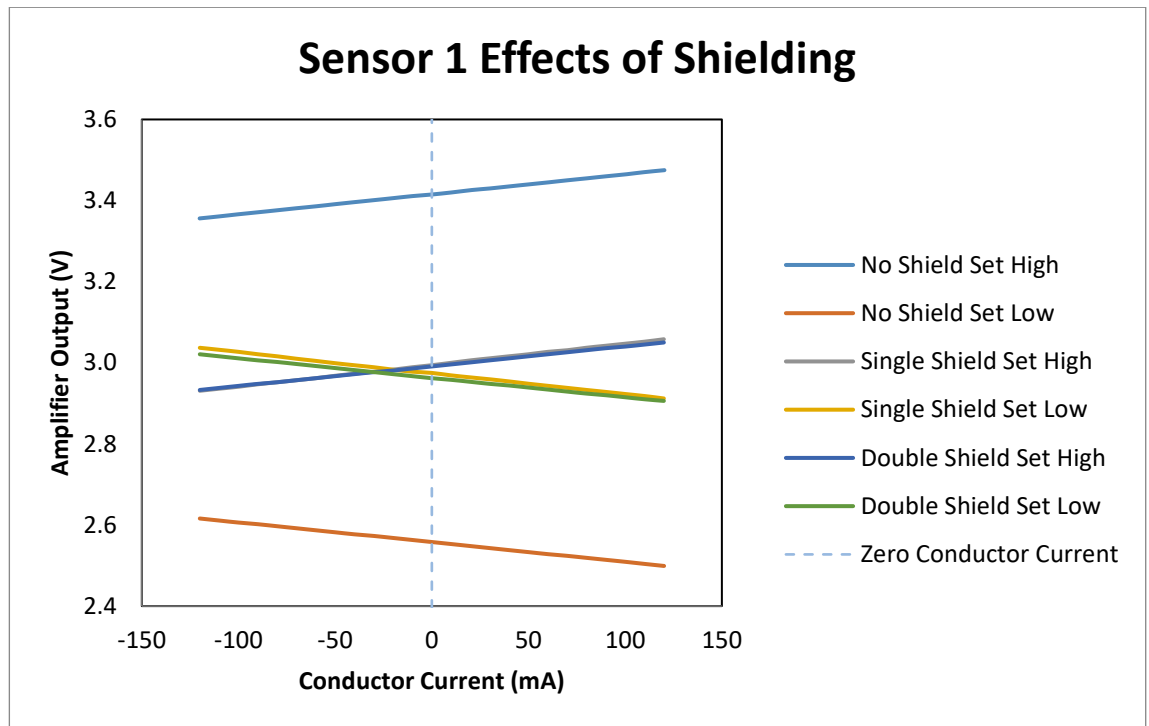
Fig. 5.28 Sensor 1 effects of shielding

It can be clearly seen from the plot of Fig. 5.28 that the effect of adding an additional screen of the same material and thickness does not change the results significantly compared to a single screen. There are slight differences in the plots for single and double screen; in particular, the single shielded set low and double shielded set low appear to have a different gain response. The difference in values of amplifier output voltage between a single and double shield set low at a conductor current of -120 mA is taken from Table A.2.2 and Table A.2.3 in appendix A :

Single shielded Sensor 1 set low output at -120 mA is 3.037 volts

Double shielded Sensor 1 set low output at -120 mA is 3.021 volts

This gives a difference of 16 mV.

There is a similar difference in response for the single and double shield set high, only in this case to a lesser extent.

The reason for the change in gain between single and double shielding may be accounted for by considering that any external field is concentrated in the shielding

material and the effects that the structure of the enclosure relative to the field has on the measurement.
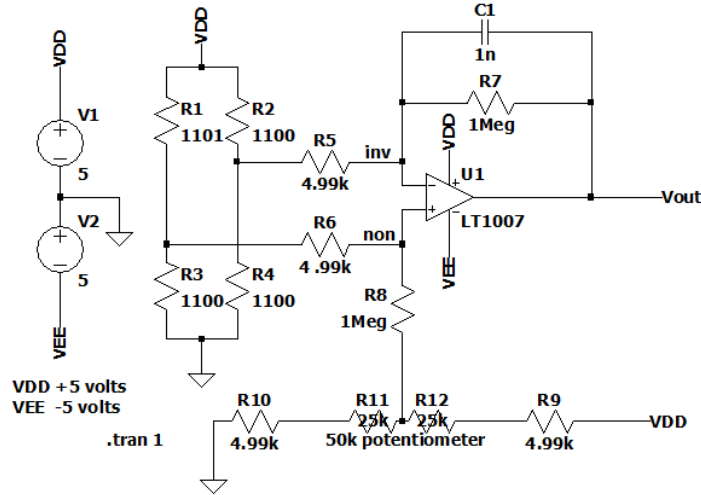
Fig. 5.29 Circuit double shielded fully offset low gain (adapted from [41, p.13])

The final tests undertaken with shielded enclosures were with a double shielded enclosure. The circuit is shown in Fig. 5.29, it is the same set up as used for the multiple sensor test bed shown in Fig. 5.16 other than; the adjustment of the offset for the sensor resistive bridge circuit makes use of a 50 kΩ high resolution potentiometer. This is to provide fine offset adjustment over a wider range, enabling adjustment of the zero current amplifier output voltage to be set at 2.5 volts DC.

The configuration in Fig. 5.29 is for the low gain output. The values of *R5* and *R6* were changed from 4.99 kΩ to 2 kΩ to provide a high gain output.

The values of *R5* and *R6* were again changed from 2 kΩ to 1 kΩ to provide a very high gain output

The values of V_{out} were recorded in Table   A.2.7 for both low, high and very high gain outputs. They were recoded for positive values of current in the range from 0 to +120 mA against amplifier output voltage; the results are plotted in Fig. 5.30.
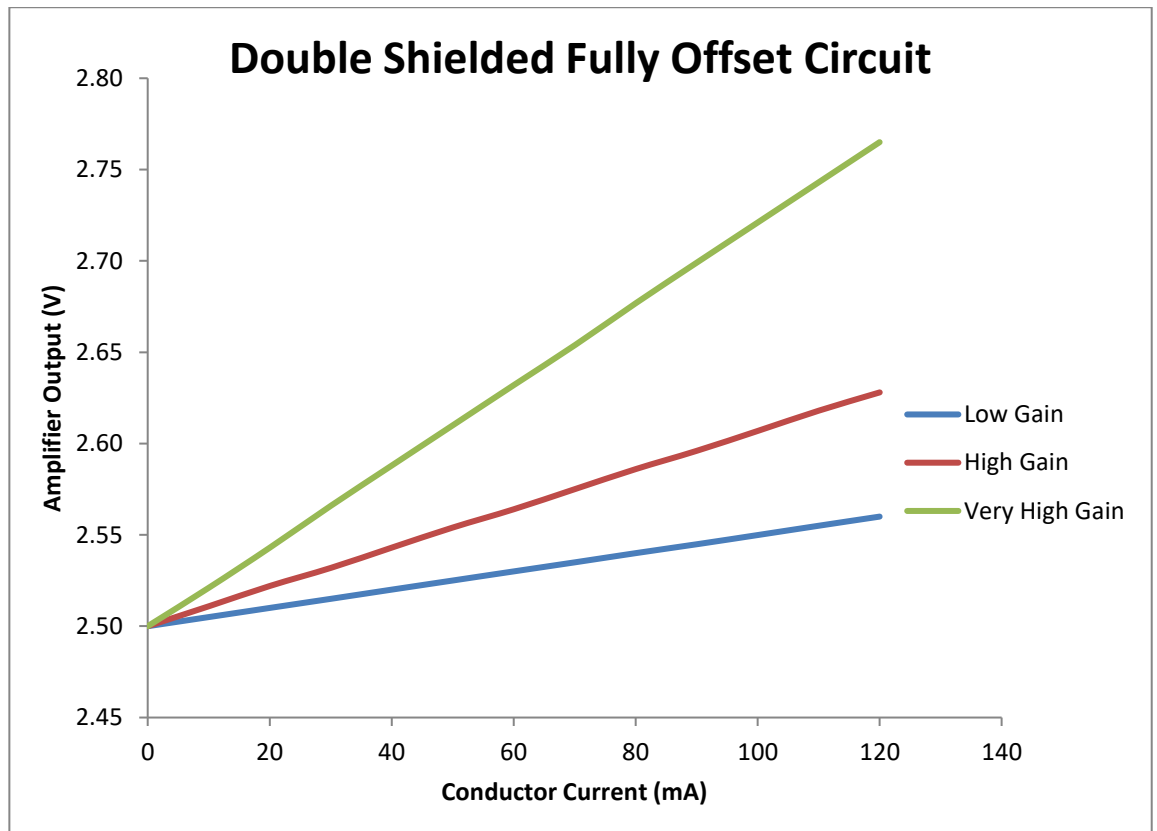
Fig. 5.30 Double shielded fully offset circuit

The plot clearly shows the linear response of the amplifier output for both low, high and very high gain.

For low gain, the sensitivity is given by:

Range of conductor current = 120-0 =120 mA

Range of amplifier output = 2.560 -2.500 = 60 mV

Giving low gain sensitivity of: 60 / 120 = 0.5 mV / mA

For high gain the sensitivity is given by:

Range of conductor current = 120 – 0 = 120 mA

Range of amplifier output = 2.628 – 2.500 = 128 mV

Giving high gain sensitivity of: 128 / 120 = 1.06 mV / mA

For very high gain the sensitivity is given by:

Range of conductor current = 120 – 0 = 120 mA

Range of amplifier output = 2.765 – 2.500 = 265 mV

Giving very high gain sensitivity of: 265 / 120 = 2.21 mV / mA

5.2.4 DETECTION CIRCUIT TEST BED

The test layout illustrated in Fig. 5.31 is used to simulate the switching and loading conditions of the detection circuit described in section 4.2.2 and section 4.3 that are used for safety critical point detection.

The aim of the tests is to prove that the sensors provide a response that can be used to carry out the analysis described in section 4.3. In particular the waveforms that provide data on the success or otherwise of the point moves.
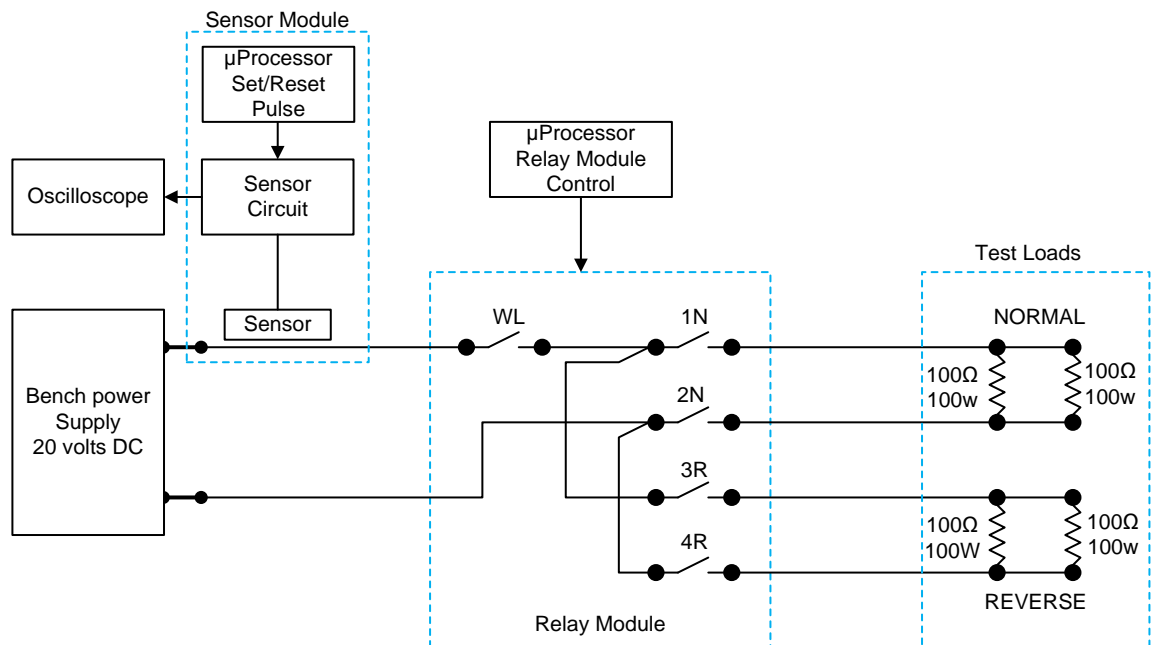
Fig. 5.31 Detection circuit test layout 01

The test set-up in Fig. 5.31 is set up to mimic the point detection circuit illustrated in Fig. 4.14. The relay module contacts are switched by the output pins of the relay module controller microprocessor.

Table 5.3 Detection Circuit Test Layout Equipment

Equipment	Description
Power Supply-Single 0-30 V DC 0-3 Amps	ISOTECH303DD DC Power Supply
Sensor Circuit	See Fig. 5.16
Sensor	HMC1021 1-Axis magnetic sensor
Relay Module control (μProc)	Arduino Mega2560
Oscilloscope	PicoScope 2406B PC oscilloscope 4 Channel 50 MHz bandwidth 500 MS/s
Relay Module	Sunfounder 5 volt 8 channel relay interface unit
Load	50Ω (2 x 100Ω) 50 W resistors in parallel)

The test bed layout is shown in Fig. 5.32; showing the relay module, test loads and relay module controller mounted on the board to the right of the picture. The double screened enclosure is to the extreme right.

The sensor module comprised of resistive bridge operational amplifier circuit mounted on a bread board are shown to the centre left together with the set-reset circuit mounted on a breadboard with associated pulse timing microprocessor.

The circuit has been built to accommodate further testing to capture variations in timing of the various contacts to simulate point operation and fault modes. However, the series of tests described below are undertaken to ascertain the capabilities of the sensor and sensor circuitry in capturing pulses of various durations and the integrity of the waveform produced.
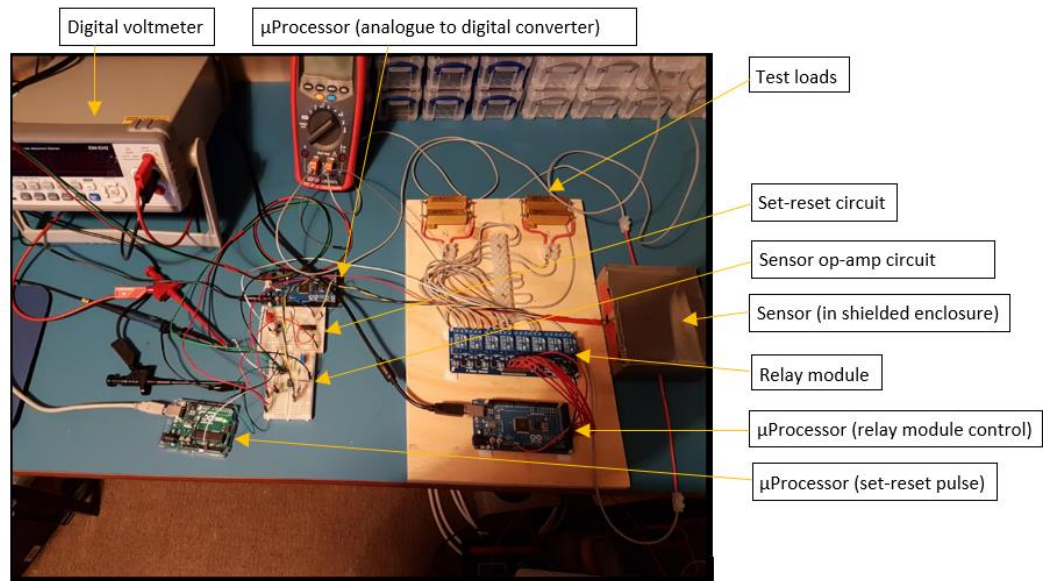
Fig. 5.32 Detection circuit test bed
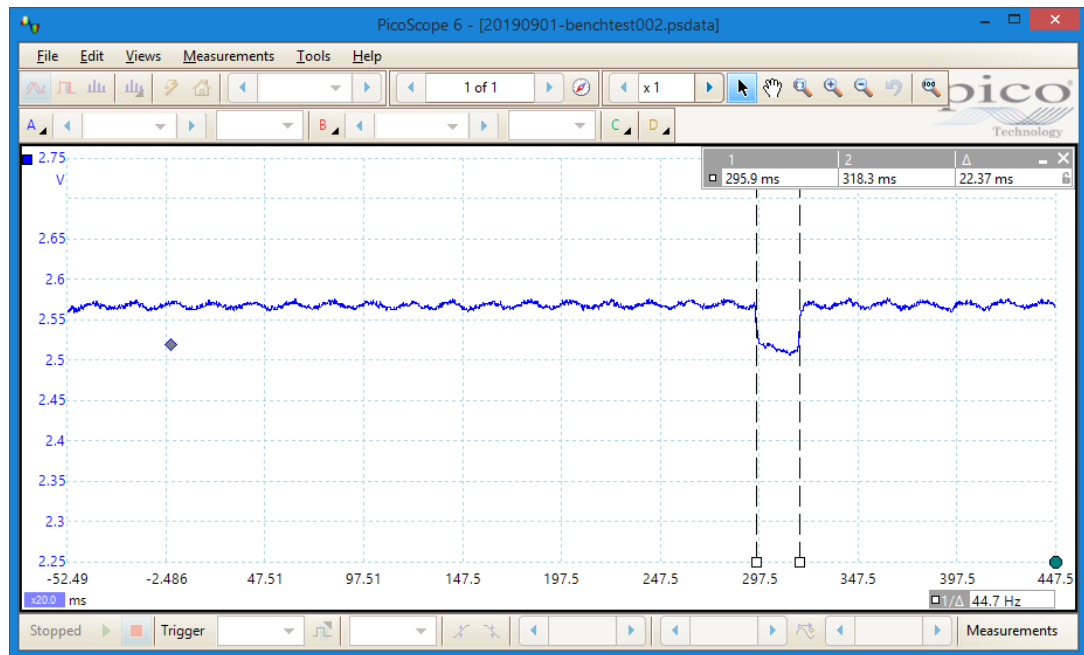
Fig.5.33 Detection circuit test bed 20 mS trace

Fig.5.33 shows the waveform captured by the oscilloscope with the relay control microprocessor set up to switch the relays of and then back on for 20 mS. The oscilloscope was connected across the output of the sensor amplifier. Note the 50 Hz noise on the trace due to mains pick up in the test leads.
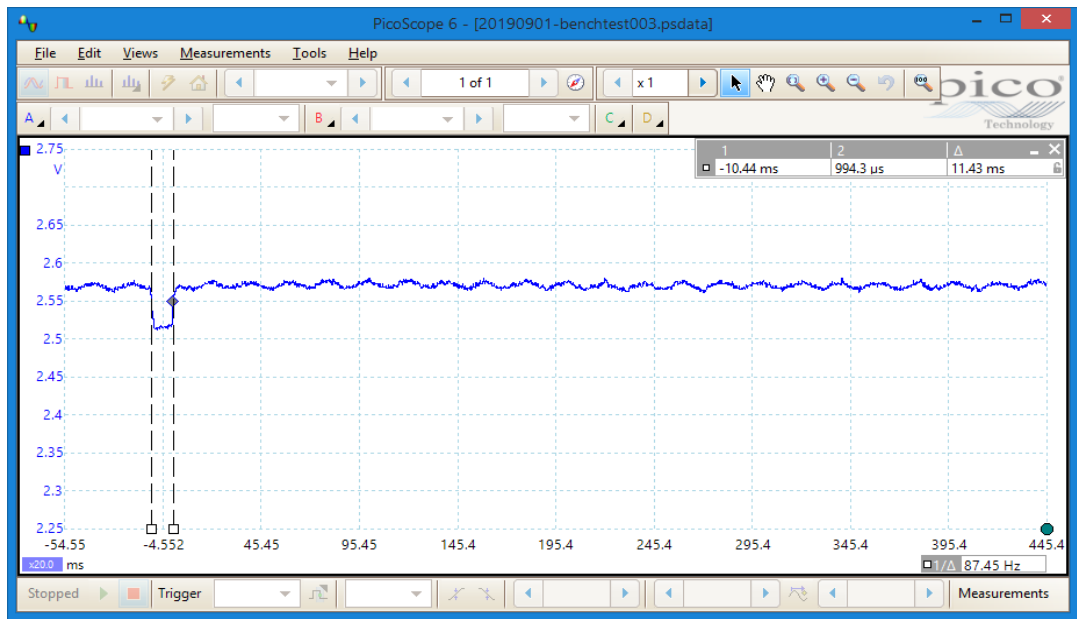
Fig. 5.34 Detection circuit test bed 10 mS trace

Fig. 5.34 shows the output of the bridge amplifier circuit with the relay set to switch off and back on in 10 mS.
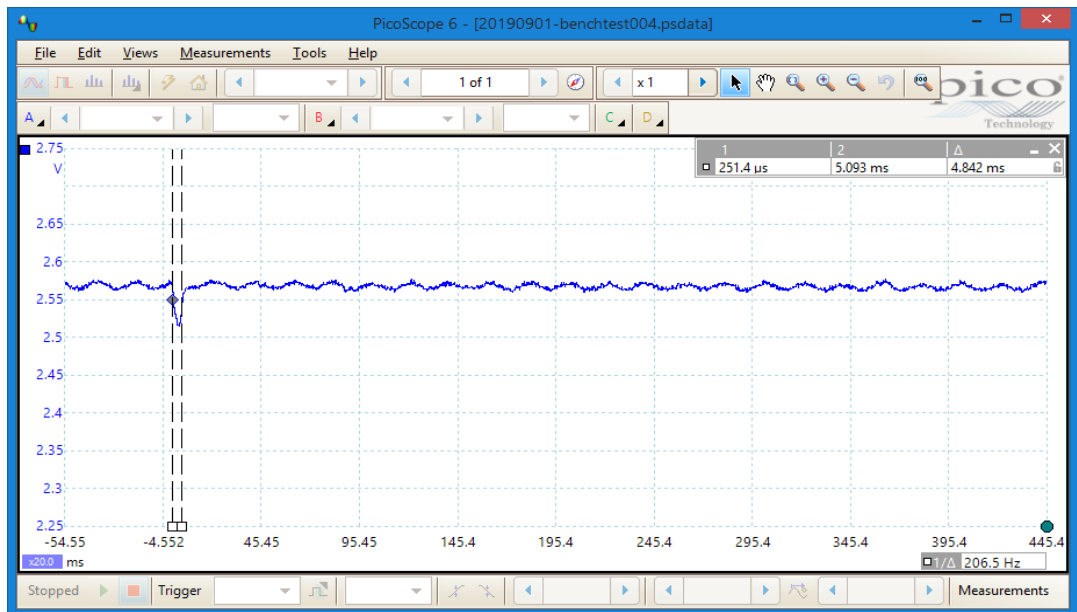
Fig. 5.35 Detection circuit test bed 5 mS

Fig. 5.35 shows the output of the bridge amplifier circuit with the relay set to off and back on in 5 mS.

The traces show that the sensor and associated circuit has the ability to detect pulses down to at least 5 mS duration.

5.3   POINT THROW ACCELEROMETER MEASUREMENT

As described in section 4.4 the flange way gap must be 105 mm at the lock stretcher position, which is 127 mm from the extreme tip of the switch; this is according to LU standard S2536 Maintenance of Points [28].

The objective of bench testing is to simulate the movement of the point switch across the flange gap during the point throw operation, and to capture the characteristic outputs from an accelerometer unit. The acceleration of the linear actuator, both in starting and stopping is not expected to be of a great enough magnitude to change the accelerometer output by a great deal. The tests include the introduction of simulated shock loading due to jamming or loose mechanical linkages causing sharp changes to the acceleration forces on the test bed.

The bench testing is a demonstration of the basic apparatus that could be used for in-house testing prior to field testing. The initial field testing could take place at a training facility with fully operational point machines. This could provide a test stage for the point movement scenario, but not the passage of a train scenario.

A description of the sensor to be used for the bench testing and the test apparatus used to carry out the testing is given in the following sections, followed by the accelerometer test and results.

5.3.1   ACCELEROMETER TEST
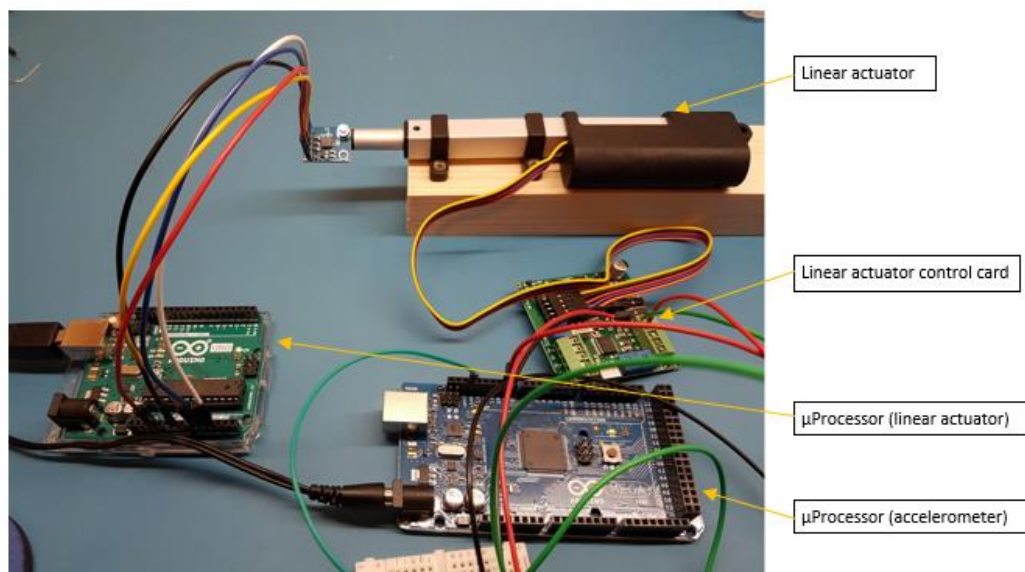
Fig. 5.36 Accelerometer test setup

The benchtop accelerometer test layout can be divided into two sections one for the linear actuator and the other for the accelerometer.

Accelerometer Board
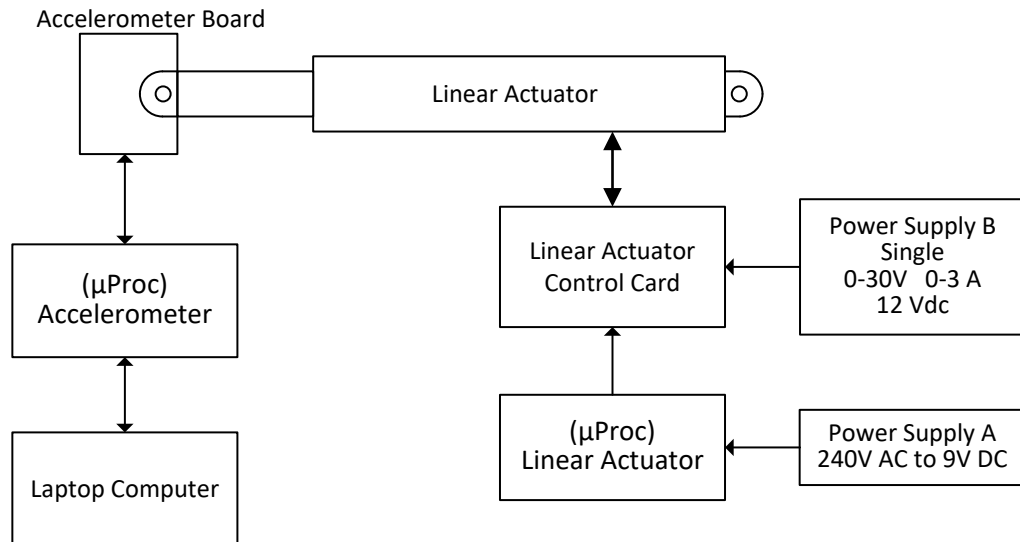
Fig. 5.37 Accelerometer test layout

Table 5.4 Accelerometer Test Equipment

Equipment	Description
Power Supply A: 240V AC to 9V DC unregulated PSU (600 mA) 9VPSU-600	240V AC to 9V DC power supply to feed linear actuator µProcessor.
Power Supply B: Single 0-30 V DC 0-3 Amps	ISOTECH303DD DC Power Supply
Accelerometer	ADXL335 mounted on break-out board
µProcessor (Accelerometer)	Arduino Uno R3
Linear Actuator	Actuonix P16-100-64-12-P
Linear Actuator Control Card	Actuonix LAC
µProcessor (Linear Actuator)	Arduino Mega2560
Laptop Computer	MATLAB Software Application Installed

The linear actuator layout comprises the actuator, which is connected to the linear actuator control card via a ribbon cable. The ribbon cable assembly is comprised of 5 cables, two provide the feed to the motor and three are connected to a potentiometer that provides feedback to the control card of the position of the actuator, providing closed loop control. The linear actuator has a power supply connected to it to provide power for the motor drive and associated control circuitry on the card. A microprocessor analog pin programmed as an output is connected to the card that provides the RC variable pulse width signal that acts to command the actuator to the desired position.

The accelerometer break out board is fixed to the moving clevis of the actuator with a small nut and bolt.

The connections between the board and the accelerometer microprocessor are comprised of a 3.3V DC supply; a ground connection and three outputs from the x, y and z axes outputs. These axes outputs are connected to analog pins A0, A1 and A2 respectively on the microprocessor board, the ground and supply are connected to the corresponding connections on the microprocessor board. The output is in the form of a voltage that represents the acceleration forces experienced in each of the three orthogonal axes. The serial data output from the accelerometer microprocessor board is received at the serial port of a compruter; MATLAB application software then converts the data into an animated plot and saves the data to a csv file for further analysis.

The stroke of the actuator is representative of the distance that the point switch rails travel between the normal and reverse position, which is fully open to close against the rail.

The tests comprise powering the actuator back and forth with a pause at each end of the stroke, which is fully extended and fully retracted. Following on from the initial static test the actuator is set to move; during the movement of the actuator the outputs of the accelerometer are connected to the analog input pins of an Arduino Uno microprocessor.

A MATLAB support package for Arduino hardware allows for the output to be recorded directly into the MATLAB application, where it is run as an animated

output providing "real time" viewing of the accelerometer output. The MATLAB script also saves the accelerometer output in a csv format.

The tests carried out are:

- With the actuator is at rest.

- With the actuator moving back and fore.

- With the end of the test bed being moved in the x-axis in a range of approximately five millimetres.

- With the end of the test bed being moved in the y-axis in a range of approximately five millimetres.

- With the end of the test bed being moved up and down in the z-axis in a range of approximately five millimetres.
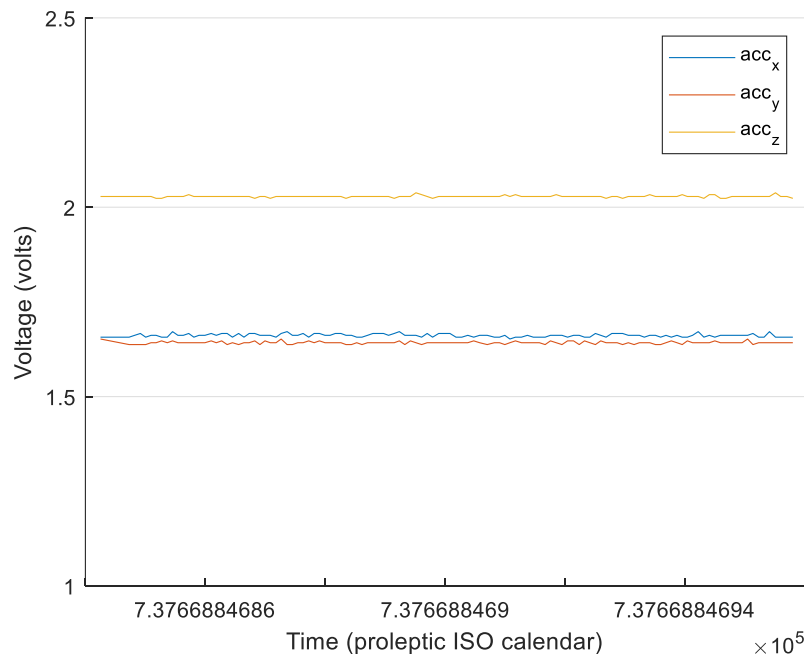
Fig. 5.38 Accelerometer readout static

The plots in Fig. 5.38 are for a period of approximately 20 seconds with the linear actuator in a static position. The output voltage of the accelerometer for each of the three axes is plotted against the proleptic ISO calendar which represents a serial date from a fixed, pre-set date which is January 0 year 0000 as a whole and fractional number of days.

Note that the amplitude of the voltage for the z axis is a greater value that those for the x axis and y axis; this is because the value represents the force of gravity which is constant acceleration acting in the z axis.
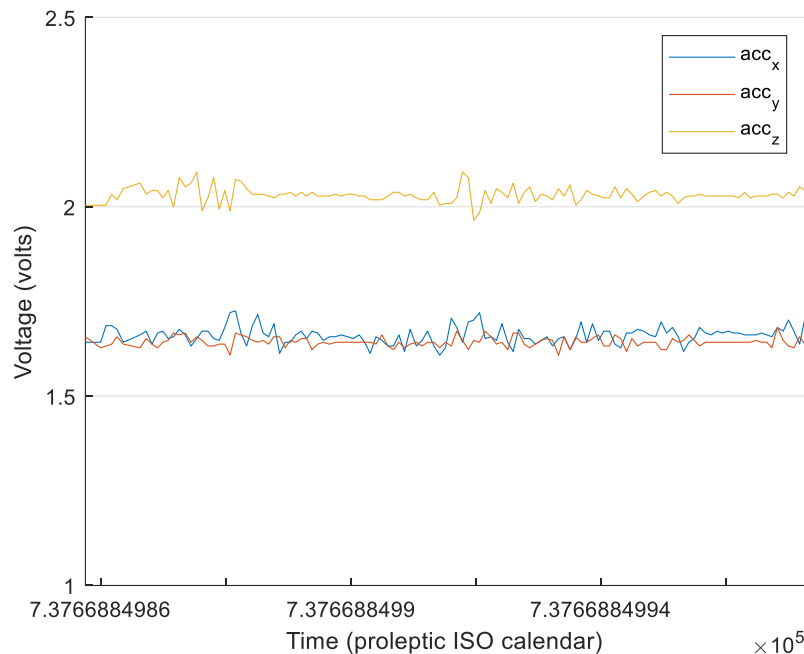
Fig. 5.39 Actuator movement only

The linear actuator was then cycled through its whole stroke length back and fore for approximately 20 seconds as represented in Fig. 5.39. It is clear from the plots that the start and finish of a stroke cycle is discernible in the traces for the x-axis and y-axis. The x-axis is expected as this is the axis along the length of the actuator; however, the clearest trace appears to be the z-axis. Movement in the y axis is limited as expected as there is no lateral movement at the end of the actuator. The "flutter" in the x-axis and z-axis traces is due to the actuator controller hunting for its position at the end of the stroke.
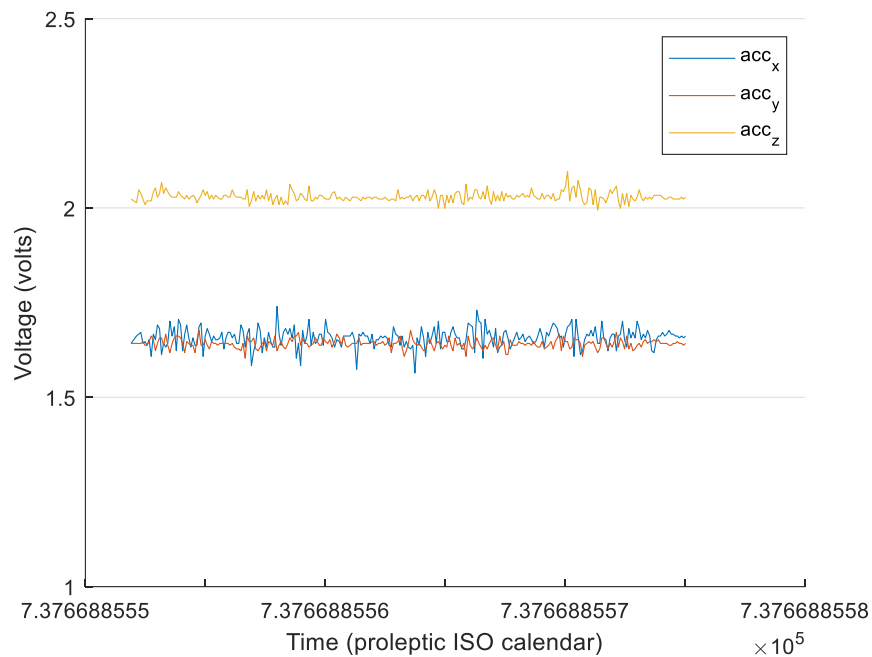
Fig. 5.40 X-axis movement

The plot of axes in Fig. 5.40 represents the case where the x axis is moved back and forth by a couple of millimetres, at the same time as the actuator is moving back and forth for its full stroke length. The sharp change in amplitude; both in a positive and negative sense are clearly evident. Note that the distinctions for end of stroke length evident in Fig. 5.39 are not clearly evident in this plot.
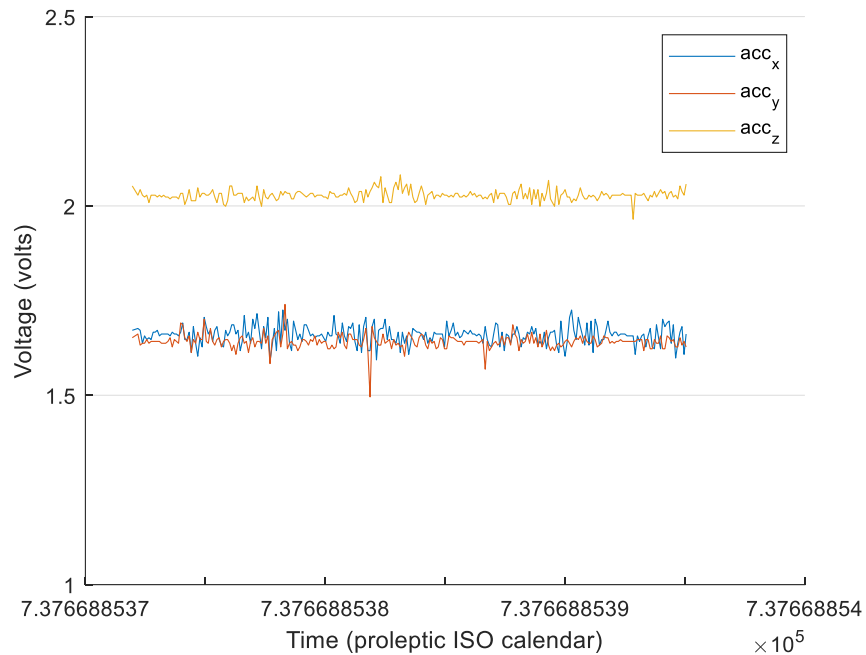
Fig. 5.41 Y-axis movement

The case where the y-axis is moved at the same time as the actuator is cycled back and forth through the stoke length is shown in Fig. 5.41. The movement of the y-axis is clearly discernible. There is also a lot of change in the trace of the x-axis; this is probably due to the limitations of isolating the movement in individual axes with the current test layout. Again, the differentiation for end of stroke length is not clearly evident.
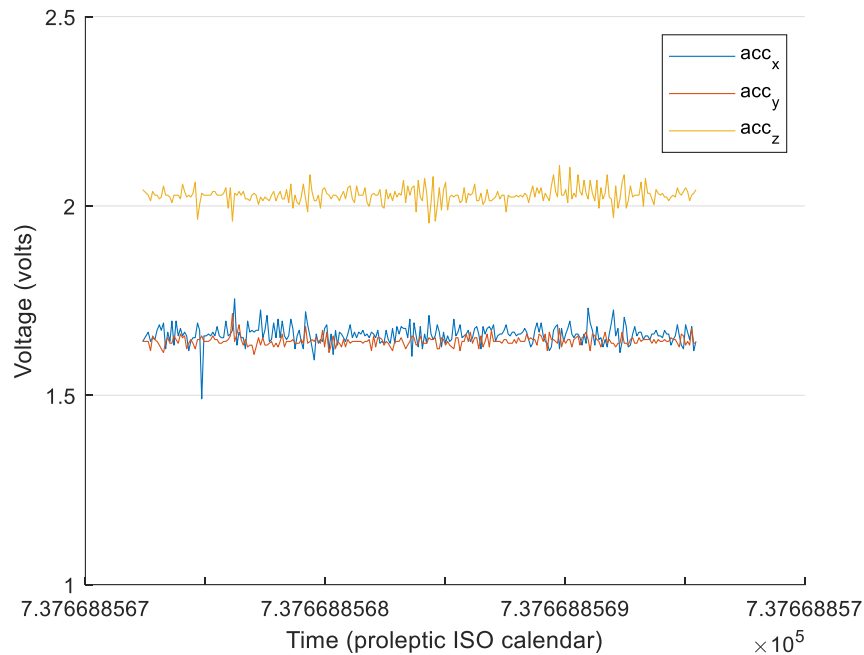
Fig. 5.42 Z-axis movement

The plot for z-axis movement in Fig. 5.42 seems to indicate movement in all three axes. The peak amplitudes appear to be more distinct in the x-axis. Again, the limitations of the test bed in isolating the movement to individual axes is probably partly responsible. However, there is expected to be movement in the x-axis as the arc of the vertical movement changes the acceleration force in the x-axis.
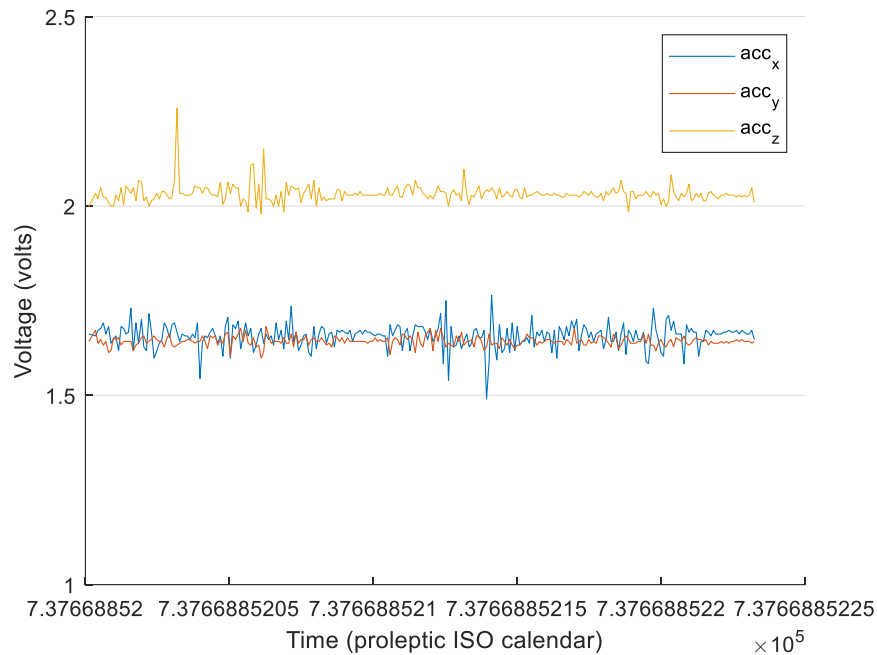
Fig. 5.43 All 3 axes movement

The movement of all three axes when the actuator is moving back and forth produces the accelerometer outputs as shown in Fig. 5.43. The y-axis appears to have limited change in its output. This could be as a result of the test being not very representative of movement in three axes. The trace for y-axis movement in Fig. 5.41 clearly shows the expected output for movement in the y-axis, but this is not present in the plot for all three axes. The x-axis and z-axis clearly show changes in direction as expected.

The benchtop testing of the accelerometer outputs that can be expected during the movement of the points is only intended as a demonstration. It shows the type of test set up that is required to investigate the use of accelerometers mounted on point mechanisms as a monitoring tool. The outputs are indicative of the nature of the signals that are output in the three axes of movement for a linear actuator when other axial movement is present.

The outputs from the basic demonstration raise questions over how the signals are best analysed. The sampling rate for the benchtop testing is comparatively low compared with other analogue to digital converter equipment on the market, although further testing is needed to confirm the best balance between sampling rates, signal analysis and useful data obtained.

The development of the use of accelerometers in proposed manner could use the basic equipment as a starting point and progress to testing on point mechanisms in a rail industry training school. These training schools have multiple point types and are vastly experienced in introducing failure modes as part of delivering training objectives.

It is expected that the output from simulated fault data will indicate particular trends leading to particular faults.

Once the equipment has been refined to a sufficient state, including the development of the local wireless network for data collection, then field trials could take place on the railway with the correct safety approvals in place.

6 CONCLUSIONS

This project set out to explore means of providing information on equipment performance, in particular for point machines. The use of two particular sensors was explored, a current sensing device in detail and a discussion on the use of accelerometers to monitor acceleration forces on point machines.

The current sensor used for testing was chosen to test its ability to measure low values of current in a conductor and be non- intrusive to the circuit being measured. The first attempts at getting a response from the sensor, that gave a reflection of the current in the conductor, confirmed that the sensitivity of the sensors was such that they were capable of measuring very low levels of magnetic field. This was expected as the manufacturer data indicated they were developed for applications for measurement down to tens of micro gauss. This also meant that they needed to be shielded form unwanted fields that could affect the accuracy of the conductor current measurement.

The sensors are intended to be used in signalling equipment rooms, within cabinets that contain control cable termination frames. The cabinets in which they are to be used consist of multiple cables with direct current and power frequency currents running through them; the sensors need to be able to operate in very close proximity to other cables carrying direct current and alternating current at power frequency. The sensors need to measure the value of current within the feed cable for the point circuit being monitored and should not be subject to interference to magnetic fields produced by other circuits.

The first set of bench tests with a multiple sensor array was with the intention of testing if the multiple sensors gave a similar output to each other, for the same value of conductor current. There was no current flowing in the conductor when the following observations were made. The oscilloscope trace shown in Fig. 5.10 for the bridge amplifier output and set-reset pulse, indicated that the set-reset circuit was working, also that there was a significant swing around the offset voltage of 2.5 volts between the output voltage for set and reset pulses. The offset was adjusted to 2.5 volts with a potentiometer in the non-inverting input leg of the operational amplifier circuit. When the orientation of the field was changed the output was as show in Fig. 5.11, the swing around the offset voltage being greatly reduced.

The set and reset pulses are called 'set high' and 'set low' to reflect the output of the bridge amplifier circuit when the pulse signal is removed to hold the output high or low. This significant swing is because the external magnetic field immediately realigns the magnetic domains in the resistive elements and changes the resistance of the sensor bridge elements. The swing in output is around the 2.5 volt offset voltage as the set reset pulse effectively changes the polarity of the resistive bridge. When the orientation is changed, as illustrated in Fig. 5.11, the external field is not incident with the easy axis of the sensor, and the change in sensor bridge elements due to domain realignment is not as great. The outputs for the sensors shown in Fig. 5.19 still show that the output is linear for both sensors for high and low gain configurations of the amplifier circuit.

The next set of sensor testing introduced an enclosure where the position of the sensor could be more consistent. The position of the enclosure on the test bench was also maintained for all enclosure tests; although this did not provide a magnetic field free environment it did attempt to provide consistency for shielded and non-shielded enclosure testing.

The enclosure testing was carried out using sensor 1, with no-shielding, single layer of shielding and a double layer of shielding. The plot of Fig. 5.28 clearly shows that the effect of shielding greatly reduced the offset voltage with zero conductor current. The effect of introducing a second layer of shielding had very little effect on reducing the offset further. The remaining offset can be accounted for by there being no provision for offset adjustment using a potentiometer in the non-inverting input leg of the operational amplifier circuit in this test circuit configuration.

The bridge amplifier circuit was modified to include a high resolution potentiometer in the non-inverting leg of the circuit, this was to provide a means of setting the offset voltage at 2.5 volts with a greater degree of accuracy than the potentiometer used for the multiple sensor tests.

The test results represented by Fig. 5.30 are for three configurations of the amplifier circuit to produce three levels of gain. All three traces have an origin at 2.5 volts and produce a linear response for the range of conductor current between 0 and 120 mA.

The shielded enclosure test configuration was then used to test the ability of the sensor and associated circuit to measure pulses produced by the switching of a

load across relay contacts. The aim was to see what the output of the circuit was for varying pulse widths. The oscilloscope traces in section 5.2.4 illustrate the responses to pulse widths between 20 milliseconds and 5 milliseconds. They indicate that the pulses are clearly discernible as a change in output level.

The accelerometer testing was carried out to demonstrate the type of sensor that may be used to perform monitoring of the acceleration forces on point switches. A decision was made early in the project that the testing that could take place on accelerometer trends for point machines was best developed in a railway training facility. The next stage of testing would need to involve equipment found in test houses for vibration analysis, or possibly move straight to a railway training facility where point machines are available. This testing could then be used to investigate the accelerometer outputs under fault conditions. Development of analysis and monitoring techniques can then take place.

The detection current testing indicates that they could be used for non-intrusive measurement of detection currents. There needs to be further development and testing of shielding that could be provided for the sensor itself that would not be too big to install in the termination cabinets. The leads from multiple sensors could then be taken to a local processing unit containing the bridge amplifier and set-reset circuits. The output from the amplifier circuits could then be processed prior to sending to a centralised processing unit.

The microprocessors that have been used for this testing have relatively low sampling rates and further testing should investigate the use of processors with enhanced features to develop the local processing of sensor outputs.

The application of the sensors for timing of point detection, and therefore monitoring point performance, does not require the sensitivity that the sensor is capable of providing; it only needs to provide a signal that allows for detection of a change in voltage level. However, there are other current and magnetic field sensing applications in the railway environment where the sensor capabilities could be fully explored.

7 REFERENCES

[1] D.J. Smith, *Reliability Maintainability and Risk*, 8th ed. Oxford: Elsevier, 2011.

[2] *Signalling functional requirements*, LU category 1 standard S1195, A6, London, 2013.

[3] *4LM System Architecture & Interface Requirements Specification*, Rev0007, Thales GTS, Vélizy-Villacoublay, France.

[4] *4LM Typical Bookwiring* Version 8, Thales GTS, Vélizy-Villacoublay, France.

[5] R. M. Goodall and C. Roberts, "Concepts and Techniques for Railway Condition Monitoring," in *IET International Conference on Railway Condition Monitoring*, Birmingham, UK, 29-30 Nov. 2006, pp. 90-95. Available: doi:10.1049/ic:20060050.

[6] T. Asada and C. Roberts, "Improving the dependability of DC point machines with a novel condition monitoring system," *Proceeding of the Institution of Mechanical Engineers, Part F: Journal of Rail and Rapid Transit, vol. 227, no. 4,* 2013, pp. 322-332, Accessed on: Mar. 21, 2020. [online].Available: doi: 10.1177/0954409713481748.

[7] J. Han, M. Kamber, and J. Pei, *Data Mining Concepts and Techniques*, 3rd ed. Burlington, Mass.: Elsevier, 2012.

[8] C. M. Bishop, *Pattern Recognition and Machine Learning*, New York : Springer, 2006.

[9] T. Asada, C. Roberts, and T. Koseki, "An algorithm for improved performance of railway condition monitoring equipment: Alternating-current point machine case study," *Transportation Research Part C*, vol. 30, pp. 81-92, 2013, Accessed on: Apr. 7, 2020. [online]. Available: doi: 10.1016/j.trc.2013.01.008.

[10] B. Hao, C. Roberts, and C. Goodman, "A generic fault detection and diagnosis approach for railway assets," in *International Conference on Railway Engineering - Challenges for Railway Transportation in Information Age*, Hong Kong, 25-28 March 2008, pp. 1-8. Accessed on: Mar. 29, 2020. [online]. Available: https://www.researchgate.net/publication/224364199_A_generic_fault_det ection_and_diagnosis_approach_for_railway_assets/link/5718d2fd08aed 43f63232986/download

[11] F. P. García Márquez, C. Roberts, and A. M. Tobias, "Railway point mechanisms: Condition monitoring and fault detection," *Proceedings of the Institution of Mechanical Engineers, Part F: Journal of Rail and Rapid Transit,* vol. 224, no. 1, 2009, pp. 35-44, Accessed on: Mar. 19, 2020. [online]. Available: doi: 10.1243/09544097jrrt289.

[12]   HSE press release, E087:03–29, May 2003. *Train Derailment at Potters Bar 10 May 2002 a Progress Report,* HSE Investigation Board, May 2003 Accessed on: Mar. 19, 2020. [online]. Available: http://158.132.155.107/posh97/private/accident-investigation/Potters-Bar-Report.pdf

[13]   *Derailment at Grayrigg*, *23 February 2007,* Report 20/2008, v5 July 2011, Rail Accident Investigation Branch, Department for Transport, London, 2011. Accessed on: Mar. 19, 2020. [online]. Available: https://assets.publishing.service.gov.uk/media/547c9037ed915d4c0d000199/R202008_081023_Grayrigg_v5.pdf

[14]   W. J. Zwanenburg, "A Model for the Life Expectancy Of Railway Switches And Crossings For Maintenance And Renewal Planning In Asset Management Systems," *WIT Transactions on the Built Environment,* vol. 103*,* pp. 765-773, 2008. Accessed on: Mar. 28, 2020. [online]. Available: doi: 10.2495/CR080741.

[15]   D. Rama and J.D. Andrews, "A reliability analysis of railway switches," Proc. of the Institution of Mechanical Engineers, Part F: *Journal of Rail and Rapid Transit*, vol. 227, 4, pp. 344-363, Mar. 2013. Accessed on: Mar. 19, 2020. [online]. Available: http://citeseerx.ist.psu.edu/viewdoc/download?doi=10.1.1.983.892&rep=rep1&type=pdf

[16]   V. L. Markine, M. J. M. M. Steenbergen, and I. Y. Shevtsov, "Combatting RCF on switch points by tuning elastic track properties," *Proc. of 8th Int. Conf. on Contact Mechanics and Wear of Rail/Wheel Systems,* Florence, 2009. vol. 271, no. 1, S.L. Grassie, E. Magel, and P.J. Mutton, Eds. 2011, pp. 158-167, 2011. Accessed on: Mar. 27, 2020. [online]. Available: https://doi.org/10.1016/j.wear.2010.10.031

[17]   A. Johansson *et al.*, "Simulation of wheel–rail contact and damage in switches & crossings," *Proc. of 8th Int. Conf. on Contact Mechanics and Wear of Rail/Wheel Systems,* Florence, 2009. vol. 271, no. 1, S.L. Grassie, E. Magel, and P.J. Mutton, Eds. 2011, pp. 472-481. Accessed on: Mar. 27, 2020. [online]. Available: https://doi.org/10.1016/j.wear.2010.10.014.

[18]   J. Xiao, F. Zhang, and L. Qian, "Numerical simulation of stress and deformation in a railway crossing," *Engineering Failure Analysis,* vol. 18, no. 8, pp. 2296-2304, 2011. Accessed: Mar. 22, 2020. [online]. Available: https://doi.org/10.1016/j.engfailanal.2011.08.006

[19]   W. Jin *et al.*, "Development and evaluation of health monitoring techniques for railway point machines," in *2015 IEEE Conf. on Prognostics and Health Management (PHM)*, 22-25 June 2015, pp. 1-11, Accessed: Feb. 24, 2020. [online]. Available: doi: 10.1109/ICPHM.2015.7245016.

[20]   H. Yin, "The self-organizing maps: Background, theories, extensions and applications." *Computational intelligence: a compendium*, J. Fulcher, Ed., Berlin: Springer, 2008, pp. 715-762.

[21]   J. B. Yu and L. F. Xi, "Using an MQE chart based on a self-organizing map NN to monitor out-of-control signals in manufacturing processes," *Int. Journal of Production Research,* vol. 46.21, pp. 5907 - 5933, Oct. 2008. Accessed: Mar. 22, 2020. [online]. Available: doi: 10.1080/00207540701358729.

[22]   J. Sa, Y. Choi, Y. Chung, H. Kim, D. Park, and S. Yoon, "Replacement Condition Detection of Railway Point Machines Using an Electric Current Sensor," *Sensors,* vol. 17, no. 2, Feb. 2017. Accessed: Feb. 24, 2020. [online]. Available: doi: 10.3390/s17020263.

[23]   J. Sa, Y. Choi, Y. Chung, J. Lee, and D. Park, "Aging Detection of Electrical Point Machines Based on Support Vector Data Description," *Symmetry,* vol. 9, no. 12, p. 290, 2017. Accessed: Feb. 24, 2020. [online]. Available: doi: 10.3390/sym9120290.

[24]   V. Atamuradov, K. Medjaher, F. Camci, P. Dersin, and N. Zerhouni, "Degradation-level Assessment and Online Prognostics for Sliding Chair Failure on Point Machines," *IFAC PapersOnLine,* vol. 51, no. 24, pp. 208-213, 2018. Accessed: Mar.11, 2020. [online]. Available: doi: 10.1016/j.ifacol.2018.09.579.

[25]   M. Hamadache, S. Dutta, R. Ambur, O. Olaby, E. Stewart, and R. Dixon, "Residual-based Fault Detection Method: Application to Railway Switch & Crossing (S&C) System," in *2019 19th International Conference on Control, Automation and Systems (ICCAS)*, Jeju, Korea, 15-18 Oct. 2019, pp. 1228-1233. Accessed on: Feb. 24, 2020. [online]. Available: doi: 10.23919/ICCAS47443.2019.8971747.

[26]   "Infrastructure, turnouts." The Railway Technical Website. http://www.railway-technical.com/infrastructure/. (accessed Apr. 23, 2020).

[27]   *Points, Unit 5, Four Foot Points*, *Edition B*, Signals Training Unit, London, March 2007.

[28]   *Maintenance of Points,* LU Standard S2536, Issue A7, London Underground, London, June 2014.

[29]   LUL Signalling Design Handbook Principles and Applications, Applications – Catalogue of Signalling Equipment M7382 A1, Sept 2002.

[30]   *Elementary Signals, Unit 5, ed. A*, Signals Training Unit, London, (London Underground Training Manual).

[31]   *4LM Station Controller Subsystem (SCS) Requirements Specification (SURS), 3CU 14021 0032 DTZZA,* Revision 04, Thales GTS, Vélizy-Villacoublay, France.

[32]   *4LM System Design Overview (SDO),3CU 14021 0028 DSZZA,* Revision 10, Thales GTS, Vélizy-Villacoublay, France.

[33] *Signalling and Signalling Control-Concept and Requirements,* LU Standard S1196, Issue A4, London Underground, London, Nov. 2011.

[34] Nexans, Paris, France. *C62 Type 1 Cable, Technical Specification, 2016-20050815-TS-01*, Revision 03. (October 2017). Accessed: Mar. 21, 2019. [online]. Available: https://www.nexans.co.uk/eservice/UK-en_GB/pdf-family_30678/Essential_6_U_UTP_Cable.pdf

[35] *Station Controller Subsystem (SCS) Software Architecture Design, 3CU 14021 0096 DSZZA*, Revision 04, Thales GTS, Vélizy-Villacoublay, France.

[36] J, de Reffye, P. Dersin, "Mechanical reliability of a point system," *IFAC Proceedings*, Vol. 43, Issue 3, 2010, pp 86-9. Accessed: Apr. 11, 2020. [online]. Available: doi: 10.3182/20100701-2-PT-4012.00016.

[37] I.S. Grant and W.R. Phillips, *Electromagnetism*, 2nd ed. Chichester: John Wiley and Sons, 1990.

[38] L. Quéval, "BSmag Toolbox User Manual," Tech. report, Dept. Elect. Eng., University of Applied Sciences, Düsseldorf, Germany, Apr. 2015. Accessed June. 06, 2019.[online] Available: http://www.lqueval.com

[39] T.R. Maguire and R.I. Potter, "Anisotropic magnetoresistance in ferromagnetic 3d alloys," *IEEE Transactions on Magnetics*, vol. 11, issue 4, pp.1018-1038, July 1975. Accessed: May 20, 2019. [online]. Available: doi: 10.1109/TMAG.1975.1058782.

[40] Honeywell, Plymouth, MN, USA. *Set/reset function for magnetic sensors. manufacturer's application note AN213 900298*. (Aug. 2002). Accessed: Apr. 14, 2019. [online]. Available: https://aerospace.honeywell.com/content/dam/aero/en-us/documents/learn/products/sensors/application-notes/AN213_Set_Reset_Function_of_Magnetic_Sensors.pdf

[41] Honeywell, Plymouth, MN, USA. *1- and 2- Axis magnetic sensors HMC1001/1002/1021/1021 datasheet.* (Apr. 2019). Accessed: June 8, 2019. [online]. Available: https://www.alldatasheet.com/datasheet-pdf/pdf/543272/HONEYWELL-ACC/HMC1001.html

[42] H.W. Ott, Noise Reduction Techniques in Electronic Systems, 2nd ed. New York: John Wiley and Sons, 1988.

[43] Aaronia AG, Strickscheid, Germany. *Magnetic field shielding foil/shielding sheet Aaronia MagnoShield FLEX datasheet, Rev 1.6.* (Sep. 20, 2016). Accessed May 12, 2019. [online]. Available: https://docplayer.org/37420407-Magnetic-field-shielding-foil-shielding-sheet-aaronia-magnoshield-flex.html

[44] M. Hamarat, S. Kaewunruen, M. Papaelias, and M. Silvast, "New Insights from Multibody Dynamic Analyses of a Turnout System under Impact Loads," *Applied sciences,* vol. 9, no. 19, p. 4080, Sep. 2019. Accessed: Apr. 12, 2020. [online]. Available: doi: 10.3390/app9194080.

[45] X. Liu and V. L. Markine, "Train hunting related fast degradation of a railway crossing-condition monitoring and numerical verification," *Sensors,* vol. 20, no. 8, p. 2278, 2020, Accessed: Apr. 12, 2020. [online]. Available: doi: 10.3390/s20082278.

[46] *Electromagnetic Compatibility (EMC) with LU Signalling System Assets,* LU Standard S1193, Issue A4, London Underground, London, April 2017.

[47] *Railway Applications. Electromagnetic Compatibility. General*, BS EN 50121-1:2017, British Standards Document, BSI, Jan. 2017.

[48] 4LM Induced Voltage Study, Revision 5, Thales GTS, Vélizy-Villacoublay, France.

[49] C. R Paul, *Introduction to Electromagnetic Compatibility*, 2nd ed. Hoboken: John Wiley and Sons, 2006.

[50] *Fire Safety Performance of Materials*, LU Standard 1-085, Issue A4, London Underground, London, Dec. 2015.

[51] Honeywell, Plymouth, MN, USA. *Vehicle detection using AMR sensors*: *manufacturer's application note AN218*. (Aug. 2005). Accessed: June 12, 2019. [online]. Available: https://www.yumpu.com/en/document/view/26492389/an218-vehicle-detection-using-amr-sensors

[52]   N.S. Nise, *Control Systems Engineering*, 4th ed. Hoboken: John Wiley and Sons, 2004.

[53]   A. Williams and F. Taylor, Electronic Filter Design Handbook, 4th ed. New York: McGraw Hill, 2006.

[54] Analog Devices, Norwood, MA, USA. *Three-Axis Accelerometer Data Sheet manufacturer's application note ADXL335, D07808-0-1/09(0), Rev 0.* (Jan. 2009). Accessed: June 8, 2019. [online]. Available: https://www.analog.com/media/en/technical-documentation/data-sheets/ADXL335.pdf

[55] Actuonix Motion Devices, Victoria, BC, Canada. *Linear motion series-P16, datasheet Rev B.* (Sept. 2016). Accessed: June 8, 2019. [online]. Available: https://s3.amazonaws.com/actuonix/Actuonix+P16+Datasheet.pdf

[56] Actuonix Motion Devices, Victoria, BC, Canada. *Linear Actuator Control Board datasheet.* (2017). Accessed: June 8, 2019. [online]. Available: https://s3.amazonaws.com/actuonix/Actuonix+LAC+Datasheet.pdf

[57] P. Horowitz and W. Hill, *The art of electronics*, 2nd ed. Cambridge: CUP, 1989.

Appendix A   DETECTION CIRCUIT CURRENT

A.1   Multiple Sensor Array Test Results

Table   A.1.1 Multiple sensor array results for sensor 1

Multiple Sensor		Multiple Sensor	
Sensor 1		Sensor 1	
Low Gain		High Gain	
mA	Vout	mA	Vout
120.20	2.610	120.00	2.729
110.00	2.600	110.30	2.711
100.20	2.590	100.00	2.695
90.00	2.590	90.00	2.675
80.80	2.580	80.60	2.657
70.50	2.570	70.04	2.638
59.98	2.560	59.95	2.622
50.01	2.550	49.97	2.607
39.96	2.540	40.01	2.589
29.94	2.540	30.00	2.569
20.01	2.530	20.03	2.554
10.06	2.520	10.06	2.533
0.00	2.510	0.00	2.516
-10.14	2.490	-10.00	2.498
-20.00	2.480	-20.00	2.482
-30.03	2.470	-30.01	2.464
-40.05	2.460	-39.98	2.449
-49.95	2.450	-50.44	2.430
-60.00	2.440	-60.15	2.414
-69.90	2.430	-70.00	2.395
-80.30	2.420	-80.30	2.378
-90.10	2.410	-89.90	2.363
-100.50	2.410	-100.30	2.343
-110.00	2.400	-110.00	2.327
-120.30	2.390	-120.00	2.312

The recorded values are for multiple sensor test bed sensor 1 in a multiple sensor test setup. The range of values is recorded for testing with low and high gain configuration of the bridge differential operational amplifier circuit.

Table   A.1.2 Multiple sensor array results for sensor 3

Multiple Sensor		Multiple Sensor	
Sensor 3		Sensor 3	
Low Gain		High Gain	
mA	Vout	mA	Vout
120.00	2.600	120.00	2.745
110.20	2.590	110.00	2.727
100.10	2.580	100.00	2.708
90.10	2.570	90.00	2.687
80.60	2.560	80.00	2.669
70.20	2.550	70.00	2.651
60.08	2.540	60.00	2.632
50.21	2.530	50.00	2.614
40.04	2.520	40.00	2.593
30.01	2.510	30.00	2.574
19.99	2.510	20.00	2.555
10.00	2.500	10.00	2.535
0.00	2.490	0.00	2.512
-10.08	2.480	-9.99	2.499
-19.95	2.470	-19.94	2.485
-30.06	2.460	-30.00	2.464
-40.03	2.450	-39.97	2.448
-49.99	2.440	-50.03	2.427
-59.95	2.430	-59.96	2.408
-70.10	2.420	-70.10	2.385
-80.00	2.410	-80.90	2.365
-90.00	2.400	-90.05	2.343
-100.00	2.390	-100.40	2.327
-110.00	2.380	-110.30	2.295
-120.00	2.370	-120.00	2.276

The recorded values are for multiple sensor test bed sensor 3 in a multiple sensor test setup. The range of values is recorded for testing with low and high gain configuration of the bridge differential operational amplifier circuit.

A.2   Enclosure Test Results

Table   A.2.1 Non-shielded enclosure sensor 1 test results

Sensor 1			Sensor 1	
No Shield			No Shield	
Set High			Set Low	
mA	**Volts**		**mA**	**Volts**
120.30	3.475		120.10	2.499
109.60	3.470		110.10	2.504
100.80	3.465		100.50	2.509
90.30	3.460		90.20	2.514
80.40	3.455		80.00	2.519
70.00	3.450		69.90	2.524
60.40	3.445		60.20	2.528
50.20	3.440		50.20	2.533
40.10	3.435		40.04	2.538
30.17	3.430		30.05	2.543
20.69	3.426		20.06	2.548
10.07	3.420		10.07	2.553
0.00	3.415		0.00	2.558
-10.10	3.411		-9.98	2.563
-19.97	3.406		-20.03	2.568
-30.03	3.401		-30.00	2.573
-40.29	3.396		-40.05	2.577
-50.20	3.391		-50.00	2.582
-59.60	3.386		-60.10	2.587
-70.20	3.381		-70.10	2.592
-80.10	3.376		-80.10	2.597
-90.20	3.371		-90.10	2.602
-100.50	3.366		-100.00	2.606
-109.90	3.361		-110.00	2.611
-120.10	3.356		-120.00	2.616

The recorded values are sensor test bed sensor 1 in a non-shielded enclosure test setup. The range of values is recorded for testing with the set-reset pulses held set low and set high.

Table   A.2.2 Single-shielded enclosure sensor 1 test results

Sensor 1			Sensor 1	
Single Shield			Single Shield	
Set High			Set Low	
mA	**Volts**		**mA**	**Volts**
120.00	3.058		120.00	2.912
109.90	3.052		110.10	2.918
99.90	3.047		100.00	2.923
89.90	3.042		90.30	2.928
79.80	3.037		80.00	2.933
70.10	3.031		70.30	2.938
60.00	3.027		60.40	2.943
50.00	3.021		50.60	2.948
39.90	3.016		40.00	2.954
30.00	3.011		30.50	2.959
20.10	3.006		19.90	2.964
10.10	3.000		9.90	2.969
0.00	2.994		0.00	2.975
-10.00	2.989		-10.00	2.978
-20.10	2.983		-20.00	2.983
-30.10	2.978		-30.00	2.989
-40.10	2.973		-40.20	2.994
-50.00	2.968		-50.00	2.999
-60.10	2.962		-60.60	3.005
-70.10	2.957		-70.10	3.010
-80.00	2.952		-80.00	3.016
-90.00	2.947		-89.90	3.021
-99.90	2.941		-100.00	3.027
-110.20	2.936		-109.90	3.032
-120.00	2.931		-120.00	3.037

The recorded values are sensor test bed sensor 1 in a single shielded enclosure test setup. The range of values is recorded for testing with the set-reset pulses held set low and set high.

Table   A.2.3 Double-shielded enclosure sensor 1 test results

Sensor 1			Sensor 1	
Double Shield			Double Shield	
Set High			Set Low	
mA	**Volts**		**mA**	**Volts**
120.00	3.050		120.00	2.906
110.10	3.045		110.10	2.910
100.00	3.040		100.00	2.915
90.00	3.036		90.00	2.920
80.00	3.031		80.10	2.924
70.10	3.026		69.90	2.929
60.00	3.021		60.00	2.934
49.90	3.016		49.90	2.939
40.10	3.011		39.90	2.944
29.90	3.006		30.10	2.948
20.10	3.001		20.10	2.953
10.00	2.996		10.00	2.958
0.00	2.991		0.00	2.962
-10.00	2.986		-10.00	2.967
-20.00	2.981		-20.00	2.972
-29.90	2.977		-29.90	2.977
-40.00	2.972		-40.00	2.982
-50.00	2.967		-50.00	2.987
-60.00	2.962		-59.90	2.992
-70.00	2.957		-70.00	2.997
-80.00	2.952		-80.00	3.002
-90.00	2.948		-90.00	3.006
-100.10	2.943		-100.10	3.011
-110.00	2.938		-110.00	3.016
-120.00	2.933		-120.00	3.021

The recorded values are sensor test bed sensor 1 in a double shielded enclosure test setup. The range of values is recorded for testing with the set-reset pulses held set low and set high.

Table   A.2.4 Non-shielded enclosure sensor 2 test results

Sensor 2			Sensor 2	
No Shield			No Shield	
Set High			Set Low	
mA	**Volts**		**mA**	**Volts**
120.00	3.167		120.00	2.219
110.00	3.162		110.20	2.223
100.10	3.158		100.20	2.226
90.00	3.152		90.10	2.231
80.00	3.147		79.90	2.237
70.10	3.142		69.80	2.241
60.10	3.137		60.00	2.246
49.90	3.132		50.10	2.251
40.10	3.127		39.90	2.256
30.00	3.122		29.90	2.261
20.00	3.117		20.10	2.265
10.10	3.112		10.00	2.270
0.00	3.107		0.00	2.276
-10.10	3.103		-9.90	2.282
-20.10	3.098		-19.90	2.288
-30.00	3.094		-29.90	2.292
-40.00	3.089		-39.90	2.297
-50.00	3.084		-50.00	2.302
-60.00	3.077		-60.10	2.307
-70.00	3.072		-70.00	2.312
-80.10	3.067		-80.10	2.317
-90.00	3.062		-90.20	2.322
-100.00	3.057		-99.90	2.326
-110.00	3.052		-110.00	2.332
-120.00	3.047		-120.00	2.336

The recorded values are sensor test bed sensor 2 in a non-shielded enclosure test setup. The range of values is recorded for testing with the set-reset pulses held set low and set high.

Table   A.2.5 Single-shielded enclosure sensor 2 test results

Sensor 2			Sensor 2	
Single Shield			Single Shield	
Set High			Set Low	
mA	**Volts**		**mA**	**Volts**
120.00	2.778		120.00	2.621
109.90	2.772		110.00	2.626
100.10	2.768		100.10	2.632
89.90	2.762		90.00	2.637
80.30	2.757		80.00	2.642
69.80	2.752		70.00	2.647
60.00	2.746		60.00	2.653
50.10	2.741		50.00	2.658
40.60	2.736		40.01	2.663
30.03	2.730		30.08	2.668
20.07	2.725		19.97	2.673
9.99	2.720		10.03	2.678
0.00	2.715		0.00	2.684
-10.06	2.711		-10.00	2.689
-20.01	2.705		-20.00	2.695
-30.08	2.700		-30.00	2.700
-40.20	2.695		-40.10	2.705
-50.00	2.689		-50.20	2.711
-59.80	2.684		-60.10	2.716
-70.00	2.679		-70.10	2.721
-80.00	2.673		-80.00	2.726
-89.90	2.668		-90.00	2.731
-100.10	2.663		-100.10	2.737
-110.00	2.656		-110.00	2.742
-120.00	2.651		-120.00	2.747

The recorded values are sensor test bed sensor 2 in a single shielded enclosure test setup. The range of values is recorded for testing with the set-reset pulses held set low and set high.

Table   A.2.6 Offset applied to non-shielded results

Sensor 1 No Shield Set High		Offset		Sensor 1 No Shield Set Low		Offset	
mA	Volts	Volts	Volts	mA	Volts	Volts	Volts
120.30	3.475	0.308	3.167	120.10	2.499	0.282	2.217
109.60	3.470	0.308	3.162	110.10	2.504	0.282	2.222
100.80	3.465	0.308	3.157	100.50	2.509	0.282	2.227
90.30	3.460	0.308	3.152	90.20	2.514	0.282	2.232
80.40	3.455	0.308	3.147	80.00	2.519	0.282	2.237
70.00	3.450	0.308	3.142	69.90	2.524	0.282	2.242
60.40	3.445	0.308	3.137	60.20	2.528	0.282	2.246
50.20	3.440	0.308	3.132	50.20	2.533	0.282	2.251
40.10	3.435	0.308	3.127	40.04	2.538	0.282	2.256
30.17	3.430	0.308	3.122	30.05	2.543	0.282	2.261
20.69	3.426	0.308	3.118	20.06	2.548	0.282	2.266
10.07	3.420	0.308	3.112	10.07	2.553	0.282	2.271
0.00	3.415	0.308	3.107	0.00	2.558	0.282	2.276
-10.10	3.411	0.308	3.103	-9.98	2.563	0.282	2.281
-19.97	3.406	0.308	3.098	-20.03	2.568	0.282	2.286
-30.03	3.401	0.308	3.093	-30.00	2.573	0.282	2.291
-40.29	3.396	0.308	3.088	-40.05	2.577	0.282	2.295
-50.20	3.391	0.308	3.083	-50.00	2.582	0.282	2.300
-59.60	3.386	0.308	3.078	-60.10	2.587	0.282	2.305
-70.20	3.381	0.308	3.073	-70.10	2.592	0.282	2.310
-80.10	3.376	0.308	3.068	-80.10	2.597	0.282	2.315
-90.20	3.371	0.308	3.063	-90.10	2.602	0.282	2.320
-100.50	3.366	0.308	3.058	-100.00	2.606	0.282	2.324
-109.90	3.361	0.308	3.053	-110.00	2.611	0.282	2.329
-120.10	3.356	0.308	3.048	-120.00	2.616	0.282	2.334

The tables show the effects off adding an offset to the results of sensor 2 with respect to sensor 1. This offset has then been added to the results for sensor 2. This has been carried out for both set high and set low pulses held at set high and set low.

Table   A.2.7 Double shielded fully offset circuit results

Low Gain			High Gain			Very High Gain	
4.99 kΩ			2 kΩ			1 kΩ	
Sensor 1			Sensor 1			Sensor 1	
Double Shield			Double Shield			Double Shield	
Set High			Set High			Set High	
mA	**Volts**		**mA**	**Volts**		**mA**	**Volts**
0.00	2.500		0.00	2.500		0.00	2.500
10.02	2.505		10.10	2.511		10.00	2.521
19.99	2.510		20.00	2.522		20.02	2.543
30.06	2.515		30.10	2.532		30.06	2.566
39.96	2.520		40.00	2.543		40.03	2.588
49.97	2.525		50.00	2.554		50.02	2.610
60.01	2.530		60.00	2.564		60.02	2.632
70.10	2.535		70.00	2.575		70.10	2.654
80.00	2.540		80.00	2.586		80.10	2.677
90.30	2.545		90.00	2.596		90.00	2.699
100.20	2.550		100.10	2.607		100.00	2.721
110.00	2.555		110.02	2.618		110.00	2.743
120.00	2.560		120.02	2.628		120.00	2.765

The table records the value of the bridge operational amplifier with three different gain configurations. The sensor enclosure is double shielded, and a high resolution potentiometer has been use to adjust the offset at the input to the operational amplifier. The readings have all been taken with the set-reset pulse set high.

Appendix B   MICROPROCESSOR CODE

B.1   Detection Circuit Test Bed Code

Table   B.1.1 Detection circuit test bed code

```
_8_channel_relay_low_Development_01A

//the relays connect to
int IN1 = 41;
int IN2 = 42;
int IN3 = 43;
int IN4 = 44;
int IN6 = 46;

#define ON   0
#define OFF  1
void setup()
{
  relay_init();//initialize the relay
}

void loop() {
  //delay (5000);

  relay_SetStatus(ON,ON,OFF,OFF,ON);
  delay(2000);//delay 2s
  relay_SetStatus(OFF,OFF,OFF,OFF,ON);
  delay(500);//delay 2s

}
void relay_init(void)//initialize the relay
{ |
  //set all the relays OUTPUT
  pinMode(IN1, OUTPUT);
  pinMode(IN2, OUTPUT);
  pinMode(IN3, OUTPUT);
  pinMode(IN4, OUTPUT);
  pinMode(IN6, OUTPUT);
 // relay_SetStatus(ON,ON,ON,OFF ,OFF);//turn off all the relay
}
//set the status of relays
void relay_SetStatus( unsigned char status_1, unsigned char status_2,unsigned char status_3,
                      unsigned char status_4, unsigned char status_6  )
{
  digitalWrite(IN1, status_1);
  digitalWrite(IN2, status_2);
  digitalWrite(IN3, status_3);
  digitalWrite(IN4, status_4);
  digitalWrite(IN6, status_6);


}
```

The code contained in Table B.1.1 is used to provide the control of the relay module. The contacts of the relay module are opened and closed to represent the state of the equivalent contacts in a wayside point detection circuit. Pins 41, 42, 43, 44 and 46 are programmable as input/output pins on the microprocessor board

and are set as outputs; they drive contacts 1N, 2N, 3R, 4R and WL respectively. The status of the pins is then set high or low as required to represent the operation of the point circuit.

The timing element is represented by setting up delays in software loops. The code is only developed to the point where it can provide timed pulses of various durations to accommodate the limited testing at this stage.

Appendix C   ACCELEROMETER CODE

C.1   MATLAB code

```matlab
clear a
a =arduino('COM5','Uno');

%% Create a graph for accelerometer readings
figure
ax = axes;
ax.YGrid = 'on';
ax.YLim = [1,2.5];
cmap = ax.ColorOrder;
h1 = animatedline('Color',cmap(1,:));
h2 = animatedline('Color',cmap(2,:));
h3 = animatedline('Color',cmap(3,:));
legend({'acc_x','acc_y','acc_z'});
xlabel('Time (proleptic ISO calendar)');
ylabel('Voltage (volts)');

    xX = 0;
    xY = 0;
    xZ = 0;
    xt = 0;

%% Collect data from accelerometer and update plot live
tic
while toc <20
%%Get new data to plot
    t    =    datetime('now','TimeZone','local','Format','d-MMM-y
HH:mm:ss.ms ');
    t = datetime('now');

    b = readVoltage(a,'A0');
    c = readVoltage(a,'A1');
    d = readVoltage(a,'A2');




    %% Add points to animation
    addpoints(h1,datenum(t),b)
    addpoints(h2,datenum(t),c)
    addpoints(h3,datenum(t),d)
    xX = [xX,b];
    xY = [xY,c];
    xZ = [xZ,d];
    xt = [xt,datenum(t)];

    drawnow
% %    Time elapsed for data collection
     te = toc;

end
```

The MATLAB code is used to communicate with the Arduino Uno that reads the voltages output from the accelerometer unit. The values are serially transmitted to a laptop via USB. The MATLAB script then provides an animated plot of all three axes values, the values are also saved to file for further analysis.

- END OF DOCUMENT -